To the Graduate Council:

I am submitting herewith a dissertation written by Ernest Clayton Crosby entitled "Simulation of the Effects of Contour Coal Strip Mining on Stormwater Response and Suspended Sediment Yield in the New River Watershed, Tennessee." I recommend that it be accepted in partial fulfillment of the requirements for the degree of Doctor of Philosophy, with a major in Civil Engineering.

Donald E. Overton

Donald E. Overton, Major Professor

We have read this dissertation and recommend its acceptance:

Wayne T. Davis

Roger A. Minear

[illegible]

Accepted for the Council:

L. Evans Roth

Vice Chancellor
Graduate Studies and Research

SIMULATION OF THE EFFECTS OF CONTOUR COAL STRIP MINING ON STORMWATER RESPONSE AND SUSPENDED SEDIMENT YIELD IN THE NEW RIVER WATERSHED, TENNESSEE

A Dissertation

Presented for the

Doctor of Philosophy

Degree

The University of Tennessee, Knoxville

Ernest Clayton Crosby

August 1979

DEDICATION

This dissertation is dedicated to my wife, father and mother.

ACKNOWLEDGEMENTS

This research was supported in part by funds provided by the U.S. Department of Energy under Contract Number EY-76-S-05-4946.

The author wishes to express his sincere appreciation to Dr. Donald E. Overton, Major Professor and Advisor, for his guidance and encouragement during his study.

Sincere appreciation is expressed to the author's committee: Roger A. Minear, Wayne T. Davis, and Gerald L. Vaughn, for their suggestions, assistance and support.

Special thanks are given to Miss Gail Ferguson, who typed the manuscript and to Miss Karengay Chen, who drafted the figures.

ABSTRACT

Water and soil are two of man's most valuable resources and often the most abused. The impact of misuse frequently results in dramatic effects such as floods, soil erosion, droughts and unwanted deposition of soil. Repeatedly, these consequences are caused by an inability to quantify the effects of land use changes on stormwater runoff and soil erosion in small watersheds. With this in mind, a mathematical model for simulating stormwater response and suspended sediment yield in strip mined watersheds was developed. This model consisted of a storm hydrograph simulator, a watershed suspended sediment load simulator and a site erosion simulator. The storm hydrograph simulator, TENN-I, has been optimized for the Tennessee Valley and can be used for both gauged and ungauged watersheds. The watershed soil load simulator, LOAD-I, was based upon development of a suspended load modulus that can be derived from storm hydrographs and sedigraphs. The site specific soil erosion model, ERODE-I, was based upon soil erosion mechanics and overland flow. Erosion, runoff, sediment delivery and total loads were simulated for storm events on both a real time basis and on a design storm basis. A regionalization scheme associated with the model permitted simulation of the effects of alternative development scenarios on stormwater and suspended load. Comparisons of the model are made with suspended sediment yields from watersheds which have undergone coal contour strip mining and urbanization.

This model's ability to relate a watershed's stormwater runoff and sediment load to measurable, quantifiable, and readily comparable quantities provides a powerful tool to evaluate the effects of land use change before the fact.

TABLE OF CONTENTS

LIST OF TABLES

LIST OF FIGURES

FIGURE | PAGE

FIGURE PAGE

CHAPTER I

INTRODUCTION

Prevailing economics since the advent of the oil tariffs in 1973 and current efforts of the United States toward energy self-sufficiency virtually insure the continuing demand for both surface and underground coal. In 1955, 465 million tons of coal were mined in the United States with surface mining accounting for 26 percent of the total. By 1971, surface mining accounted for 50 percent of the total mined and by 1975 it accounted for 55 percent of the 647 million tons mined [1]. As the role of coal in the nation's energy supply expands, the share from surface mining will continue to increase since a large portion of domestic coal reserves are surface mineable.

Although the majority of surface mined coal is located in the West; Central and Southern Appalachia--consisting of West Virginia, Kentucky (eastern), Virginia, Tennessee and Alabama--are major producers. Twenty-eight percent of the 355 million tons of coal surface mined in 1975 was produced from this region [2]. In the last decade as much as 80 percent of the annual electricity consumed by the Eastern United States has been produced with Appalachian coal [3]. This coal is generally higher in sulfur content than western coal. This is a detracting attribute, but it is offset by its higher average heat content--12,500 Btu per pound as compared to 7,000 Btu per pound of western coal [4]. Further, local economics and close proximity to eastern electric producers will insure the continued demand of coal from the region.

Surface mining operations in Tennessee since the 1940's have disturbed in excess of 53,000 acres [5]. It is estimated that some 7,700 additional acres of Tennessee's remaining 59,400 acres of strippable reserves will be disturbed between 1980 and 1985 [6]. These mining operations have primarily been confined to mountain top removal and contour stripping techniques since Tennessee's coal reserves are located predominantly in mountainous regions with steep slopes. This strip mining has and will bring about alterations in quantity and quality of surface water within the mined watersheds. While the impacts from mining on steep slopes are similar to all surface mining conducted in the eastern United States, the severity of the impacts increases as the degree of slope increases [6]. This is particularly true because of the increased difficulty in dealing with problems of erosion, runoff and land stability on steeper slopes. If the past can be any indication of the future, then detriment to water quality due to excess soil eroded sediment and spoil related additions to the runoff water may be expected [7].

In order to optimize the trade-off between environmental impact and coal mining production, management of mined areas must come to grips with the problem of balancing adverse environmental impacts with the economics of strip mining subject to the political, legal, social and jurisdictional constraints. This process has become so critical that the United States Congress passed Public Law 95-87, The Surface Mining Control and Reclamation Act of 1977, to establish regulatory control under which coal could be mined while maintaining minimum acceptable environmental impact [8]. Under this act, the Department of Interior has established an Office of Surface Mining and Enforcement and a permanent regulatory program [9].

Under this regulatory program, an attempt is being made to minimize the change in water quality and quantity resulting from increased surface mining. Initially, this will necessitate simulation of the environmental effects of strip mining on watershed runoff. This can be accomplished for steep mountainous terrain if the hydrologic and erosion responses of the mined areas are correlated with watershed basin outflow and suspended sediment responses by mathematical simulation.

Statement of Problem

The transition of basin watershed outflow and suspended sediment responses during mining have been attributed to strip mining on virgin watersheds [10]. In addition, it has been postulated that a major mechanism for pollutant injection into the watershed hydrologic system is by erosion and subsequent suspension in runoff [11]. Hence, it becomes evident that the best possibility for selecting an optimum feasible policy for managing contour strip mined areas must include the use of a mathematical model for simulating the hydrologic and erosion responses on a scientific deterministic basis.

Research Objectives

The objective of this research is to evaluate the effects of steep contour coal strip mining on stormwater response and suspended sediment yield for small watersheds using mathematical modelling. The New River Basin, Tennessee, has been selected as being representative of small watersheds in Eastern Tennessee undergoing this type of disturbance and will be used as such for an in-situ study.

To accomplish this objective, simulation of the following processes will be required for both the watersheds and the in situ mining site:

1. Stormwater response,
2. Erosion,
3. Sediment Yield.

The simulation techniques used possess the following characteristics:

1. The models were developed on a physical basis, i.e. deterministic,
2. The parameters have physical significance,
3. The models are accurate,
4. The models are experimentally verified,
5. The structure of the models is not so complicated as to be intractable.

CHAPTER II

LITERATURE REVIEW

Prior to model formulation, an extensive literature review was conducted in order to (a) trace the historical development of models relating surface runoff, erosion and sedimentation process; (b) determine the formulation of those models; and (c) establish a present state of the art.

Stormwater Response Simulation

Stormwater is the direct runoff response of a basin or site to rainfall [12]. The simulation of this runoff response is a relatively new hydrologic tool and is based upon two fundamental hydrologic principles, unit hydrograph theory and kinematic overland flow theory.

Unit Hydrograph Theory

In the 1930's, Sherman [13, 14, 15] introduced the unit hydrograph as a hydrograph of runoff resulting from a unit of rainfall excess occurring at a uniform rate, uniformly distributed over a watershed in a specified duration of time. From this unit hydrograph it was postulated that for a given area, for any rain or series of rains, the runoff hydrograph could be computed by a simple summation process [14, 16, 17, 18, 19]. This last assumption, the principal of superposition, states that the unit hydrograph reflects all basin characteristics to the degree that the runoff rate is simply proportional to the runoff volume for a rainfall excess of a given duration. Expressed in mathematical modeling terms, the system model must be lumped, time invariant and linear [12].

Unit hydrograph theory is extensively used today, although there are serious questions about its assumptions. Although validity of the basic theory was not seriously questioned until the late 1950's, Johnstone and Cross [18] indicated as early as 1949 that the basic assumptions of the unit hydrograph model were not entirely sound. It is now known that a basin acts less as a lumped parameter system as its size decreases. Uniform rainfall distribution and intensities seldom occur in nature. As for the assumption of linearity, much proof that hydrologic systems violate that assumption has been presented in recent literature by many investigators such as Parsad [19], Nash [20], O'Donnell [21], Amorocho and Orlob [22], Amorocho [23], Overton [24] and others. It is generally accepted now that the assumptions of linearity and time-invariance are not strictly correct. They are adopted, however, because the method is still useful, simple and one of the best methods available that produces results that are acceptable for engineering and research purposes [16, 25].

In addition to analyzing gauged watersheds, Sherman's [13] technique has become an important device for transferring information from gauged to ungauged watersheds. To accomplish this, techniques have been developed to generate synthetic unit hydrographs that allegedly have similar physiographic and climatic characteristics.

Synthetic unit graph techniques have traditionally followed two avenues of approach. One approach was to statistically correlate, normally using linear regression, the physiographic characteristics of the watershed with the derived unit hydrograph such as the work of Morgan and Johnson [26], Dooge [27], Edson [28], O'Kelly [29] and others [16].

The second line of approach was to represent all unit hydrographs by a single curve or family of curves, choose a number of unit hydrograph parameters that make up the basis for defining the hydrograph and relate the parameters to the catchment characteristics. Snyder [30], Linsley [31], Eagleson [32], Taylor and Schwarz [33] and Hudlow and Clark [34] concentrated on using lag time, peak discharge and unit hydrograph time base to relate various basin characteristics in an effort to produce synthetic unit hydrographs. The United States Soil Conservation Service uses a single triangle unit hydrograph and the SCS curve number model [35] to simulate storm hydrographs. Still others, such as Commons [36], Mitchell [37], United States Soil Conservation Service [38] and Gray [37] have developed routines to produce dimensionless hydrographs that can be converted into unit hydrographs. This method is designed to eliminate the effects of basin size on the unit hydrograph.

Once the nonlinearity of the watershed response was verified [24, 40, 41, 42], several attempts were made to account for it by deriving variable unit hydrographs. Black [42] and Minshall [43] used linear regression equations to relate peak flow to rainfall intensity. Singh [44] extended this work by relating the nonlinear unit hydrograph to an equivalent instantaneous effective rainfall.

Nash [20] and Dooge [27] used a series of reservoirs amd channels where storage was directly related to flow to approximate the nonlinear storage and translation effects of natural watershed response. Prasad [19] extended that approach by allowing for unsteady conditions.

Ding [45] derived a unit hydrograph using a nonlinear, generalized Muskingum routing technique coupled with a differential correction method.

Unlike his previous investigators, Ding [45] attempted to attach physical significance to the parameters used to define the hydrograph.

Ardis [46], taking a unique approach to the problem, developed a method for deriving unit hydrographs based on the assumption that the unit hydrograph could be represented by a geometric quadrilateral configuration. This quadrilateral configuration was referred to as a unit response function (URF) and could assume a wide range of shapes. In addition, this method was also based upon the concept of partial area runoff [47, 48, 49, 50] and the concept that the unit hydrograph or URF, could vary considerably both among and within watersheds. This method has been widely used by the Tennessee Valley Authority and is often called the TVA double triangle model.

Using the partial area runoff concept, Ardis [46] assumed that the URF could be represented by two triangular shaped responses. The first triangular response represented the initial response of the watershed from riparian areas. The second triangular response represented the watersheds delayed response from non-riparian areas as they became saturated. As shown in Figure 2.1, these responses have the same initial starting time but different time base durations. When the ordinates of these two triangular responses are added together, they form the unit response function for a given watershed and storm as depicted in Figure 2.2.

The symbol nomenclature used in Figures 2.1 and 2.2 is as follows:

DT = time interval used for abstracting rainfall and streamflow discharge records in hours,

I = precipitation excess intensity in inches per hour,

I = 1.0/DT since the volume of input is one basin-inch,

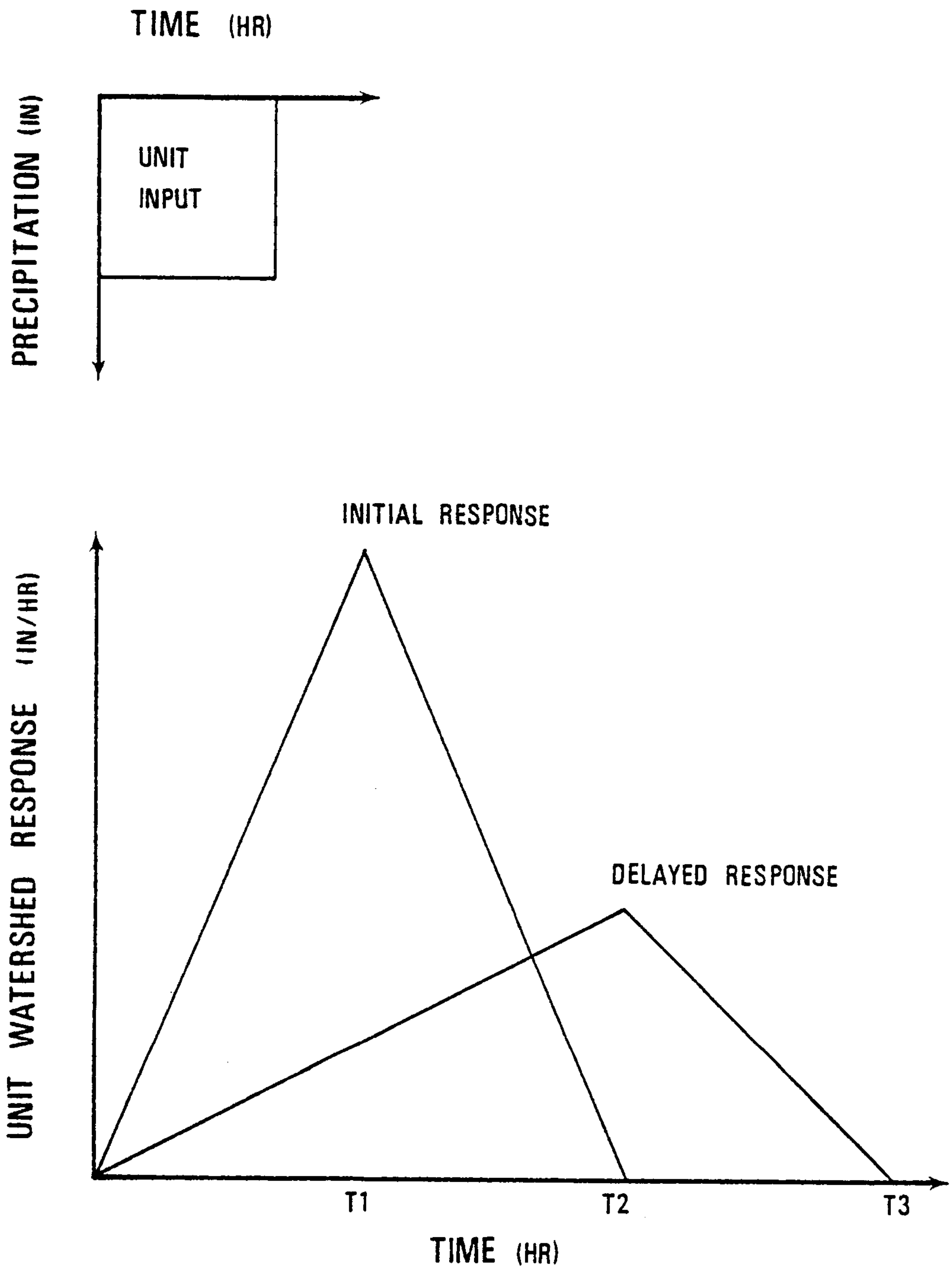

FIGURE 2.1

PARTIAL AREA RUNOFF CONCEPT REPRESENTED BY AN INITIAL AND DELAYED RESPONSE [46]

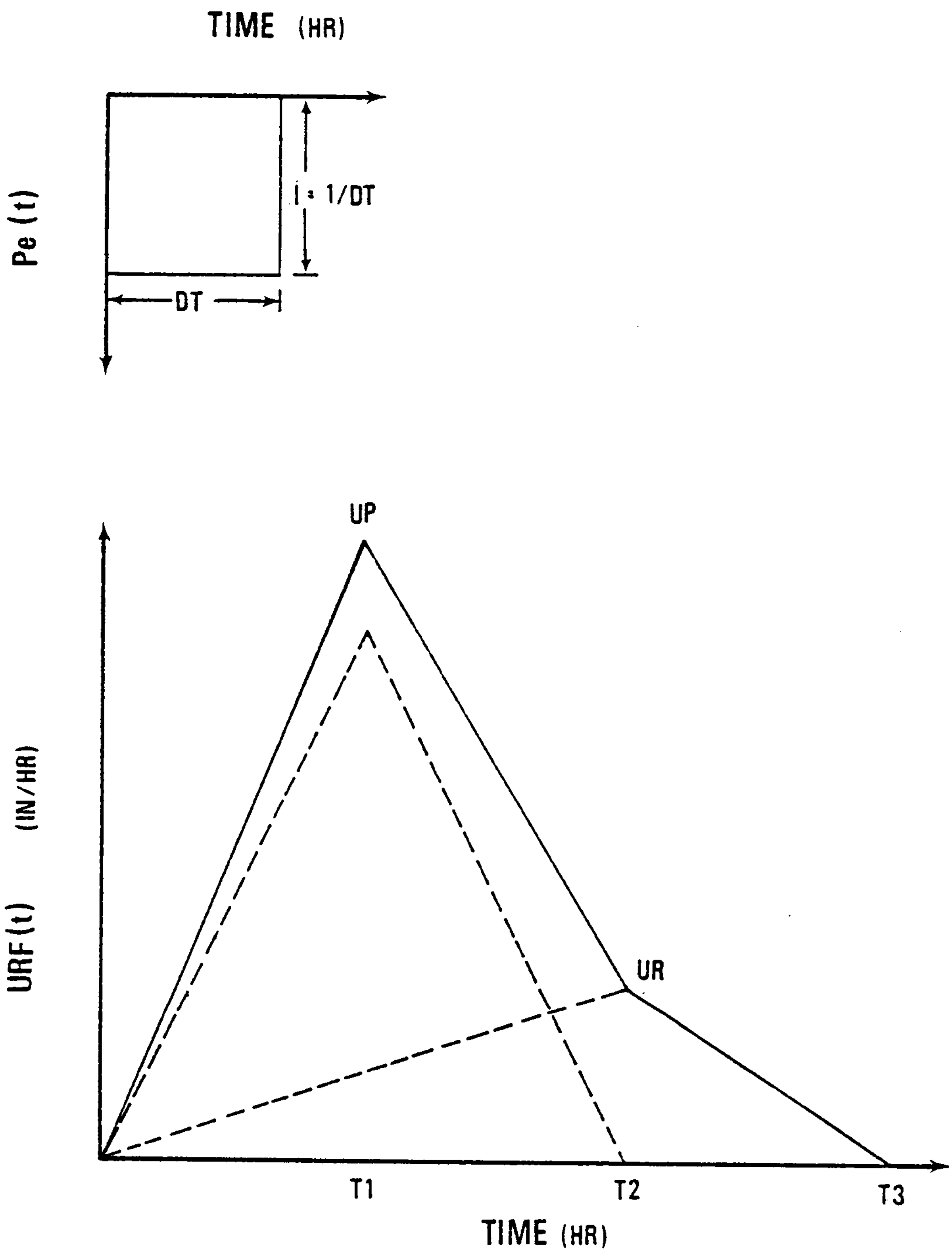

FIGURE 2.2

DOUBLE TRIANGLE MODEL FOR UNIT
RESPONSE FUNCTION [46]

Pe(t) = precipitation excess as a function of time, t, in inches per hour,

T1 = time to peak of initial response in hours,

T2 = time base of initial response and time to peak of delayed response in hours,

T3 = time to end of delayed response in hours,

UP = peak ordinate of the URF at T1 in inches per hour,

UR = peak ordinate of the delayed response at T2 in inches per hour, and

URF(t) = unit-response function ordinates as a function of time, t, in inches per hour.

To account for the nonlinearity between storms, the URF parameters are allowed to vary from storm to storm. Green [51], using a pattern search technique, developed a procedure for optimizing the URF parameters from observed storm data. Ardis [46] and later Betson [52] used this technique to study the variability of URF parameters on a total of twenty four rural and urban watersheds located mostly in the Tennessee Valley and regionalized the parameters using regression techniques.

Troxler [53] developed an alternative regionalization model using essentially the same data base as that used by Ardis [46] and Betson [52]. As a result of this investigation, he was able to relate the URF parameters to lag time, where lag time was defined as the time between occurrence of 50 percent of rainfall excess and 50 percent of runoff volume [12]. This work led Troxler [53] and Overton and Troxler [54] to relate lag time to the rainfall excess intensity using watershed lag modulus. Lag modulus is a representation of watershed geometry and roughness characteristics and can be derived from kinematic wave theory for sheet surface runoff. Lag moduli were optimized for each of the twenty-six watersheds in their study from a data base consisting of three-hundred-fifty storms. In addition, they regionalized the lag modulus for the Tennessee Valley as a function of watershed characteristics. This allowed the URF to be simulated for ungauged basins within the Tennessee Valley.

Kinematic Wave Theory

Lighthill and Whitham [55] were the first to report a study of kinematic wave theory of surface flow with their classical paper on flood movements in river channels. Since then, this theory has been extensively used to bring a more deterministic approach to both channel flow simulation and surface runoff simulation. Kinematic wave properties are governed by the equations of continuity, conservation of mass and a stage-discharge relation. This phenomenon occurs when the dynamic terms in the conservation of momentum equation are negligibly small. Kinematic flow occurs whenever a balance exists between the gravity and friction forces. This corresponds to unsteady uniform flow.

The one-dimensional conservation of mass equation is

$$\frac{\partial Q}{\partial x} + \frac{\partial A}{\partial t} = q \qquad (2.1)$$

where Q is discharge, A is cross-sectional area of flow, q is lateral inflow, and x and t are space and time coordinates. This formulation states that inflow minus the outflow of a reference volume must equal the rate of change of storage.

For the case of one-dimensional flow the conservation of momentum equation can be expressed as

$$\frac{\partial V}{\partial t} + V\frac{\partial V}{\partial x} + g\frac{\partial y}{\partial x} = g\,(S_0 - S_f) - \frac{q}{A}V \qquad (2.2)$$

where V is the mean velocity of flow, g is gravitational acceleration, S_0 is bed slope, y is depth of flow, and S_f is the friction slope, which represents the loss of momentum due to drag. This equation has been derived [12] from Newton's second law of motion and states that the sum of external forces acting on a fluid element in motion is equal to the time rate of change of linear momentum. Under this formulation, kinematic flow exists when the partial derivative terms in the equation and the lateral inflow term are negligibly small in comparison with the friction and bed slope. This reduces the momentum equation to

$$S_0 = S_f \qquad (2.3)$$

The drag force component opposing flow is essentially balanced by the weight component in the direction of flow. Hence, the fluid is not appreciably accelerating. Discharge under these conditions would be related to flow depth in the form

$$Q = a\,y^m \qquad (2.4)$$

where a and m are coefficients which characterize the state of flow.

Henderson [56] was one of the first to describe the conditions under which flow could be classified as kinematic in his paper on celerity of subsidizing flood waves. Woolhiser and Liggett [57] also examined the necessary hydraulic conditions required for the kinematic flow assumptions to be valid and concluded that much of the research and modeling previously performed in the area of overland flow had been carried out under essentially kinematic conditions.

Henderson and Wooding [58], first applied the kinematic model to flow over a uniform sloping plane. They solved the basic equations, 2.1 and 2.2, using the method of characteristics under the conditions of a steady lateral inflow of long duration resulting in a relation for discharge in the form

$$Q = a(qt)^m \tag{2.5}$$

Wooding [59, 60, 61], in a series of three papers, extended the application of kinematic wave theory to overland and channel flow components of catchment runoff from a hypothetical V-shaped watershed consisting of two rectangular planes and a straight channel. His study of the response on this elementary watershed system represents one of the first attempts to simulate catchment behavior using the kinematic wave model.

Studying the rising hydrograph of overland flow on a single plane, Woolhiser and Liggett [57] compared results obtained from the kinematic wave model and the shallow-water equations, equations 2.1 and 2.2, when the dynamic terms are not neglected. Their study disclosed that the degree of departure of the kinematic wave model from the shallow-water equations could be related by a dimensionless kinematic flow number,

$$k = \frac{S_0 L}{H_0 F_0^2} \tag{2.6}$$

where L is the length of the plane, H_0 is the flow depth and F_0 is the Froude number at equilibrium at the end of the plane, respectively. High values of k (greater than ten) indicated that gravity and friction dominated flow and consequently the kinematic hydrograph was a good approximation to that derived by the shallow water equations.

Recently, considerable development has been reported for an increasing number of complex geometric watersheds, most of which have been based upon uniform planes. Besides Wooding [59, 60, 61], Overton [62, 63] and Overton and Brakensiek [64] have developed models for various V-shaped watersheds. Woolhiser [65], Overton [62] and Singh [66] have extended kinematic wave theory to converging sections of a cone surface. Singh [64] reported a model which combines a V-shaped watershed and the converging section of a cone. Brakensiek [67], Kibler and Woolhiser [68], Overton [69] and Singh [66] have extended kinematic modeling to a cascade of planes contributing flow to a channel. These approaches have been summarized by Overton and Meadows [12].

Overton's [69] work, using cascading planes to simulate hillslope runoff had several interesting and significant results. In analyzing some 214 equilibrium hydrographs on airport runways up to 500 feet long with both concrete and simulated turf surfaces, he demonstrated that the flows were kinematic and that one dimensionless hydrograph would accurately represent all the hydrographs. This was accomplished by normalizing the hydrograph with its associated lag time. It was also demonstrated that lag time for each rising hydrograph was inversely related to the generating rainfall intensity. From lag time and the dimensionless hydrograph, he developed a variable response model, VRM, as an alternative to the tedious and expensive numerical solutions of the shallow water and kinematic wave equations. In the VRM, unsteady rainfall on uniform planes is convoluted with a response function. Hillslopes are transformed theoretically into a uniform plane, and hydrographs developed on the upper parts of the planes are transmitted to the lower end of the plane by a unique storage routing procedure.

The accuracy and flexibility of the VRM has been demonstrated on many actual and theoretical complex rainstorms, and on nonuniform planes and hillslopes. It produces results nearly as accurate as solutions obtained from the kinematic wave theory model [12].

Overton and Meadows [12] and Overton [63] have shown that the solution for the rising hydrograph associated with long steady uniform rainfall excess on a uniform plane is of the form

$$Q = (t/t_e)^m \tag{2.7}$$

where t is the time from beginning of rainfall, t_e is the time to equilibrium and m is a function of the state of flow. Time to equilibrium was also shown to be a function of the physical characteristics of the catchment and rainfall excess intensity, i_e. It was expressed as

$$t_e = f(m) * \mu/i_e^n \tag{2.8}$$

where μ is lag modulus and f(m) and n are constants which are functions of the state of flow [12, 53, 70]. Lag modulus is a single physical parameter that lumps geometry and roughness. It was first introduced by Overton [24] and is discussed extensively by Overton and Meadows [12] in relation to stormwater modeling. It is a real positive number that expresses surface runoff response as a function of the physics of the flow system for a unit rainfall excess input. As long as the system's physics are time-invariant, the lag or surface response is only a function of the input rate and a different unit hydrograph would result for each rain excess intensity. Table 2.1 lists lag modulus as derived from kinematic wave theory for two common surfaces for turbulent flow [12].

TABLE 2.1

LAG MODULI

Surface	Lag Modulus
Plane	$0.928(nL/\sqrt{S_0})^{0.6}$
Converging	$0.928(1-r)^{0.4}\ (nL/\sqrt{S_0})^{0.6}$

The nomenclature used in Table 2.1 is as follows:

n = Manning roughness factor, and

r = convergence parameter for converging surfaces.

Since the shape of a dimensionless rising overland flow hydrograph is highly sensitive to small changes in the time to equilibrium [63], time to equilibrium can be a difficult parameter to measure. Using kinematic wave theory, Overton [71] avoided this problem by showing that time to equilibrium, t_e, could be related to lag time, TL, by a factor, f(m), that is a function of the flow state

$$t_e = f(m) * TL \qquad (2.9)$$

Comparison of equations 2.8 and 2.9 shows lag time to be

$$TL = \mu/i_e^n \qquad (2.10)$$

where n is equal to (m-1)/m, and i_e is rainfall excess intensity. Overton [62] and Overton and Meadows [12] have reported values of m to be 3 for laminar kinematic flow and 5/3 and 3/2 for Manning's and Chezy's turbulent kinematic flow, respectively.

Using the turbulent Manning kinematic wave model, Overton [62] derived lag moduli for several hypothetical catchment geometries for conditions of pure sheet surface runoff where the lag modulus was a function of the geometry and associated Manning roughness coefficient.

Troxler [53] and Overton and Troxler [54] using the above models evaluated lag moduli for a number of small urban and rural watersheds in the Tennessee Valley utilizing storm rainfall and runoff data. The rainfall excess intensity was weighted to allow the larger rain bursts to contribute a greater percentage to the uniform weighted rainfall excess. This weighted rainfall excess, REI, is expressed in the following form

$$REI = \sum_{j=1}^{N} {i_{e_j}}^2 / \sum_{j=1}^{N} i_{e_j} \tag{2.11}$$

where i_{e_j} is the rainfall excess rate at the jth time increment for a storm duration of N time increments. The lag modulus model was then regionalized for the Tennessee Valley using the same basin characteristics that Betson [52] reported. Hence, once lag modulus was simulated for watersheds, storm lag times could be simulated using TVA's double triangle model [52] by convolution of the associated unit response function with the rainfall excess time distribution.

Other authors, notably Laurenson [72] and Askew [73] have developed and reported relationships for variable lag times. These authors, using data from Australian watersheds, present an expression for lag time that is similar to equation 2.10 of the form

$$TL = k'(q')^{-n'} \tag{2.12}$$

where TL is the watershed lag time, k' is a watershed constant, q' is the mean discharge and n' is an exponent that varies from 0.193 to 0.328. Unfortunately equations 2.10 and 2.12 are not directly analogous because one is based on mean channel discharge while the other uses rainfall excess intensity.

Erosion Simulation

Erosion is the connecting link between sediment sources and sediment yield. It involves the processes by which sedimentary materials are removed from a location (detachment), transported through other locations and subsequently deposited [74]. This is a selective process in which the fine-grained sediments such as clays, organic matter and amorphous materials, are transmitted farthest. Often, this fine fraction of eroded particles is involved in the sorption and transport of certain chemicals.

Erosion includes inception of particle motion, transport by traction, saltation, or suspension and deposition by single-particle settling or floculation. It is dependent upon aspects of fluid mechanics; notably, lift and drag generation, mass and momentum transport, turbulence generation and boundary and wake development. With all of these considerations it is quite understandable why the field of erosion is still largely empirical. Current technology efforts in this area are largely approximate because of the uncertainty in the knowledge of sedimentary transport principles involved. Areas in which principles and theoretical development are best understood and advanced are design of settling basins and studying fine material motion. Areas of least advancement are predicting channel capacity and sediment load.

The technology or erosion response has had three distinct avenues of approach: the unit sediment graph, the universal soil loss equation and erosion mechanics.

Unit Sediment Graph

The unit sediment graph model was first proposed by Johnson [75] in 1943 and extends the unit hydrograph theory to sediment graph analysis, producing a unit sediment graph that is analogous to a unit hydrograph. This method is applicable to small uniform watersheds where the main contributions to suspended sediment, transported in the drainage channels as the result of runoff, are derived from upland erosion, that is, from washload and not from bedload material [76, 77]. Unit sediment graph theory in addition to having the same basic assumptions and constraints of unit hydrograph theory, has the additional requirement that the loci of the hydrograph and the sediment graph must closely parallel each other [78, 79]. This method has not been widely explored and has been used mainly to estimate washload on a few gauged basins [76, 78, 79].

Universal Soil Loss Equation (USLE)

The development of USLE began with Zingg [80] first relating soil loss rates on specific agricultural sites and fields to length and percentage of slope. Shortly thereafter, Smith [81] published a similar equation that included crop and conservation practice factors and the concept of a specific soil loss limit. A regionalization of the above two equations occurred in 1946 and became known as the Musgrave Equation [82]. This equation was widely used to estimate gross soil erosion until Wischmeier and Smith [83, 84] developed and published the USLE in 1965. The USLE has the following form [85, 86]

$$A = R\ K\ L\ S\ C\ P \tag{2.13}$$

where

A = the computed soil loss per unit area on an annual basis,

R = the rainfall runoff factor, an index of the erosive force of rainfall and runoff,

K = soil erodibility factor for a specific soil on a standardized plot,

L = slope length factor to adjust actual conditions to standardized plot (72.6 feet long),

S = slope-gradient factor to adjust actual conditions to the standardized plot with a 9 percent slope,

C = cropping-management factor to adjust actual conditions to the standardized plot with cultivated continuous fallow conditions, and

P = the erosion-control practice factor, the ratio of soil loss with contouring, strip cropping, or terracing to that with straight-row farming, up-and-down slope.

The USLE model was designed to simulate long term average soil losses from sheet and rill erosion under specific conditions. It is empirical in nature and has been developed from a massive amount of runoff and soil loss data from small areas such as farm fields, rainulator plots and construction sites [85]. It cannot simulate deposition or sediment production from gullies, streambanks, and streambed erosion. It was intended to be used as a management tool to guide methodical decision making in conservation planning on a site specific basis. The underlying objective in developing the USLE was to simulate the relative erosion potential effect of producing one agricultural crop on a specific field as compared to another crop [85]. Hence, the USLE is a relative estimate of increase or decrease of erosion of one condition over another and not a prediction of absolute value.

Following the establishment of the USLE, several variations of the equation have been presented in the literature for adjusting the equations to land uses other than agricultural and to account for sediment that may have been trapped along the path from the source of the erosion to the point of measurement. Some of the extensions have taken the form of regionalization of equation factors by regression curves such as the Yound and Mutchler [87] slope factor. Others, such as Fogel, Herkman and Duchstein [88], attempted to redefine the equation factors using stochastic methods to make the USLE storm or time specific. And still others have attempted to define the USLE factors deterministically [89, 90, 91]. In spite of these developments, the USLE remains an empirical model that is highly dubious and open to considerable discussion except when used to estimate the long term average sediment generated on small areas such as farm fields or construction sites. Since the USLE was developed to simulate long term averages, it cannot be used for single storm events.

Erosion Mechanics

The importance of fundamental principles of the erosion process has been recognized since the middle 1930's by Cook [92]. Ellison [93] in 1947 presented the first extensive analysis of many of the erosion subprocesses. He pointed out that rainfall and runoff both have a detaching and a transporting capacity, and that these should be studied separately. His work has been an important cornerstone for erosion modeling in the last decade and one that has guided others [94, 95, 96, 97, 98, 99] to explore and research the various phenomena of the soil erosion process.

Modeling erosion mechanics is more complicated than surface runoff modeling since sediment transport and flow are so interrelated. It becomes difficult, if not impossible, to model sediment transport without modeling flow. Hence, the three differential equations that form the governing mathematical model of the movement of suspended sediment are the conservation of flow mass, equation 2.1, the conservation of flow momentum, equation 2.2, and the following conservation of sediment mass equation [100] for one-dimensional, infinitely wide, free surface flow

$$\frac{\partial(h\delta)}{\partial t} + (1-\lambda)\frac{\partial y}{\partial t} + \frac{\partial(hU_p\delta)}{\partial x} = \frac{\partial}{\partial x}\left(hE_p\frac{\partial\delta}{\partial x}\right) \qquad (2.14)$$

where h is depth of flow, δ is sediment concentration, t is time, λ is porosity of deposited sediment, U_p is average velocity of sediment, x is the distance in direction of flow and E_p is the particle mass transfer coefficient (See Figure A.1, Appendix A).

For conditions of negligible dispersion and quasi-steady state Foster and Meyer [101, 102] and Foster, Meyer and Onstad [103] have presented equation 2.14 in the following form

$$\frac{\partial E_B}{\partial x} = D_F + R_{DT} \qquad (2.15)$$

where D_F is the net flow shear detachment rate, R_{DT} is the net rainfall detachment rate and

$$E_B = \gamma u\delta h \qquad (2.16)$$

where E_B is the suspended sediment weight transport rate, u is the average flow velocity, γ is sediment particle specific gravity and x and h are the same as in equation 2.14. In terms of the conservation of sediment mass equation 2.14, this is equivalent to stating [100, 103]

$$R_{DT} + D_F = \frac{\partial E_B}{\partial x} = \frac{\partial(\gamma u\delta h)}{\partial x} = -\gamma(1-\lambda)\frac{\partial h}{\partial t} \qquad (2.17)$$

In formulating equations 2.15 and 2.16, Foster and Meyer [101, 102] have assumed that dispersion, the right hand term of equation 2.14, is zero and that the sediment concentration does not change with time, i.e. quasi-steady state. These are common assumptions made in the present state of the art of erosion modeling according to Simons, Richardson and Nordin [104] to achieve mathematical tractability.

In spite of the fact that the derivation [101, 102] of equation 2.15 is made directly from physical considerations, existing knowledge of erosion micromechanics used to express rainfall and runoff detachment rates is rudimentary and empirical. Foster and Meyer [101, 102] and Meyer, Foster and Fomkens [105] have expressed this interaction between flow shear detachment rate and suspended sediment weight transport rate as

$$\frac{D_F}{D_C} + \frac{E_B}{T_C} = 1 \qquad (2.18)$$

where D_C is the ultimate detachment capacity of overland flow and T_C is the ultimate transport capacity of overland flow. This is the same as assuming that a particular flow carrying less than its capacity to transport will fill this capacity according to a first-order reaction of the form [100, 101]

$$D_F = C(T_C - E_B) \qquad (2.19)$$

where C is the reaction coefficient. Experimental evidence that demonstrated the tendency for flows to entrain sediment in this manner has been presented by Meyer and Monke [97] and Willis [106].

Foster and Meyer [102, 207] have formulated transport capacity after derivations by Yalin [108] to be

$$T_C \propto (hS_0)^{3/2} \propto Z^{3/2} \tag{2.20}$$

where S_0 is the local bed slope and Z is the bottom shear stress. Bagnold [109] and Yang [110] have formulated transport capacity as being proportional to stream power, the product of bottom shear and flow velocity in the following manner

$$T_C \propto (\gamma h S_0)\ u \tag{2.21}$$

The rainfall detachment term, shown to be proportional to the square of rainfall intensity, is based upon empirical evidence of Meyer and Wischmeier [98]. The transport capacity of rainfall generated by raindrop splash has normally been shown to be negligible [100]. However, rainfall significantly reduces the flow velocity and increases tractive force, especially over rough boundary conditions and shallow flow [111].

Sediment Yield Simulation

Sediment yield is the amount of eroded material passing a geographical point, such as the outlet of a watershed or of any of its subwatersheds. Several methods are presently being used to simulate sediment yield from upland watersheds, and each presents unique data needs. In each model there is an associated uncertainty that requires a safety factor when used in a design application.

Sediment Rating Curves

The sediment rating curve model is used to relate stream discharge and sediment concentration. This relationship, expressed mathematically, takes the form

$$S_C = A\ Q^E \tag{2.22}$$

where S_C is the sediment concentration at time t, and A and E are constants determined by optimizing equation 2.22 on observed data. This model has been widely used [112, 113, 114, 115] and has been applied by Ward [116] to strip mined watersheds.

The data for this model is not easily obtained for small upstream watersheds where discharge of water and sediment vary greatly in time and space. In addition, transferring sediment rating curves to areas with differing conditions can be accomplished only with additional data for the new conditions. Hence, attempts have been made to relate watershed and hydrologic variables such as drainage area, runoff, temperature, slope, soil and cover to the observed sediment concentration and to the A and E constants of equation 2.22 for watersheds [112, 115, 117, 118]. To accomplish this, multiple regression techniques have been used with varying degrees of success employing the following type of equations

$$Y = a + \sum_{i=1}^{n} b_i x_i \qquad (2.23)$$

$$Y = \sum_{i=0}^{n} b_i x_i^{c_i} \qquad (2.24)$$

$$Y = \prod_{i=0}^{n} b_i x_i^{c_i} \qquad (2.25)$$

where x_i is the watershed or hydrologic variable, Y_i is the sediment concentration or one of the constants, A or E, from equation 2.22, and a, b_i and c_i are optimized regression coefficients.

Once the sediment concentration graph is found, it can be convoluted with the runoff hydrograph to produce the sediment yield.

Sediment Delivery Ratio

The sediment delivery ratio model is a percentage relationship between sediment yield from a watershed and the gross (total) soil loss in the watershed for similar time periods. Sediment delivery ratios have been developed for many areas of the United States and have been found to be related to drainage area [86, 119, 120]. Sediment yield is obtained from sediment delivery ratios by multiplying it by the derived quantities of watershed erosion. These sediment yield equations normally take a form similar to the following equation of the USLE by Wischmeier [85]

$$Y = E\ (DR)/w \qquad (2.26)$$

where Y is the sediment yield per unit area, E is the gross (total) soil loss, DR is the sediment delivery ratio and w is the area of the watershed above the point for which the sediment yield is being computed. Thus in operation, this method requires the measurement or determination of the total erosion that took place in the watershed for both establishment of the DR's and the gross soil loss of the event at hand.

Erosion Mechanics

In recent research [99, 100, 103], soil detachment, transport and deposition mechanics are being incorporated into hydrologic models to simulate sediment yield. This method allows the determination of sediment yield by integrating equations such as 2.14, 2.15 and 2.17 for specific conditions that exist at an erosion site. Offering great potential for refining sediment yield simulation procedures, this method places soil loss on a deterministic basis capable of analyzing individual storm events.

CHAPTER III

INVESTIGATIVE DESIGN

Model Structure

The principal objective of this research was the development of a mathematical model for simulating the stormwater and suspended sediment responses of steep contour strip (surface) mining on small mountainous watersheds and specific mining sites within those watersheds. In particular, it was desired to develop a model that can be used as a tool in simulating the stormwater related responses occurring in the New River Basin, Tennessee. The structures of these models are outlined below.

Stormwater Simulation Model

The stormwater simulation model is termed TENN-I and is a watershed stormwater hydrograph simulator. This model was originally developed to study the stormwater effects of urban watersheds [53, 54]. It has been extended herein to include mountainous regions that are undergoing contour strip mining.

This storm hydrograph simulator incorporates the TVA Double Triangle model [46, 52]. A regionalization scheme developed by Overton and Troxler [54] permits simulation of the TVA Double Triangle model parameters. TENN-I accepts a real time or design rainfall hyetograph, simulates the associated rainfall excess hyetograph using the SCS-Curve Number model, simulates the URF from selected watershed characteristics and rainfall excess, and convolutes the URF with the rainfall excess hyetograph. A flow chart, depicting the basic logic of TENN-I is shown in Figure 3.1.

The model used for distributing rainfall excess over the duration of the storm is the Soil Conservation, SCS, curve number method [38]. This method relates accumulated values of rainfall, direct runoff volume and infiltration plus initial abstraction. These quantities are illustrated in Figure 3.2. The curve number method assumes that

$$\frac{F}{S} = \frac{SRO}{P_e} \tag{3.1}$$

where F is the infiltration occurring after runoff begins in inches, S is the potential abstraction in inches, SRO is the actual direct runoff volume in inches, and P_e is the potential runoff or effective storm runoff in inches, i.e. the storm rainfall minus the initial abstraction, IA. Since infiltration can be expressed as

$$F = P_e - SRO \tag{3.2}$$

equation 3.1 can be expressed as

$$SRO = \frac{{P_e}^2}{P_e + S} \tag{3.3}$$

The initial abstraction has been estimated by SCS from an empirical relation based on data from small watersheds to be

$$IA = 0.2\ S \tag{3.4}$$

Thus

$$P_e = P - IA = P - 0.2S \tag{3.5}$$

where P is the total storm rainfall in inches. Substituting

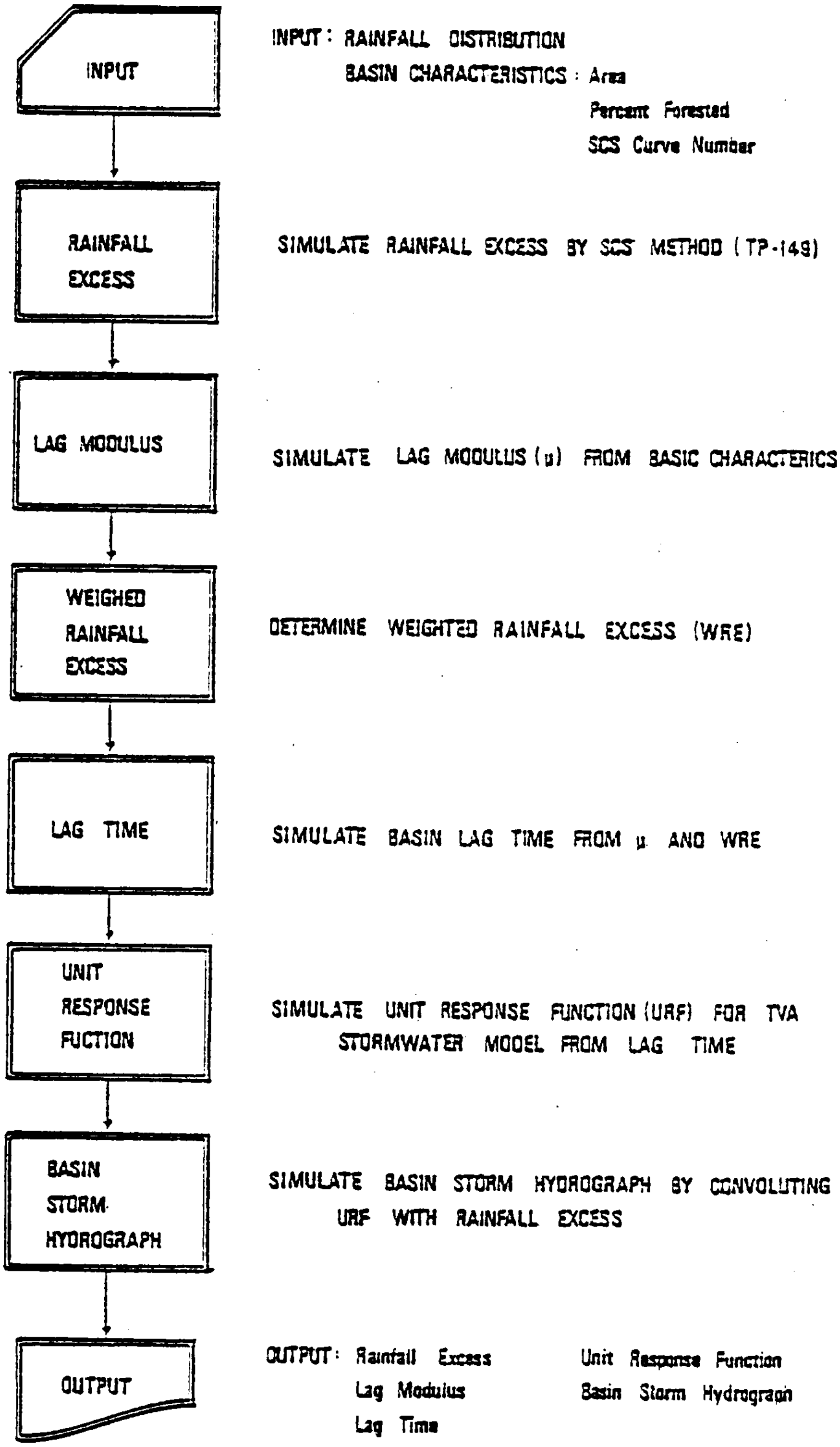

FIGURE 3.1

STORM HYDROGRAPH SIMULATOR (TENN-I)

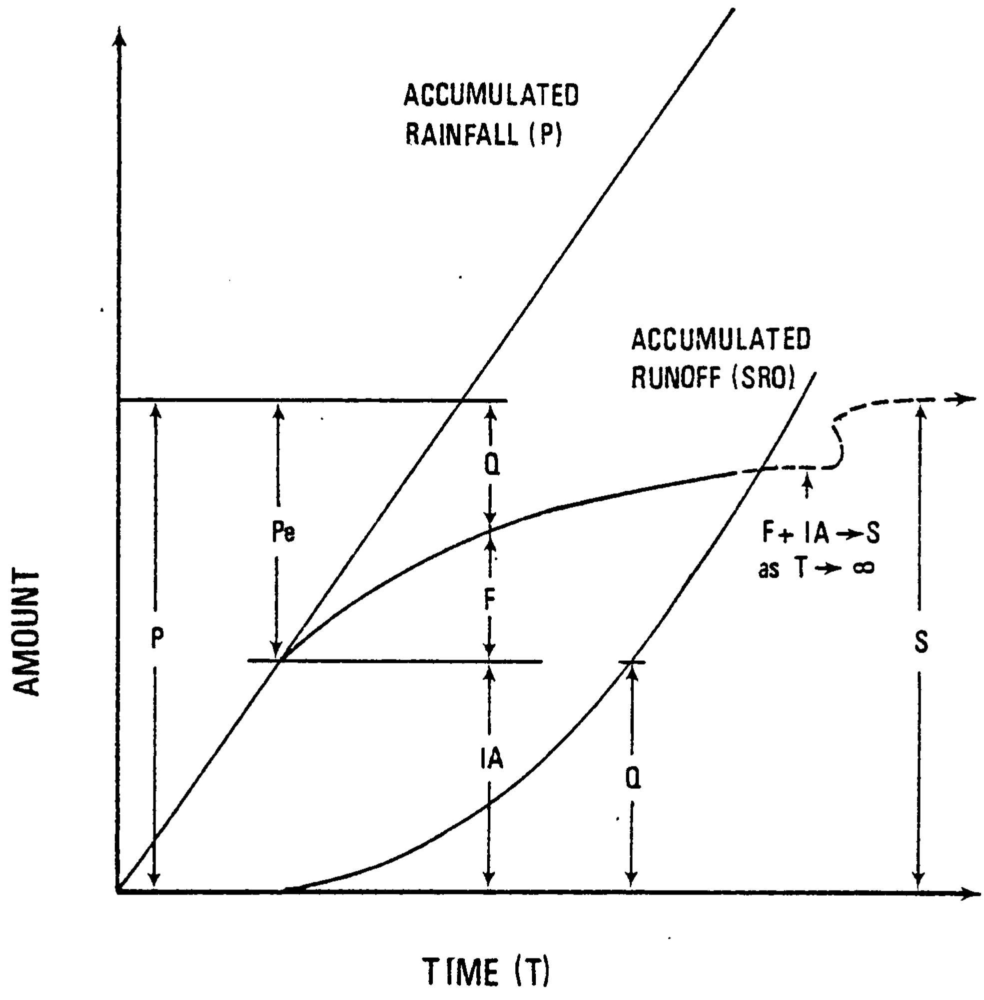

FIGURE 3.2

SCHEMATIC CURVES SHOWING RELATION EXPRESSED BY EQUATION 3.6, RELATING ACCUMULATED RUNOFF, RAINFALL, AND INFILTRATION PLUS INITIAL ABSTRACTION equation 3.5 into equation 3.3 gives the following relation for accumulated runoff

$$SRO = \frac{(P - 0.2\ S)^2}{P + 0.85} \quad . \tag{3.6}$$

Potential abstraction, S, is related to soil and cover condition of a watershed. The runoff curve number, which is also related to soil and cover conditions, is related to potential abstraction, S, by the following

$$CN = \frac{1000}{S + 10} \tag{3.7}$$

from which

$$S = \frac{1000}{CN} - 10 \ . \tag{3.8}$$

For a time distribution this method reduces to

$$SRO_i = \frac{(P_i - 0.2\ S)^2}{(P_i + 0.8\ S)} \tag{3.9}$$

where SRO_i is the total storm runoff to time i and P_i is the accumulated rainfall to time i. The distribution of rainfall excess over time is then determined by the following equation

$$P_{e_i} = SRO_i - SRO_{i-1} \tag{3.10}$$

where P_{e_i} is the rainfall excess from time i-1 to i.

Lag modulus simulation is accomplished by using a regionalization model of the form

$$\mu = C_1\ A + C_2\ PF + C_3 \tag{3.11}$$

where μ is the basin lag modulus in hours, A is the watershed area in miles, PF is the percent of area that is forested, and C_1, C_2, and C_3 are constants resulting from using principal components regression to optimize the model. Values of C_1, C_2, and C_3 can be determined by optimizing equation 3.11 for watershed storm events.

Lag time is simulated by using the Manning kinematic approximation

$$TL = \mu / i_e^{0.4} \tag{3.12}$$

The exponent in the lag time model was set equal to 0.4 in order to standardize watershed lag moduli values with sheet surface runoff. The uniform steady rainfall excess, i_e, is expressed as the weighted rainfall excess of the real time storm. The weighted rainfall excess, REI, was calculated using equation 2.11. This allows large rainfall excess a greater influence in the establishment of a simulated uniform steady rainfall excess.

The watershed unit hydrograph is simulated using the Double Triangle model URF discussed earlier. As can be seen from Figure 3.3, the URF's lag time can be calculated from the following equation

$$TL = T50 - \frac{DT}{2} \tag{3.13}$$

where T50 is the time at which the unit response function is divided into two equal volumes of one half inch. When linearity within a storm is assumed, but not from storm to storm, the watershed lag time is equivalent to the URF lag time.

As mentioned in Chapter II, lag time can be related to the URF's defining parameters [53, 54]. The URF's peak flow can be inversely related to lag time, while the time scale parameters can be related directly to lag time. Thus the URF's defining parameters may be

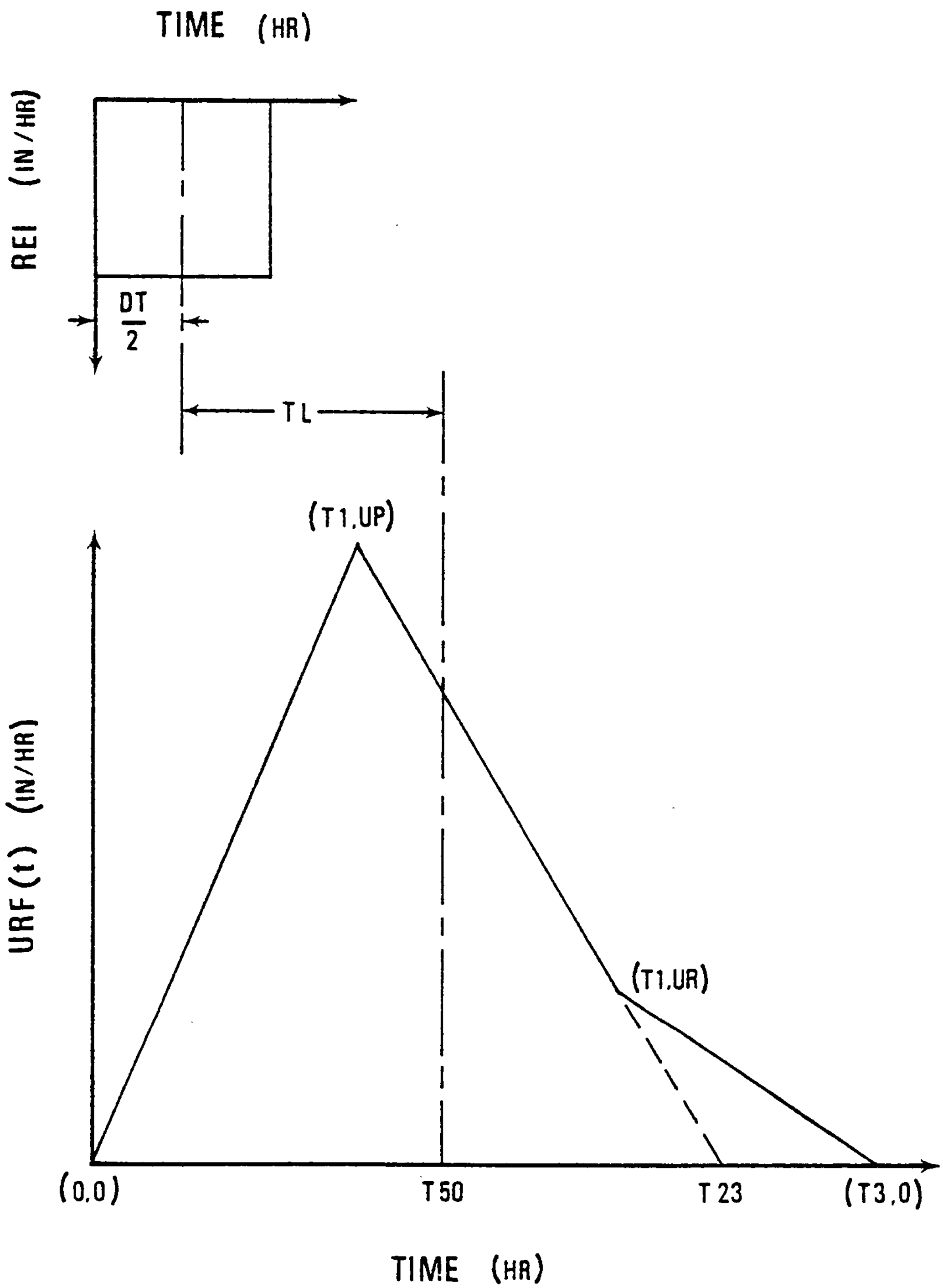

FIGURE 3.3

UNIT RESPONSE FUNCTION

expressed as

$$UP = KUP/T_L \tag{3.14}$$

$$UR = KUR/T_L \tag{3.15}$$

$$T1 = KT1 * T_L \tag{3.16}$$

$$T2 = KT2 * T_L \tag{3.17}$$

$$T23 = KT23 * T_L \tag{3.18}$$

$$T3 = KT3 * T_L \tag{3.19}$$

The physical significance of T23 can be seen from Figure 3.3. Knowing T23 allows the determination of volume of the triangle 0-T1-T23 and thus determines the triangle T23-T2-T3 since the total volume of the URF must equal one inch. KUP, KT1, KT2 and KT23 are constants for the watershed for a continuous land use and can be obtained by linear regression optimization. Once the URF is established, it is convoluted with the actual rainfall excess determined by the SCS method to produce the basin hydrograph.

Erosion Model

The Universal Soil Loss Equation (USLE) was not developed for real time storm events. Because of this, a soil loss model was developed coupling erosion mechanics and the kinematic approximation to surface runoff. This model is referred to as ERODE-I.

ERODE-I can simulate the time distribution of soil mass transport rates at the end of a mining site per unit width for a real storm or design storm rainfall time distribution. The resulting sediment transport rate curve is a function of the following:

1. Simulated storm runoff hydrograph.

2. Slope-length distribution of the site, considering it to be approximated as a cascade of planes, see Figure 3.4.

3. Specific gravity of transported material.

4. A rainfall detachment coefficient which is a function of the system resistance to raindrop detachment and kinetic energy of rainfall.

5. The coefficients which are properties of the system itself, i.e. associated with shear detachment and transport.

6. The concentration of the transported load.

A flow chart, depicting the basic logic of ERODE-I is shown in Figure 3.5.

The SCS-Curve Number (CN) model [35] was utilized for distributing excess rainfall in time over the duration of the storm. Although this model was not developed specifically for this purpose by the SCS, it has been shown to function well in this role [52, 53].

The Variable Response Model (VRM) [12, 69] was used to generate overland flow hydrographs. This model is capable of generating hydrographs from unsteady nonuniform rainfall on hillslopes that have been depicted as a cascade of planes. This is accomplished by first transforming a cascade of planes into an equivalent uniform plane. This plane is then partitioned into sections of uniform rain excess intensity. Hydrographs are simulated for each section of the plane by convoluting the time series of rainfall with a variable response function developed for planes undergoing overland flow. These hydrographs are transmitted to the end of the uniform plane by a storage routing function. The VRM

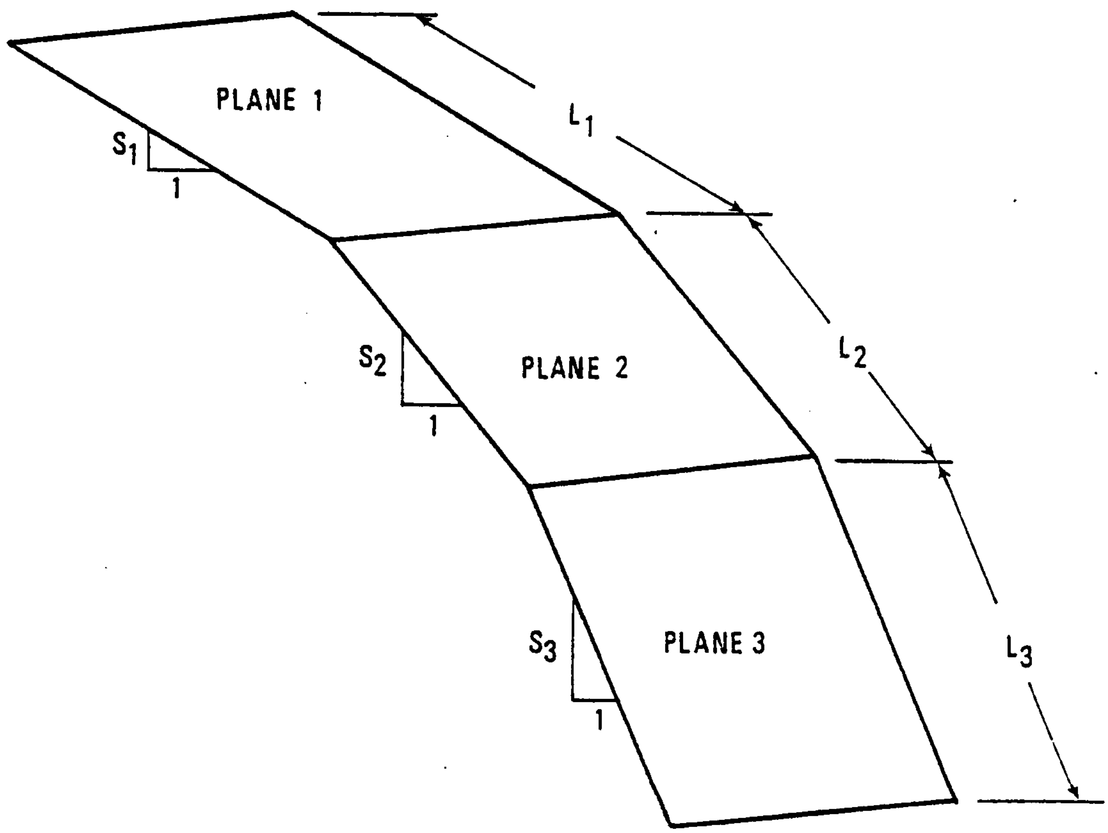

FIGURE 3.4

CASCADE OF PLANES

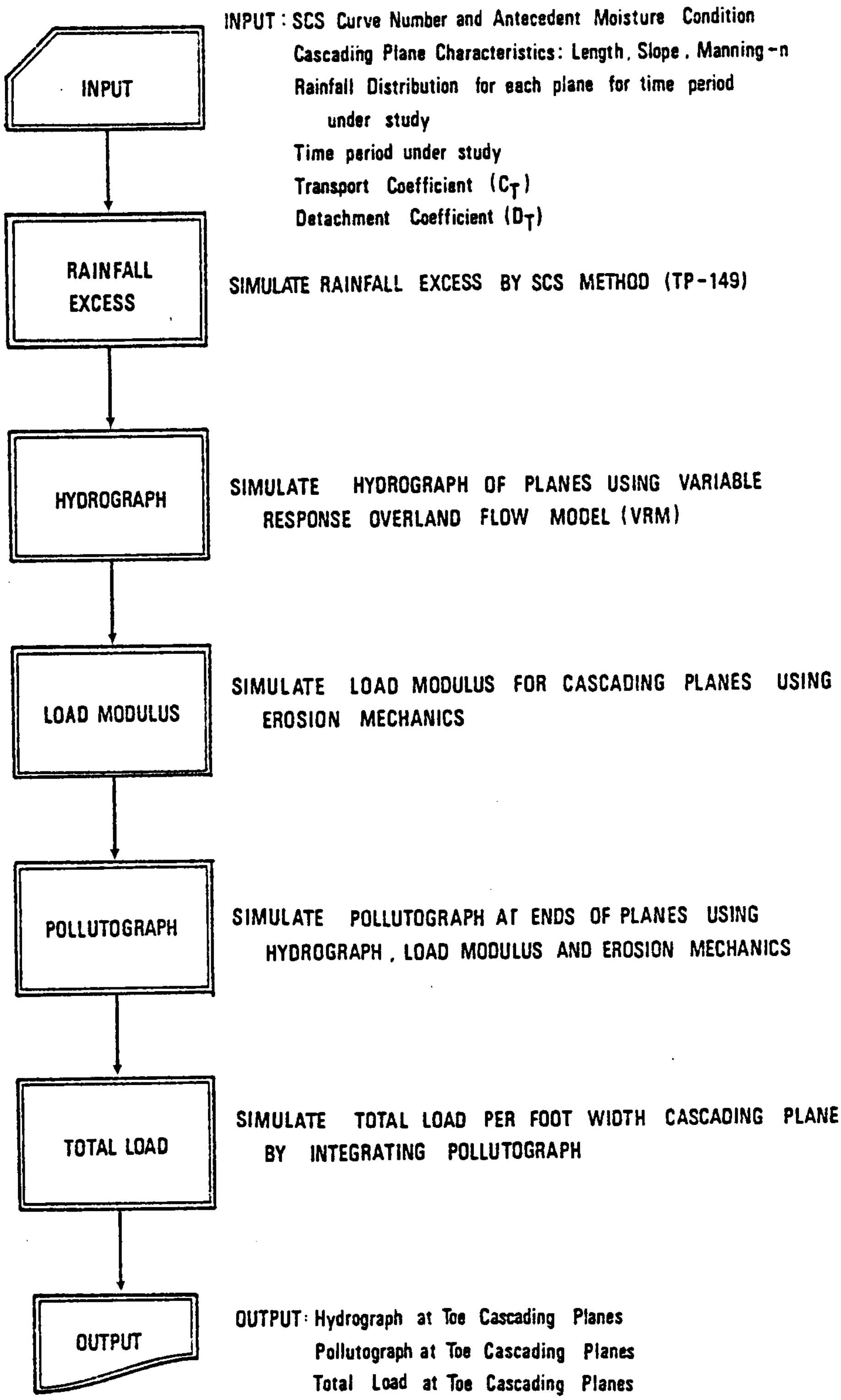

FIGURE 3.5

SOIL EROSION SIMULATOR (ERODE-I)

was selected for three reasons. First, it can simulate the physical shape of a hillslope or hillslope mining site using a cascade of planes. Second, the model is nonlinear since its response varies from storm to storm since the defining parameters change. And third, the model has been widely tested, verified on a wide range of surface runoff conditions and has been shown to be an excellent simulator of kinematic overland flow.

The erosion model developments are based on the conservation of sediment mass, equation 2.17. This conservation of sediment mass equation appears in its usual form for infinitely wide one dimensional flow planes as follows

$$\frac{\partial(h\delta)}{\partial t} + (1-\lambda)\,\frac{\partial y}{\partial t} + \frac{\partial(hU_p\delta)}{\partial x} = \frac{\partial}{\partial x}\,(hE_p\,\frac{\partial\delta}{\partial x}) \qquad (3.20)$$

This equation differs from the conservation of mass equation for a dissolved substance in that the second term on the left accounts for deposition or erosion from the bed. Also for suspended sediment, it cannot necessarily be assumed that the transport velocity, U_p, of the suspended material is the same as the flow velocity, U. As is customary and often the case for storm flows where flow is unsteady and turbulent, this assumption has been made here. The term on the right hand side of equation 3.20 accounts for dispersion of the material while it is suspended in the flow. In comparison with the effects of other processes embodied in 3.20, dispersion is normally small. Hence, dispersion will not be considered here. Under these assumptions the suspended sediment conservation of mass equation is

$$\frac{\partial(h\delta)}{\partial t} + (1-\lambda)\,\frac{\partial y}{\partial t} + \frac{\partial(hU\delta)}{\partial x} = 0 \qquad (3.21)$$

The quantities appearing in this equation are illustrated in Figure 3.6 and listed below

h = depth of flow,

δ = sediment concentration,

t = time,

λ = porosity of deposited sediment,

y = local bed elevation,

x = distance positive in direction of flow, and

μ = flow velocity, which is equal to average sediment velocity.

In this study, the conservation of sediment mass has been expressed following the basic work of Foster and Meyer [101] and has been extended from the quasi-steady state to unsteady flow conditions. Comparison of equations 2.15, 2.16, 2.17 and 3.2 indicate that weight transport rate of sediment, E_B, can be expressed as

$$D_F + R_{DT} = \frac{\partial E_B}{\partial x} - \gamma_s \frac{\partial (h\delta)}{\partial t} \tag{3.22}$$

where D_F is the flow detachment rate, R_{DT} is the rainfall detachment rate, and γ_s is the sediment particle specific gravity.

Shear detachment rate, D_F, was related to transport capacity, T_C, and E_B by the following equation

$$D_F = C(T_C - E_B) \tag{3.23}$$

where C is a reaction rate coefficient or diffusion coefficient which is a property of the settling properties of the sediment. Rearranging equation 3.23 gives

$$\frac{D_F}{CT_C} + \frac{E_B}{T_C} = 1 \tag{3.24}$$

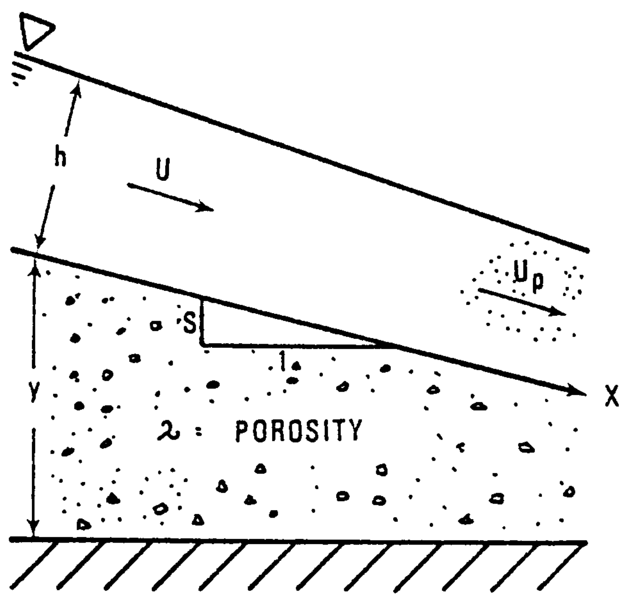

FIGURE 3.6

DEFINITION SKETCH FOR CONSERVATION OF SEDIMENT MASS

By this concept, the sediment transport rate, E_B, can never exceed the transport capacity of the flow. If E_B is ever less than T_C then additional transport material or sediment will be obtained by flow detachment, D_F. Thus the flow detachment capacity, D_C, must be a function of the unfilled transport capacity expressed as

$$D_C = C\, T_C \ . \qquad (3.25)$$

Foster and Meyer [102] have shown that Yalin's sediment transport equation [108] is a good representation of transport capacity for shallow flow. They have also simplified it for large tractive forces and shown it to be

$$T_C = C_t\, \tau^{3/2} \qquad (3.26)$$

where τ is the tractive force, and C_t is a coefficient that depends on particle size and density. An expression similar to that for T_C will be used for detachment capacity,

$$D_C = C_d\, \tau^{3/2} \qquad (3.27)$$

where C_d is a coefficient that is a function of soil's resistance to erosion by flow. Foster and Meyer [102] indicate that unpublished research available to them shows that equations 3.26 and 3.27 when used with a critical tractive force work as well on cohesive soils as on noncohesive soils.

Inserting equations 3.26 and 3.27 into 3.25 reveals that under the above assumptions and definitions that

$$C = C_d/C_t \qquad (3.28)$$

The tractive force exerted by overland flow on upland areas is distributed among many small channels (rills) at a cross section on the land profile. Instead of considering each channel individually, it is possible to consider an effective shear stress and assume it proportional to the average shear stress or tractive force developed by overland flow depth considered on a flat plane. Using the Chezy form for uniform flow equation [102],

$$y = (F/\gamma g\ S_o)^{1/3}\ q^{2/3} \tag{3.29}$$

is satisfactory for determining the average flow depth on eroding surfaces [122]. The shear stress is expressed as

$$\tau = \gamma_F\ R_h\ S_o \tag{3.30}$$

where γ_F is the density of runoff, R_h is the hydraulic radius, and S_F is the slope of the energy grade line, assumed to be equal to the slope of the land profile, S_o, because of the small depths of flow of overland runoff. With these assumptions, the effective tractive force becomes

$$\tau = C_r\ S_o^{2/3}\ q^{2/3} \tag{3.31}$$

where

$$C_r = C_{rp}\ \gamma_F\ (F/8g)^{1/3} \tag{3.32}$$

and F is the hydraulic roughness, g is the acceleration of gravity and C_{rp} is the ratio of the effective tractive force to the average tractive force as determined from average overland flow depth. Assuming C_r is constant infers that the rill pattern does not change with distance along a slope, but can change from one land profile to another as the rill pattern changes. Erosion plots that have been denuded, tilled and graded up and down slope, similar to construction work sites and strip mine spoil bank sites, often satisfy this condition. In addition, C_{rp} is for this study assumed to be unity, i.e. the tractive force from overland flow on a plane is considered to be equal to the effective tractive force.

Using these assumptions, detachment capacity, D_C, and transport capacity, T_C, can be expressed as

$$T_C = C_t\, C_r^{3/2}\, S\, q = C_T\, S\, q \tag{3.33}$$

$$D_C = C_d\, C_r^{3/2}\, S\, q = C_D\, S\, q \tag{3.34}$$

where

$$C = C_d/C_t = C_D/C_T\ . \tag{3.35}$$

Combining equation 3.22, 3.24 and 3.25 produces

$$\frac{D_F}{D_C} + \frac{\{D_F + R_{DT} + \gamma_s \frac{\partial(\delta h)}{\partial t}\}}{T_C} + \frac{f(t)}{T_C} = 1 \tag{3.36}$$

where f(t) is the constant of integration obtained when equation 3.22 is integrated. Differentiating equation 3.36

$$\frac{\partial\ D_F/D_C}{\partial x} + \frac{D_F}{T_C} + \frac{R_{DT}}{T_C} + \frac{\gamma_s}{T_C}\frac{\partial(\delta y)}{\partial x} = 0 \tag{3.37}$$

and combining 3.33, 3.34 and 3.37, results in

$$\frac{\partial}{\partial x}\left(\frac{D_F}{C_D\, S\, q}\right) + \frac{D_F}{C_T\, S\, q} + \frac{R_{DT}}{C_T\, S\, q} + \frac{\gamma}{C_T\, S\, q}\frac{\partial \delta y}{\partial t} = 0\ . \tag{3.38}$$

For a given soil, C_D and C_T can be expected to be constant over a cross section of the plane at a given distance x, then

$$\frac{\partial D_F}{\partial x} + C\, D_F = -C\, R_{DT} - C\, \gamma_s \frac{\partial(\delta h)}{\partial t} \quad . \tag{3.39}$$

Under the assumption of constant rainfall detachment, constant slope on a plane and constant rainfall excess intensity, there is a closed form solution to equation 3.39. Considering the right hand side of equation 3.39 to be F(t), there is a general solution and a particular solution. The general solution is

$$D_F = F_1(t)\, e^{-cx} \tag{3.40}$$

and the particular solution when D_F is constant is

$$D_F = -R_{DT} - \gamma_s \frac{\partial(h\delta)}{\partial t} \; . \tag{3.41}$$

This results in a complete solution

$$D_F = F_1(t)\, e^{-cx} - R_{DT} - \gamma_s \frac{\partial(hy)}{\partial t} \; . \tag{3.42}$$

By combining equations 3.23, 3.33 and 3.42 an expression results that specifies the sediment transport rate when erosion occurs on a plane surface from overland flow

$$E_B = -e^{-cx} \frac{F(t)}{C} + \frac{R_{DT}}{C} + \frac{\gamma_s}{C} \frac{\partial(h\delta)}{\partial t} + C_T\, S\, q \; . \tag{3.43}$$

The computation of a sediment transfer rate for a given geometrical runoff/erosion surface can thus be determined by solving equation 3.43 for a specific set of initial boundary conditions. The initial and boundary conditions for a cascade of planes such as that shown in Figure 3.4 (page 38) are as follows

$$\text{plane 1:} \quad E_{B_1}(0,t) = 0 \tag{3.44}$$

$$E_{B_1}(L_1,t) = E_{B_2}(0,t) \tag{3.45}$$

plane 2: $$E_{B_2}(0,t) = E_{B_1}(L_1,t) \tag{3.46}$$

$$E_{B_2}(L_2,t) = E_{B_3}(0,t) \tag{3.47}$$

plane 3: $$E_{B_3}(0,5) = E_{B_2}(L_2,t) \tag{3.48}$$

$E_{B_3}(L_3,t)$ = sediment transport rate at end of site, plane 3.

All planes in the cascade are considered dry at time equal zero. The inflow hydrograph coming from the previous plane in the cascade establishes the flow at the upstream boundary for time greater than zero. No flow enters at the upstream boundary of plane one. The sediment transport rate graph from the previous plane establishes the sediment rate at the upstream boundary. No erosion other than rainfall detachment occurs at the upstream boundary of plane one.

For a single plane, the initial sediment transport rate is

$$E_B(0,t) = -e^{-c(0)} \frac{F(t)}{C} + \frac{R_{DT}}{C} = 0 \tag{3.49}$$

and the sediment transport rate at the end of the plane at $x=L_1$ is

$$E_B(L_1,t) = (1-e^{-cx}) \frac{R_{DT}}{C} + \frac{\gamma_s}{C} \frac{\partial(h\delta)}{\partial t} + C_T\, S\, q \;. \tag{3.50}$$

Similarly, by applying the initial and boundary conditions above, the sediment transport rate at the end of any plane may be found.

To determine the sediment load at the end of a series of cascading planes, equation 3.49 can be integrated over the rain storm and runoff duration. For the case of the single plane considered above, equation 3.50 would be integrated in the following manner to obtain the total load per unit width, L,

$$L = \int_0^t E_B(L_1,t)dt = \int_0^t \{(1-e^{-cx})\ \frac{R_{DT}}{C} + \frac{\gamma_s}{C}\frac{\partial h\delta}{\partial t} + C_T\, S\, q\}\ dt \quad (3.51)$$

where t is the time lapse from beginning of the storm to runoff termination.

It has been observed from rainfall simulator experiments that after initial periods of rainfall, sediment concentrations became essentially constant [122]. Thus the sediment concentration term in equation 3.24 can be expressed as

$$\frac{\partial h\delta}{\partial t} = \delta\ \frac{\partial h}{\partial t}\ . \quad (3.52)$$

And from kinematic flow theory [12], the change in flow depth with respect to time can be shown to be equal to the rainfall excess intensity. Therefore, equation 3.51 becomes

$$L = \int_0^T (1-e^{-cx}\ \frac{R_{DT}}{C})dt + \int_0^T \frac{\gamma_s}{C}\ \delta\ i_e\ dt + \int_{t_1}^{t_2} C_T\, S\, q\ dt \quad (3.53)$$

where T is the storm duration, t_1 is the beginning of runoff, t_2 is the end of runoff, and i_e is rainfall excess intensity. Integrating equation 3.53 results in the following

$$L = (1 - e^{-cx})\ \frac{R_{DT}}{C}\ T + \frac{\gamma_s}{C}\ \delta\ R\emptyset_e + C_T\ S\ \forall_W \quad (3.54)$$

where $R\emptyset_e$ is the rainfall excess and $\forall_W$ is the volume of runoff per unit width. Multiplying by the plane width and dividing by rainfall excess and plane area, equation 3.54 becomes

$$\frac{L}{x\ R\emptyset_e} = \frac{1 - e^{-cx}}{xc}\ R_{DT}\ \frac{T}{R\emptyset_e} + C_T\ S + \frac{\gamma_s\delta}{cx}\ . \quad (3.55)$$

Under storm loads, which generate the heaviest loads, and for the case of constant δ and γ_s, the sediment concentration can be represented by a constant

$$\mu_s = \gamma_s \ \delta = \frac{L}{x \ R\emptyset_e} \tag{3.56}$$

where μ_s is the load modulus. Combining equations 3.35, 3.55 and 3.56 results in

$$\mu_s = \frac{1 - e^{-cx}}{cx - 1} R_{DT} \frac{T}{R\emptyset_e} + \frac{C_D \ S \ L}{(cx-1)} \, . \tag{3.57}$$

Once load modulus has been determined from equation 3.57, the sediment transport rate can be determined from either equation 3.50 for a single plane or 3.49 for multiple planes.

In situations of long slopes where sediment transport approaches transport capacity, equation 3.50 is closely approximated by

$$E_B = C_T \ S \ q \tag{3.58}$$

and equation 3.57 is closely approximated by

$$\mu_s = \frac{C_T \ S \ L}{cx-1} \, . \tag{3.59}$$

Sediment Yield Model

A sediment yield model was developed for small watersheds in the New River Basin as a function of the surface mining taking place there. This model, known as LOAD-I, simulates the pollutograph, i.e. the load rate curve and hydrograph associated with storm hydrographs. The linkage of the pollutograph and the hydrograph is accomplished through the use of the load modulus. This load modulus was simulated for surface mined watersheds as a function of selected watershed characteristics. Figure 3.7 presents an outline of the logic of LOAD-I.

If the concentration of suspended sediment is known, then the instantaneous load rate can be related to the basin hydrograph as follows

$$SL = \delta_L Q \tag{3.60}$$

where SL is the instantaneous load rate in units of mass per time, Q is the hydrograph in units of volume per time, and δ_L is a concentration relating mass of sediment to volume of flow. Under conditions of low flow, δ_L varies substantially. But under storm conditions there is evidence that δ_L is constant. Rainulator tests on erosion plots indicate that the concentration is essentially constant for steady rainfall excess [122]. It has been further postulated [122] that the sediment concentration would approach constant values during storm flows because the flow transport capacity would be approached. During storm flows where sediment is readily available for transport, sediment loads are known to increase to higher concentrations than during low flow. These are the concentrations and flows of interest. Using this premise, a study of five urban watersheds in Tennessee and Kentucky during storm conditions has shown that the suspended sediment load appears to be related to storm flow by a constant value [122]. Hence, the suspended sediment yield, SY, model for mined basins was selected to be

$$SY = \mu_W Q \tag{3.61}$$

where μ_W is the watershed load modulus or analogous constant concentration.

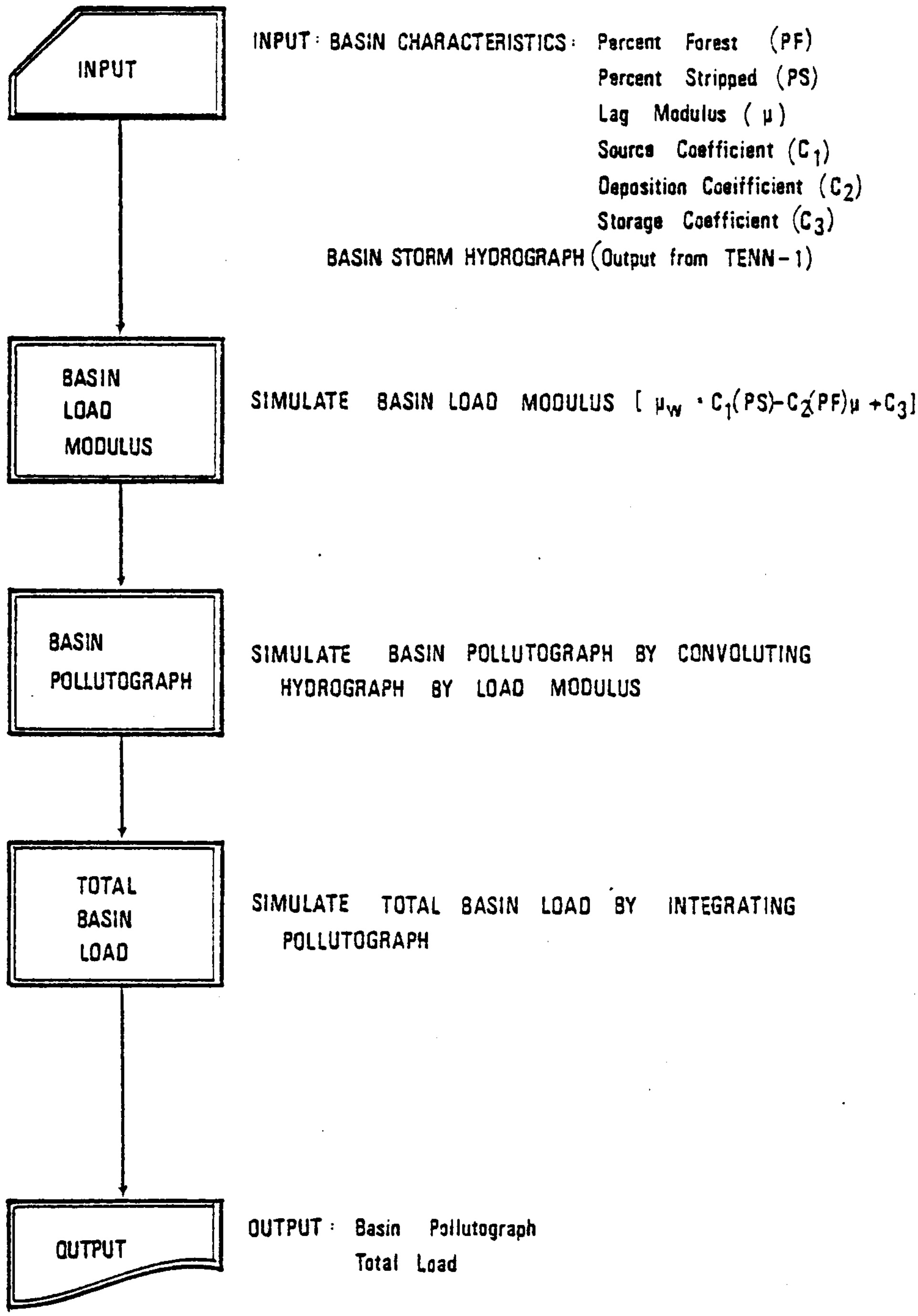

FIGURE 3.7

SUSPENDED SEDIMENT LOAD SIMULATOR (LOAD-I)

The load modulus for the watershed sediment yield model was formulated from a mass balance of suspended sediment load within a watershed. Under this concept, it can be reasoned that the watershed suspended sediment load results from the summation of the sediment loads produced, deposited and stored within the basin. Hence the watershed sediment load, L_W, for a storm could be expressed as

$$L_W = L_S + L_B - L_D \qquad (3.62)$$

where L_S is the watershed sediment load stored, L_B is the sediment load produced from denuded areas such as spoil banks, and L_D is the load deposited in the watershed, such as the forested areas.

Further, the watershed load may be represented as

$$L_W = \mu_W \, RD_W \, A_W \qquad (3.63)$$

where μ_W is the watershed load modulus in units of mass per surface area per depth of surface runoff volume, RD_W is the watershed surface runoff volume as depth, and A_W is the watershed drainage area.

The source load or spoil bank erosion load was expressed as

$$L_B = \mu_B \, RD_B \, A_B \qquad (3.64)$$

where μ_B is the source load modulus in units of mass per surface area per surface volume as depth, RD_B is the source surface runoff volume as depth, and A_B is the source or spoil bank area.

The deposited load or load deposited in the forested areas can be expressed as

$$L_D = \mu_D \, RD_F \, A_F \qquad (3.65)$$

where μ_D is the watershed deposition modulus in units of mass per surface area per surface volume runoff as depth, RD_F is the surface runoff volume as depth of the deposited or forested area, and A_F is the deposited or forested area. Combining 3.62, 3.63, 3.64 and 3.65 results in

$$\mu_W = \mu_B \left(\frac{RD_B}{RD_W}\right)\left(\frac{A_B}{A_W}\right) - \mu_D \left(\frac{RD_F}{RD_W}\right)\left(\frac{A_F}{A_W}\right) + \frac{L_s}{RD_W\ A_W} \ . \qquad (3.66)$$

The surface runoff ratios in equation 3.66, RD_B/RD_W and RD_F/RD_W, are considered storm constants. The area ratios can further be expressed as percentages using the following:

$$PF = 100 \left(\frac{A_F}{A_W}\right) \qquad (3.67)$$

$$PS = 100 \left(\frac{A_B}{A_W}\right) \qquad (3.68)$$

where PF is the percent of watershed forested or in which sediment was deposited, and PS is the percentage of watershed mined or in which source erosion occurs. This allows equation 3.66 to be represented as

$$\rho_W = C_1\ PS - C_2\ \mu\ PF + C_3 \qquad (3.69)$$

where

$$C_3 = \frac{L_s}{RD_W\ A_W} \qquad (3.70)$$

and μ is the watershed lag modulus which is considered to be proportional to the deposition modulus, μ_D. C_1 is an index of erosion load generated per percent watershed mined. C_2 is an index of the load deposited in the watershed. The sediment storage modulus, C_3, is an index of the sediment stored on the watershed that is available for transport when the transport capacity of the flow has not been filled, i.e. an average background level of suspended sediment.

Equation 3.69 provides a model for simulating load modulus as a function of three constants and two measurable basin quantities, percent forest and percent mined. The coefficients C_1, C_2 and C_3 can be optimized from observed watershed data. These constants are related to mining practice, i.e. changing land use, overburden characteristics and physiographic measures of a watershed.

Once μ_B has been determined the suspended yield may be determined by convoluting the load modulus with the hydrograph to produce the loadograph. The total storm load may be determined by integrating the loadograph over time.

Data Network

Study Area

The New River watershed basin, shown in Figure 3.8, is located in the northeastern counties of the Tennessee coal field, which occupies large portions of the eastern part of the state. This basin has a drainage area of 382 square miles and is completely contained in Anderson, Campbell, Morgan and Scott counties. This area has historically produced 70 percent of Tennessee's annual coal output.

Intensive contour strip mining in the New River basin began in 1940, but less than one percent of the basin area had been disturbed by 1955. Since 1955, the rate of strip mining disturbance has increased dramatically. By 1965 the amount of area disturbed rose to 2.25 percent and increased to 5 percent in 1974 as shown in Figure 3.9.

The New River basin, a sub-basin of the Big South Fork Cumberland River basin, is characterized by generally rugged terrain ranging in

FIGURE 3.8

TOPOGRAPHIC MAP OF THE NEW RIVER WATERSHED, TENNESSEE [123].

FIGURE 3.9

EXTENT OF CONTOUR STRIP COAL MINING IN THE NEW RIVER WATERSHED, TENNESSEE, FROM 1943 TO 1974 [123].

elevation from 1100 feet to 3300 feet with an average watershed slope of 25 percent or approximately 14.5 degrees.

The climatic conditions of this region reveal an average moderate temperature of 55 degrees Fahrenheit, a rainfall normally in excess of 50 inches per year, and a snowfall of 17 inches per year. The majority of this precipitation occurs in the Winter and Spring months.

The coal productive horizons are normally found in rock formations of the early Pennsylvanian age. These consist largely of conglomerates, sandstones, siltstones and shales. The coal seams located in these materials are normally level bedded and located on steep terrain.

The soils in this region are classified predominantly as moderately deep to deep, loamy and clayey soils on mountainous topography. These soils are dominated by mountains that occupy the highest landscape in the watershed. The soils on the narrow ridge tops and upper slopes are generally well drained, moderately deep and have clay subsoils and silty clay topsoils. The middle and lower slopes are dominated by moderately deep to deep, well-drained silty clay loam soils. These soils often have stoney surfaces and subsurfaces [123].

To obtain detailed information on the influence of mining activities on the New River Basin, six of its secondary watersheds were selected for study. Watershed location and descriptions are listed in Table 3.1 and 3.2. Initially three of the basins were virgin, having no mining activity. Disturbance to the virgin watersheds from mining commenced in 1975 in Anderson Branch and in 1977 in Bowling Branch. Lowe Branch was the only watershed that remained unmined through the period of observation from the beginning of 1975 through the end of

TABLE 3.1

STUDY WATERSHED LOCATIONS

Watershed	Map Designation (Fig. 3.8)	USGS/TVA Map Sheet No.
Anderson Branch	B	128 SW (Norma)
Bill's Branch	D	129 NW (Fk. Mtn.)
Bowling	E	128 SW (Norma)
Green Branch	F	129 NW (Fk. Mtn.)
Indian Fork	A	129 NW (Fk. Mtn.)
Lowe Branch	C	128 SW (Norma)

Source: Tung [123].

TABLE 3.2

WATERSHED DESCRIPTIONS

Watershed	Area (Acres/Miles^2)	Average Slope (%) Water-shed	Average Slope (%) Stream Bed	Average Elevation (Ft.)
Anderson Branch	518/0.81	34.1	18.4	1890
Bill's Branch	429/0.67	38.4	26.0	2408
Bowling	1402/2.19	32.5	7.4	1968
Green Branch	883/1.38	36.8	17.6	2287
Indian Fork	2765/4.32	38.1	8.4	2313
Lowe Branch	589/0.92	31.9	12.6	1820

Source: Tung [123].

1977. Green Branch experienced mining activity up through 1975 but has had no active surface mining since. Indian Fork has the longest history of mining activity. Mining in this Basin began in 1952 and culminated in 1976. The land disturbance resulting from surface mining these watersheds are shown in Table 3.3. In addition, Green Branch and Indian Fork have deep mining operations taking place in the watershed. These deep mines, however, seem to have little or no effect on the watersheds' runoff and sediment response. Bill's Branch has undergone strip mining from 1974 through 1975.

During the history of surface mining these watersheds, two major types of mining have occurred--steep contour strip mining and mountain top removal. Mountain top removal has occurred only in the Anderson Creek watershed. This method of surface mining is an adaptation of area mining to contour mining. Where coal seems to lie near tops of mountains, ridges, knobs, or knolls, they can be strip mined. The entire tops are removed down to the coal seam in a series of parallel cuts. Excess overburden that cannot be retained on the mined area is transported to head-of-hollow fills, stored on ridges, or placed in natural depressions and, until recently, on natural slopes adjacent to mining areas. This method produces large plateaus of level, rolling land that may have great value in mountainous areas. The extent of mountain top removal in Anderson Branch is small in comparison to total acreage--about 3.5 percent--but represents almost 40 percent of the mining occurring there.

The rest of the surface mining in the watersheds has consisted of the conventional steep contour strip mining method. This consists

TABLE 3.3

WATERSHED DISTURBANCE DUE TO SURFACE MINING

Watershed	Date	Strip Mining (Linear Miles)	Strip Mining (Acres)	Mountain Top Removal (Acres)	Roads (Linear Miles)
Anderson Branch	11/03/75	0.92	1.5		0.00
	11/18/76	1.95	42.0		0.00
	10/17/77	1.83	28.0	18.0	0.00
Bill's Branch	11/03/75	1.70	46.4		5.59
	10/18/76	1.70	46.4		5.59
	10/17/77	1.70	46.4		5.59
Bowling	11/03/75	0.00	0.0		3.31
	10/18/76	0.00	0.0		3.31
	10/17/77	2.16	44.0		3.31
Green Branch	11/03/75	5.34	213.0		6.63
	10/18/76	5.34	213.0		6.63
	10/17/77	5.34	213.0		6.63
Indian Fork	11/03/75	15.61	538.0		7.99
	10/18/76	16.48	552.0		7.99
	10/17/77	16.48	552.0		7.99
Lowe Branch	11/03/75	0.00	0.0		0.00
	10/18/76	0.00	0.0		0.00
	10/17/77	0.00	0.0		0.00

of removing the overburden from the coal seam, starting at a hillside outcrop and proceeding to mine around the hillside. The cut appears as a contour line would around the mountain, thus the name. Traditionally, overburden has been cast down the hillside and stacked along the outer edge of the bench as shown in Figure 3.10. After uncovering the seam, the coal is removed and successive cuts are made until the overburden becomes too great for economical recovery of the coal.

When Indian Fork was mined, the original backfilling practice, shown in Figure 3.9 (page 56), was used. This results in high backwalls ranging from a few feet to approximately a hundred feet in some areas. In addition to exposed highwalls the spoil on the bench often leaves depressions next to the highwall that collect stormwater. Green Branch has a combination of this practice and what is known as a partial back to contour spoil bank. This method is illustrated in Figure 3.11. This method differs from the original backfilling practice in that the headwall is partially covered and the bench is graded to allow stormwater to run off and not be collected in depressions. Spoil is still placed downslope. Green Branch is mined about 40 percent by this method. The rest of the study watersheds, except for Lowe Branch, have used this latter method. Table 3.4 lists the characteristics of these spoil banks throughout the watersheds. In this Table, Indian Fork has no road width because the upper slope is considered to be the total bench width.

Data Acquisition

Watershed runoff modeling data, i.e. rainfall and runoff data, was acquired in conjunction with the Knoxville office of the U.S.

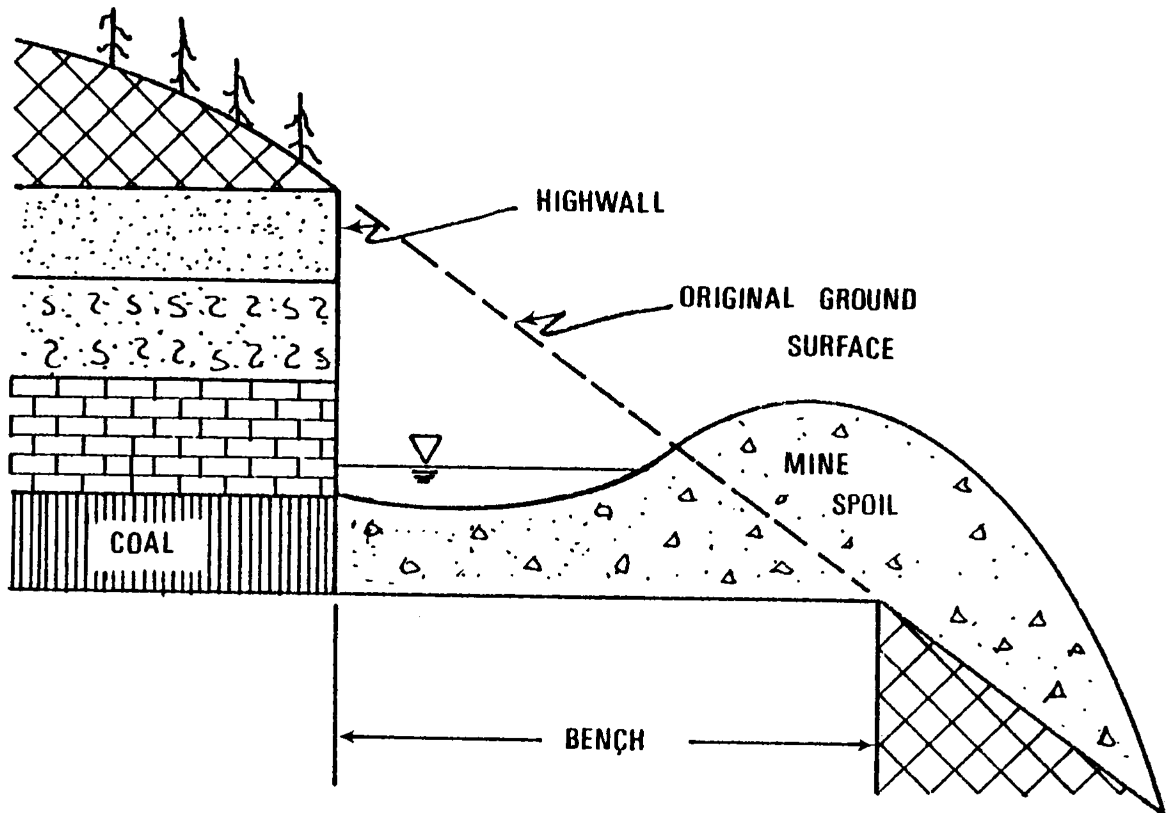

FIGURE 3.10

ORIGINAL BACKFILLING PRACTICE

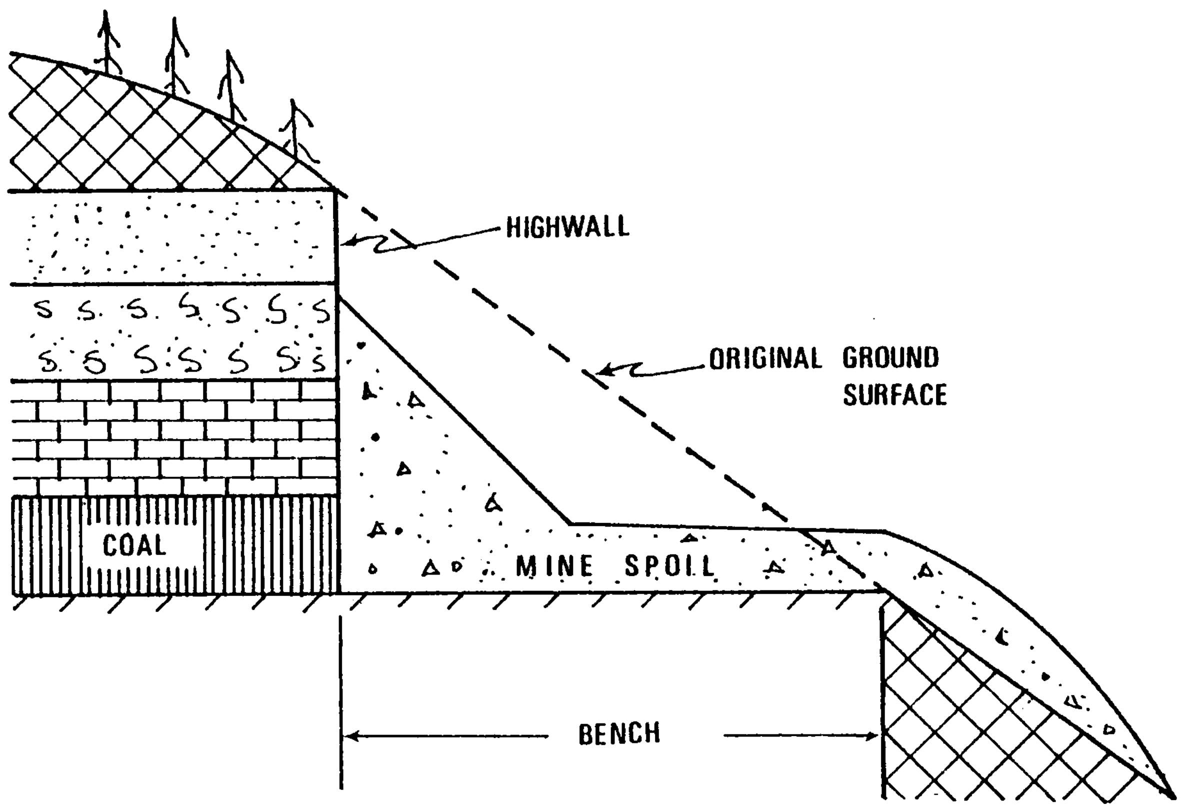

FIGURE 3.11

PARTIAL BACK TO CONTOUR PRACTICE

TABLE 3.4

SPOIL BANK CHARACTERISTICS

Watershed		Anderson Branch		Bill's Branch		Bowling Branch		Green Branch		Indian Fork	
		Length (ft)	Slope (°)	Length (ft)	Slope (°)	Length (ft)	Slope (°)	Length (ft)	Slope (°)	Length (ft)	Slope (°)
Upper Slope Length	Minimum	44	25	65	20	50	7	40	24	44	<2
	Average	95	28	84	23	70	12	100	30	160	<2
	Maximum	350	31	263	29	190	30	340	39	195	<2
Road/Flat Bench		40	-	35	-	30	-	45	-	-	-
Lower Slope Length	Minimum	70	26	60	29	100	28	100	32	95	25
	Average	155	28	105	39	140	32	160	38	210	30
	Maximum	265	32	340	53	528	37	352	49	360	45

Geological Survey. Each gauging station consisted of a weir and a continuous five-minute digital stage gauge with a synchronized rainfall monitor.

Watershed sediment yield data was obtained at the watershed gauging stations as grab samples. Samples were taken during storm flow conditions at designated locations upstream but close to the weir station. Samples were taken at mid-depth in the streams. The suspended sediment samples were analyzed using a tarred Gooch crucible with a 934 AH Reeve Angel filters. Suspended solids were determined using two different sample sizes. One hundred milliliters of the grab sample was filtered when concentrations were not visibly high. Fifty milliliter samples were filtered otherwise. Filtered samples were dried for at least two hours at 105^{o} C and were dessicated for at least thirty minutes before final weight determination. The samples were not replicated. The above suspended sediment samples were collected and analyzed in the Department of Civil Engineering (Environmental Engineering), The University of Tennessee.

All storm data, including rainfall, stage, flow and suspended solids, were placed on a computer information system and are part of the digitized computer file on New River Basin maintained by the Department of Civil Engineering, The University of Tennessee.

Data necessary to evaluate ERODE-I was not available from the New River Basin watersheds. The data necessary to evaluate this site specific erosion model must consist of rainfall excess distribution, site specific geometry, runoff hydrograph and suspended sediment loadograph. Because of these restrictions, data that was highly reliable was sought from areas with similar soil types and land slopes. The final data selected came from rainulator studies performed by the Agriculture Research Service, U.S. Department of Agriculture on Hawaii soils [124]. These data are not presented in this study because of its voluminous nature, but is summarized and further discussed in Appendix A. The reason for using the Hawaii data was threefold. First, the data were published, reliable and presented in a well documented form [124]. Secondly, these data represented the steepest slopes for which data of this nature are available, up to 16 percent. And finally the soil types are similar to those reported in the New River Basin watersheds.

CHAPTER IV

RESULTS

Stormwater Simulation Model

Unit Response Function

A data base of 54 storms was used in this study to evaluate TENN-I. This data base consisted of watershed outflow hydrographs and their associated rainfall distribution. From these hydrographs, the unit hydrograph from each storm was represented by the TVA double triangle URF. The URF for each storm was optimized by using the pattern search method described by Ardis [46]. Tables 4.1 through 4.4 list these optimized URF parameters. Lag time for each URF was calculated using equation 3.1 and is displayed in the above-mentioned tables. The coefficients of determination displayed in these tables represent the relative fit of the observed hydrograph to the storm hydrograph simulated by convoluting the optimized URF for each storm with its associated optimized rainfall excess time distribution. The weighted rainfall excess intensity, REI, was calculated using equation 2.11.

Each URF was normalized so that the variation in the URF's shape as a function of lag time could be observed. Normalization was accomplished by multiplying the ordinates, flow, by lag time and by dividing the time scale by lag time. This maintains a unit volume. Parameters of the normalized URFs are listed in Tables 4.5 through 4.8. The variation in the normalized URF parameters was analyzed using linear regression. The regressions were performed using equations 3.14 through 3.19 while assuming a zero intercept. Thus the constants KUP, KUR,

TABLE 4.1

OPTIMIZED URF USING TVA MODEL - ANDERSON BRANCH

Date	DT (HR)	T1 (HR)	T2 (HR)	T3 (HR)	UP (IN/HR)	UR (IN/HR)	TL (HR)	REI (IN/HR)	R^2
12/25/75	0.25	4.50	6.75	60.00	0.080	0.026	14.8	0.152	0.97
12/25/75	0.50	6.50	15.00	71.50	0.048	0.020	17.6	0.113	0.96
12/31/75	0.25	5.00	6.25	39.25	0.120	0.036	9.1	0.070	0.98
12/31/75	0.50	2.5	21.00	39.50	0.064	0.017	9.9	0.078	0.97
01/26/76	0.25	1.75	2.25	14.50	0.160	0.129	4.6	0.080	0.99
02/18/76	0.25	2.00	4.50	28.50	0.191	0.043	4.7	0.200	0.99
03/28/76	0.25	1.00	3.00	13.75	0.200	0.109	3.7	0.350	0.94
03/29/76	0.25	1.00	5.75	24.50	0.203	0.035	3.4	0.360	0.98
05/15/76	0.25	0.25	2.50	9.50	0.259	0.146	2.5	0.047	0.98
05/28/76	0.25	0.25	3.75	12.75	0.224	0.093	2.9	0.073	0.99
06/20/76	0.25	0.50	1.50	16.75	0.063	0.065	7.3	0.528	0.98
06/21/76	0.25	0.75	6.25	40.75	0.115	0.032	7.8	0.245	0.99
11/25/76	0.25	0.75	7.00	24.75	0.146	0.041	4.6	0.147	0.99

TABLE 4.2

OPTIMIZED URF USING TVA MODEL - BILL'S BRANCH

DATE	DT (HR)	T1 (HR)	T2 (HR)	T3 (HR)	UP (IN/HR)	UR (IN/HR)	TL (HR)	REI (IN/HR)	R^2
07/04/75	0.08	0.33	0.92	4.42	1.249	0.209	0.6	0.270	0.99
07/08/75	0.25	0.75	2.00	6.00	0.610	0.148	1.2	0.138	0.93
08/10/75	0.25	0.50	1.75	10.00	0.671	0.087	1.0	0.029	0.98
10/08/75	0.25	2.25	2.50	9.25	0.265	0.191	3.2	0.032	0.96
10/17/75	0.25	0.50	5.00	12.50	0.176	0.093	3.5	0.242	0.98
11/07/75	0.25	1.00	2.25	12.75	0.297	0.113	3.0	0.086	0.92
11/12/75	0.25	1.25	2.50	21.75	0.224	0.070	5.1	0.306	0.99
11/30/75	0.25	0.75	1.25	17.50	0.201	0.104	4.9	0.596	0.91
12/25/75	0.25	4.50	7.50	45.50	0.125	0.026	7.1	0.104	0.99
12/25/75	0.50	2.00	12.00	45.00	0.094	0.020	7.2	0.102	0.98
12/31/75	0.25	1.75	2.75	17.75	0.221	0.087	4.5	0.093	0.98
01/03/76	0.25	0.75	5.50	21.25	0.123	0.065	5.5	0.073	0.99
01/25/76	0.25	1.00	4.00	17.25	0.240	0.064	3.0	0.216	0.98
02/18/76	0.25	1.50	11.50	32.00	0.113	0.023	5.8	0.192	0.96
02/21/76	0.25	0.25	1.75	12.00	0.467	0.100	1.8	0.034	0.99
03/05/76	0.25	1.25	2.25	7.25	0.355	0.200	2.1	0.033	0.94
03/09/76	0.25	1.25	8.25	19.00	0.128	0.053	5.0	0.151	0.98
03/21/76	0.25	0.50	4.25	19.50	0.241	0.051	2.8	0.264	0.98
03/29/76	0.25	0.50	5.25	18.25	0.166	0.063	4.0	0.520	0.99
05/15/76	0.25	0.50	7.00	25.75	0.161	0.034	4.0	0.220	0.98
05/28/76	0.25	0.50	3.75	21.75	0.225	0.054	3.4	0.439	0.98
06/19/76	0.08	0.42	0.75	2.33	1.208	0.570	0.6	0.120	0.93
06/20/76	0.08	0.25	0.92	4.42	0.858	0.291	0.9	0.622	0.97
06/25/76	0.25	0.75	3.00	8.25	0.522	0.578	1.3	0.107	0.96
07/03/76	0.25	0.50	1.75	9.25	0.441	0.140	1.8	0.150	0.86

TABLE 4.3

OPTIMIZED URF USING TVA MODEL - GREEN BRANCH

DATE	DT (HR)	T1 (HR)	T2 (HR)	T3 (HR)	UP (IN/HR)	UR (IN/HR)	TL (HR)	REI (IN/HR)	R^2
12/15/75	0.25	1.00	3.00	35.25	0.155	0.045	8.3	0.091	0.98
12/15/75	0.50	1.00	8.00	48.00	0.068	0.031	11.8	0.126	0.98
12/25/75	0.25	6.76	13.00	46.00	0.071	0.027	11.4	0.083	0.99
12/26/75	0.50	0.50	18.50	48.50	0.058	0.019	10.6	0.080	0.99
12/31/75	0.25	0.25	3.5	18.00	0.219	0.069	3.4	0.105	0.94
01/11/76	0.25	0.50	4.5	21.50	0.150	0.063	4.9	0.141	0.98
01/13/76	0.25	0.75	2.25	12.25	0.392	0.097	2.0	0.435	0.97
01/26/76	0.33	1.50	10.00	35.00	0.099	0.030	6.9	0.146	0.98
02/18/76	0.25	0.25	2.75	30.75	0.264	0.042	4.7	0.140	0.96
02/20/76	0.25	0.75	1.75	9.50	0.396	0.149	2.2	0.210	0.96
02/29/76	0.25	1.50	8.00	19.50	0.167	0.037	4.0	0.253	0.96
06/25/76	0.25	0.25	2.50	6.25	0.558	0.101	1.0	0.060	0.98

TABLE 4.4

OPTIMIZED URF USING TVA MODEL - LOWE BRANCH

DATE	DT (HR)	T1 (HR)	T2 (HR)	T3 (HR)	UP (IN/HR)	UR (IN/HR)	TL (HR)	REI (IN/HR)	R^2
06/12/75	0.08	1.58	2.17	11.75	0.461	0.099	1.9	0.235	0.95
09/23/75	0.25	0.75	3.25	12.0	0.329	0.083	2.0	0.398	0.99
10/17/75	0.25	1.25	3.00	16.25	0.293	0.075	2.8	0.063	0.99
03/29/76	0.25	1.25	6.75	22.50	0.219	0.025	3.1	0.396	0.96
05/14/76	0.25	1.75	18.00	70.00	0.046	0.017	15.2	0.156	0.99
05/14/76	0.50	1.00	18.50	71.00	0.044	0.017	15.4	0.106	0.99
05/28/76	0.25	1.00	13.50	62.25	0.054	0.021	13.7	0.108	0.98
05/28/76	0.50	1.00	13.50	60.00	0.055	0.021	13.0	0.076	0.98
06/20/76	0.25	0.75	2.25	12.00	0.335	0.111	2.5	0.512	0.98
07/03/76	0.25	1.25	7.00	23.75	0.124	0.050	5.5	0.139	0.98

TABLE 4.5

NORMALIZED URF - ANDERSON BRANCH

Date	T1/TL	T2/TL	T3/TL	UP * TL	UR * TL
12/25/75	0.36	0.85	4.04	0.848	0.348
12/31/75	0.55	0.69	4.30	1.086	0.327
01/26/76	0.38	0.50	3.15	0.738	0.593
02/18/76	0.43	0.96	6.06	0.907	0.202
03/28/76	0.27	0.80	3.72	0.746	0.403
03/29/76	0.29	1.69	7.20	0.686	0.119
05/15/76	0.10	1.00	3.80	0.635	0.365
05/28/76	0.09	1.29	4.39	0.640	0.270
06/20/76	0.07	0.21	2.30	0.460	0.475
06/21/76	0.10	0.80	5.22	0.898	0.250
11/25/76	0.16	1.52	5.26	0.668	0.189

TABLE 4.6

NORMALIZED URF - BILL'S BRANCH

Date	T1/TL	T2/TL	T3/TL	UP * TL	UR * TL
07/04/75	0.55	1.53	7.37	0.749	0.125
07/08/75	0.63	1.67	5.00	0.732	0.178
08/10/75	0.50	1.75	10.00	0.671	0.087
10/08/75	0.16	0.78	2.89	0.848	0.611
10/17/75	0.14	1.43	3.57	0.616	0.326
11/07/75	0.33	0.75	4.25	0.891	0.339
11/12/75	0.24	0.49	4.26	1.142	0.357
11/30/75	0.15	1.25	3.57	0.985	0.510
12/25/75	0.63	1.06	6.41	0.888	0.185
12/31/75	0.39	0.61	3.95	0.995	0.392
01/03/76	0.14	1.00	3.86	0.676	0.358
01/25/76	0.33	1.33	5.75	0.720	0.192
02/18/76	0.25	1.98	5.52	0.655	0.133
02/21/76	0.14	0.97	6.67	0.841	0.180
03/05/76	0.60	1.07	3.45	0.745	0.420
03/09/76	0.25	1.65	3.80	0.640	0.265
03/21/76	0.18	1.52	6.96	0.678	0.143
03/29/76	0.13	1.31	4.56	0.664	0.252
05/15/76	0.13	1.75	6.44	0.644	0.136
05/18/76	0.15	1.10	6.40	0.765	0.184
06/19/76	0.70	1.25	3.88	0.725	0.342
06/20/76	0.28	1.02	4.91	0.953	0.323
06/25/76	0.58	2.31	6.35	0.679	0.751
07/03/76	0.28	1.35	5.14	0.794	0.252

TABLE 4.7

NORMALIZED URF - GREEN BRANCH

Date	T1/TL	T2/TL	T3/TL	UP * TL	UR * TL
12/15/75	0.12	0.36	4.25	1.286	0.374
12/25/75	0.59	1.14	4.04	0.809	0.308
12/26/75	0.05	1.74	4.58	0.615	0.201
12/31/75	0.07	1.03	5.29	0.745	0.235
01/11/75	0.10	0.92	4.39	0.735	0.309
01/13/76	0.38	1.13	6.13	0.784	0.194
01/12/76	0.22	1.45	5.07	0.683	0.207
02/18/76	0.05	0.59	6.54	1.241	0.197
02/20/76	0.34	0.79	4.32	0.871	0.328
02/29/76	0.38	2.00	4.88	0.668	0.148
06/25/76	0.25	2.50	6.25	0.558	0.101

TABLE 4.8

NORMALIZED URF - LOWE BRANCH

Date	T1/TL	T2/TL	T3/TL	UP * TL	UR * TL
06/12/75	0.83	1.14	6.18	0.876	0.188
09/23/75	0.38	1.63	6.00	0.658	0.166
10/17/75	0.27	1.07	5.80	0.820	0.210
03/29/76	0.40	2.18	7.26	0.679	0.078
05/14/76	0.11	1.18	4.60	0.699	6.258
05/28/76	0.08	1.04	4.62	0.715	0.273
06/20/76	0.30	0.90	4.80	0.838	0.278
07/03/76	0.23	1.27	4.32	0.683	0.275

KT1, KT2, KT23 and KT3 were the coefficients of regression analysis and represented the best estimate of the mean coordinates of the normalized URF (NURF) parameters. The statistical analyses of the NURF parameters are listed in Tables 4.9 through 4.14. Graphical representation of the linear regression analysis is depicted in Appendix B. The variation of the normalized URF parameters and those obtained through regression analysis are shown graphically in Figures 4.1 through 4.4. The basin NURF optimized from all the New River Basin watershed URFs is shown in Figure 4.5 along with NURFs for other land uses reported by Troxler and Overton [54].

Lag Modulus

Lag modulus for each storm URF was optimized using equation 3.12. The variation of lag modulus policy space for each watershed using this equation can be observed in Table 4.15. This table also shows the policy space variation of the weighted rainfall excess intensity and lag time associated with each watershed.

Two methods were used to establish a lag modulus for each watershed. The first method simulated the watershed lag modulus as the mean of all lag modulus observed on that watershed. The second method simulated the watershed lag modulus by substituting the average watershed lag time and average watershed weighted rainfall excess intensity into equation 3.12. This lag modulus is referred to as the average lag modulus, μ_{AVG}.

Equation 3.11 was optimized using principle components regression to regionalize the lag modulus simulator. The matrix used in evaluating equation 3.11 as a regionalization model is shown in Table 4.16.

TABLE 4.9

STATISTICAL ANALYSIS FOR REGRESSION OF T1 VERSUS TL

Watershed	Regression Coefficient KT1	Coefficient of Determination	Standard Error	Lower* Confidence Level	Upper* Confidence Level
Anderson Branch	0.349	0.89	0.043	0.251	0.446
Bill's Branch	0.251	0.59	0.027	0.196	0.306
Green Branch	0.259	0.61	0.072	0.099	0.420
Lowe Branch	0.130	0.39	0.037	0.042	0.218
ALL	0.253	0.65	0.024	0.204	0.301

*Confidence Interval Computed on 95 Percent Significance Level

TABLE 4.10

STATISTICAL ANALYSIS FOR REGRESSION OF T2 VERSUS TL

Watershed	Regression Coefficient KT2	Coefficient of Determination	Standard Error	Lower* Confidence Level	Upper* Confidence Level
Anderson Branch	0.860	0.91	0.070	0.700	1.020
Bill's Branch	1.234	0.78	0.111	1.004	1.465
Green Branch	1.190	0.80	0.157	0.841	1.539
Lowe Branch	1.153	0.97	0.066	0.997	1.308
ALL	1.085	0.85	0.055	0.974	1.195

*Confidence Interval Computed on 95 Percent Significance Level

TABLE 4.11

STATISTICAL ANALYSIS FOR REGRESSION OF T23 VERSUS TL

Watershed	Regression Coefficient KT23	Coefficient of Determination	Standard Error	Lower* Confidence Level	Upper* Confidence Level
Anderson Branch	1.176	0.90	0.106	0.936	1.416
Bill's Branch	1.714	0.78	0.154	1.396	2.033
Green Branch	1.648	0.79	0.233	1.130	2.167
Lowe Branch	1.759	0.99	0.066	1.604	1.914
ALL	1.541	0.85	0.080	1.380	1.702

*Confidence Interval Computed on 95 Percent Significance Level

TABLE 4.12

STATISTICAL ANALYSIS FOR REGRESSION OF T3 VERSUS TL

Watershed	Regression Coefficient KT3	Coefficient of Determination	Standard Error	Lower* Confidence Level	Upper* Confidence Level
Anderson Branch	4.368	0.96	0.241	3.823	4.913
Bill's Branch	4.861	0.89	0.249	4.346	5.376
Green Branch	4.541	0.97	0.190	4.118	4.965
Lowe Branch	4.682	0.99	0.169	4.284	5.081
ALL	4.581	0.96	0.107	4.367	4.795

*Confidence Interval Computed on 95 Percent Significance Level

TABLE 4.13

STATISTICAL ANALYSIS FOR REGRESSION OF UP VERSUS 1/TL

Watershed	Regression Coefficient KUP	Coefficient of Determination	Standard Error	Lower* Confidence Level	Upper* Confidence Level
Anderson Branch	0.703	0.96	0.032	0.630	0.777
Bill's Branch	0.745	0.99	0.012	0.721	0.769
Green Branch	0.694	0.95	0.048	0.588	0.801
Lowe Branch	0.791	0.97	0.034	0.710	0.871
ALL	0.740	0.99	0.011	0.718	0.762

*Confidence Interval Computed on 95 Percent Significance Level

TABLE 4.14

STATISTICAL ANALYSIS FOR REGRESSION OF UR VERSUS 1/TL

Watershed	Regression Coefficient KUR	Coefficient of Determination	Standard Error	Lower* Confidence Level	Upper* Confidence Level
Anderson Branch	0.302	0.701	0.041	0.209	0.396
Bill's Branch	0.219	0.74	0.024	0.169	0.269
Green Branch	0.169	0.73	0.026	0.112	0.226
Lowe Branch	0.195	0.84	0.021	0.145	0.246
ALL	0.215	0.754	0.016	0.184	0.247

*Confidence Interval Computed on 95 Percent Significance Level

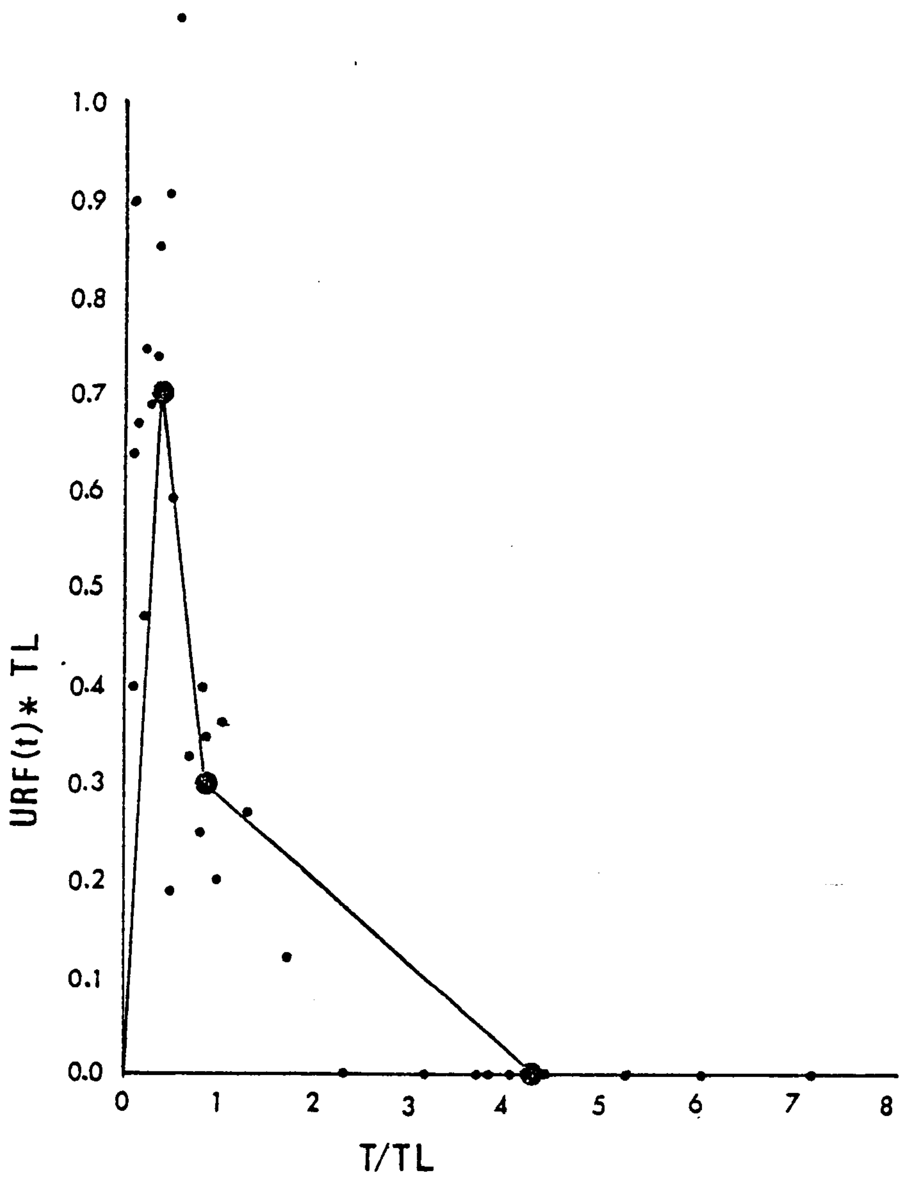

FIGURE 4.1

STATISTICAL URF VERSUS NORMALIZED URF - ANDERSON BRANCH

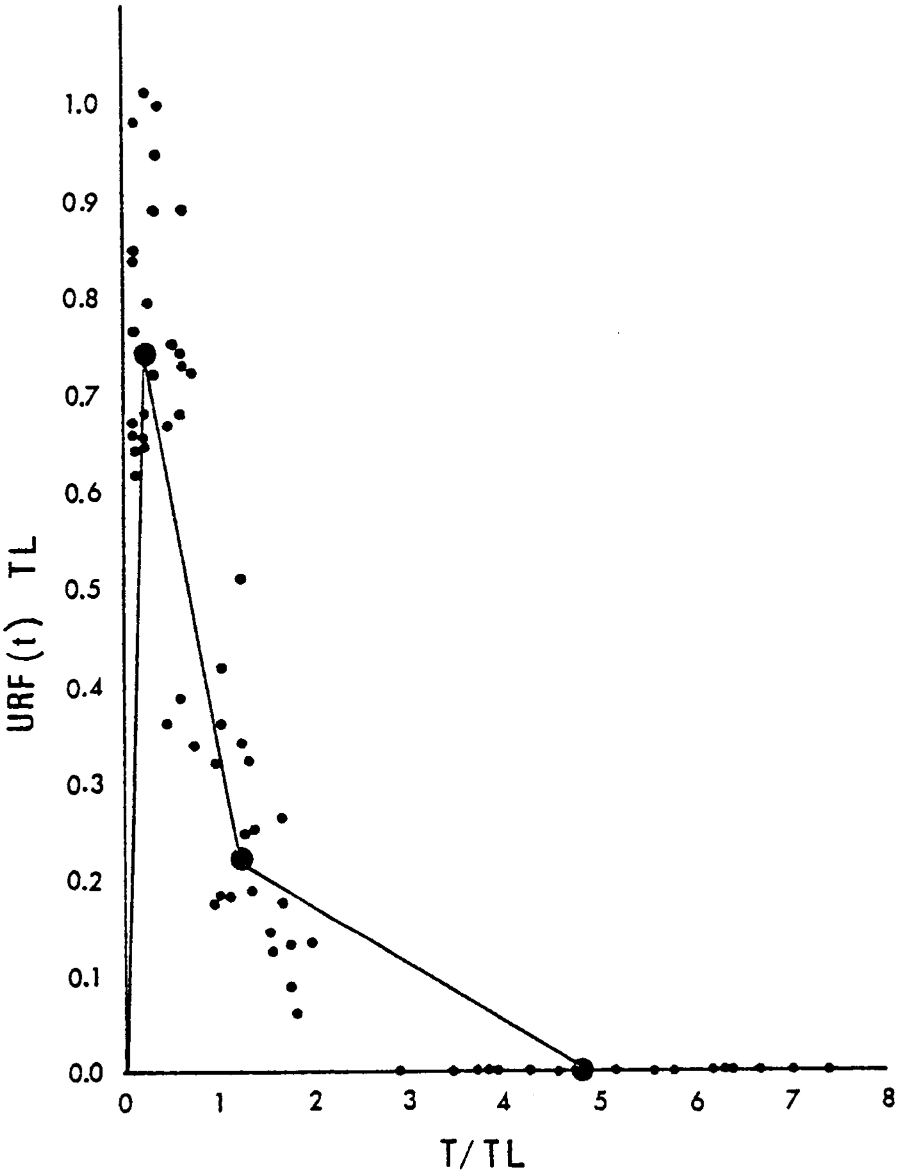

FIGURE 4.2

STATISTICAL URF VERSUS NORMALIZED URF - BILL'S BRANCH

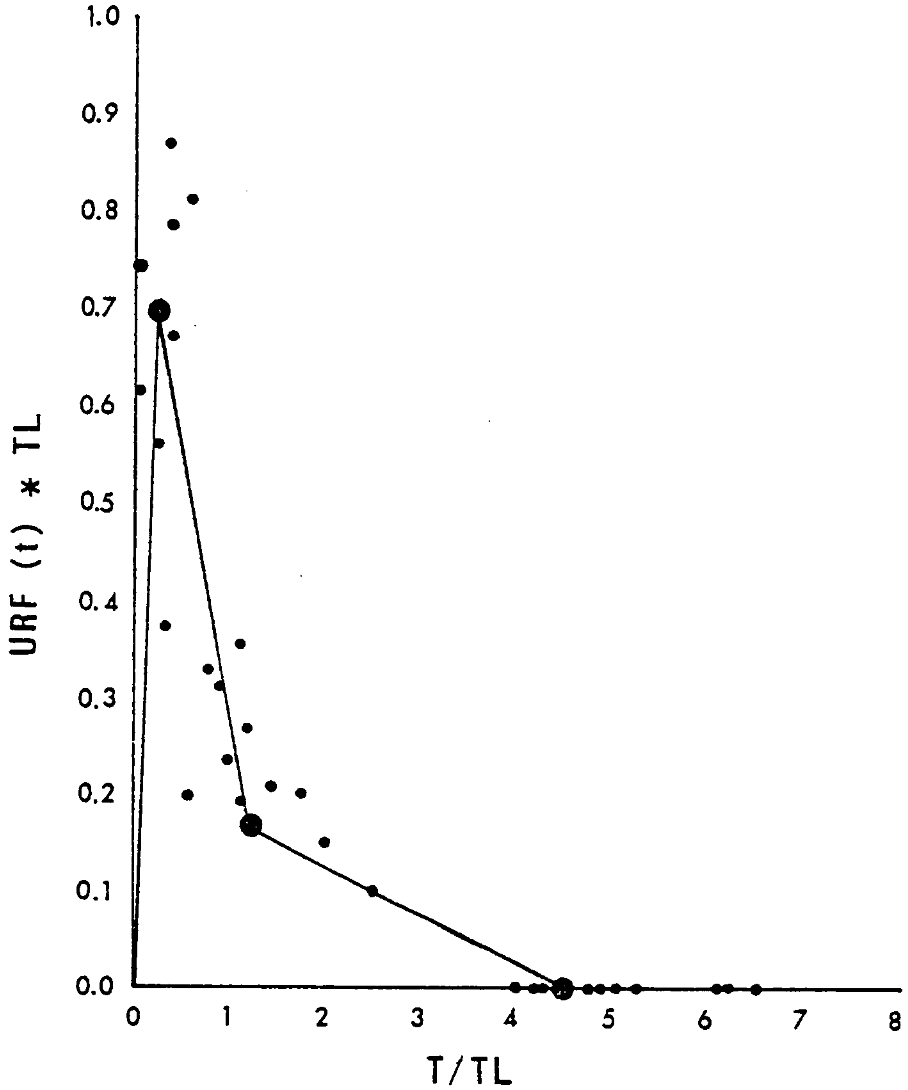

FIGURE 4.3

STATISTICAL URF VERSUS NORMALIZED URF - GREEN BRANCH

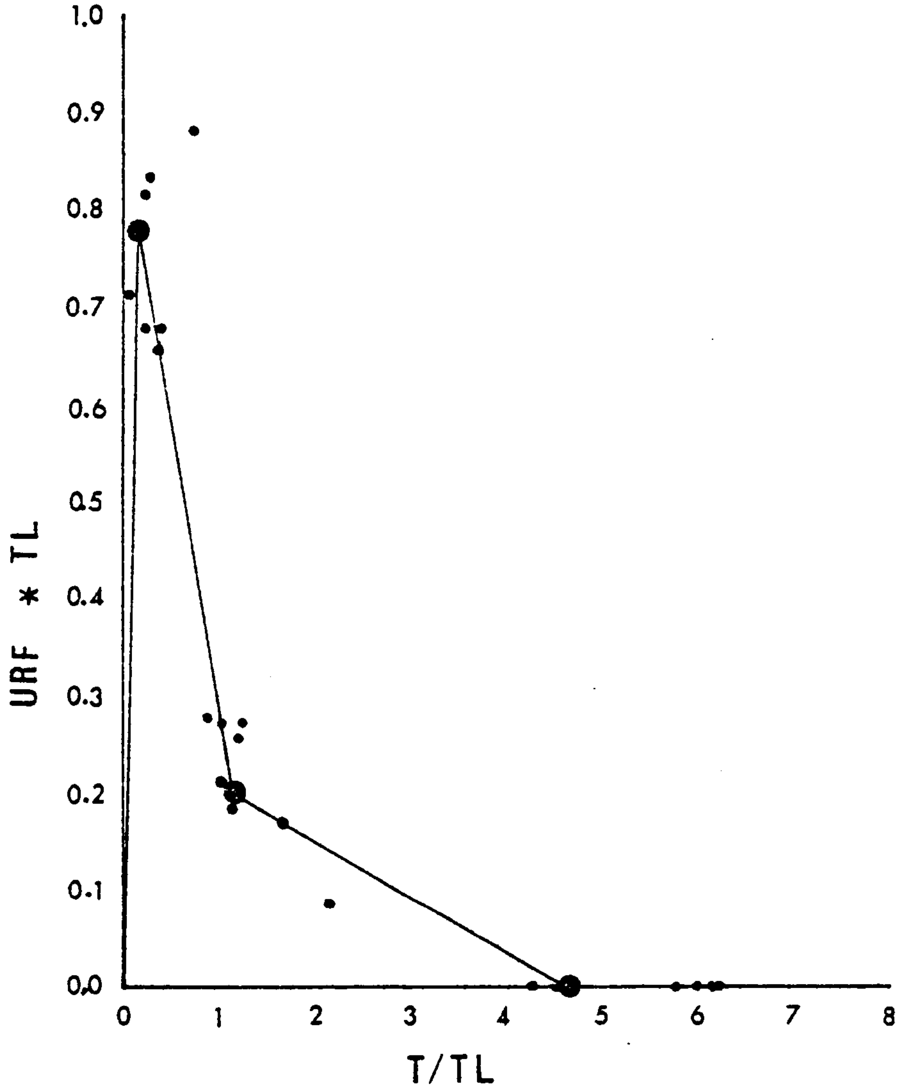

FIGURE 4.4

STATISTICAL URF VERSUS NORMALIZED URF - LOWE BRANCH

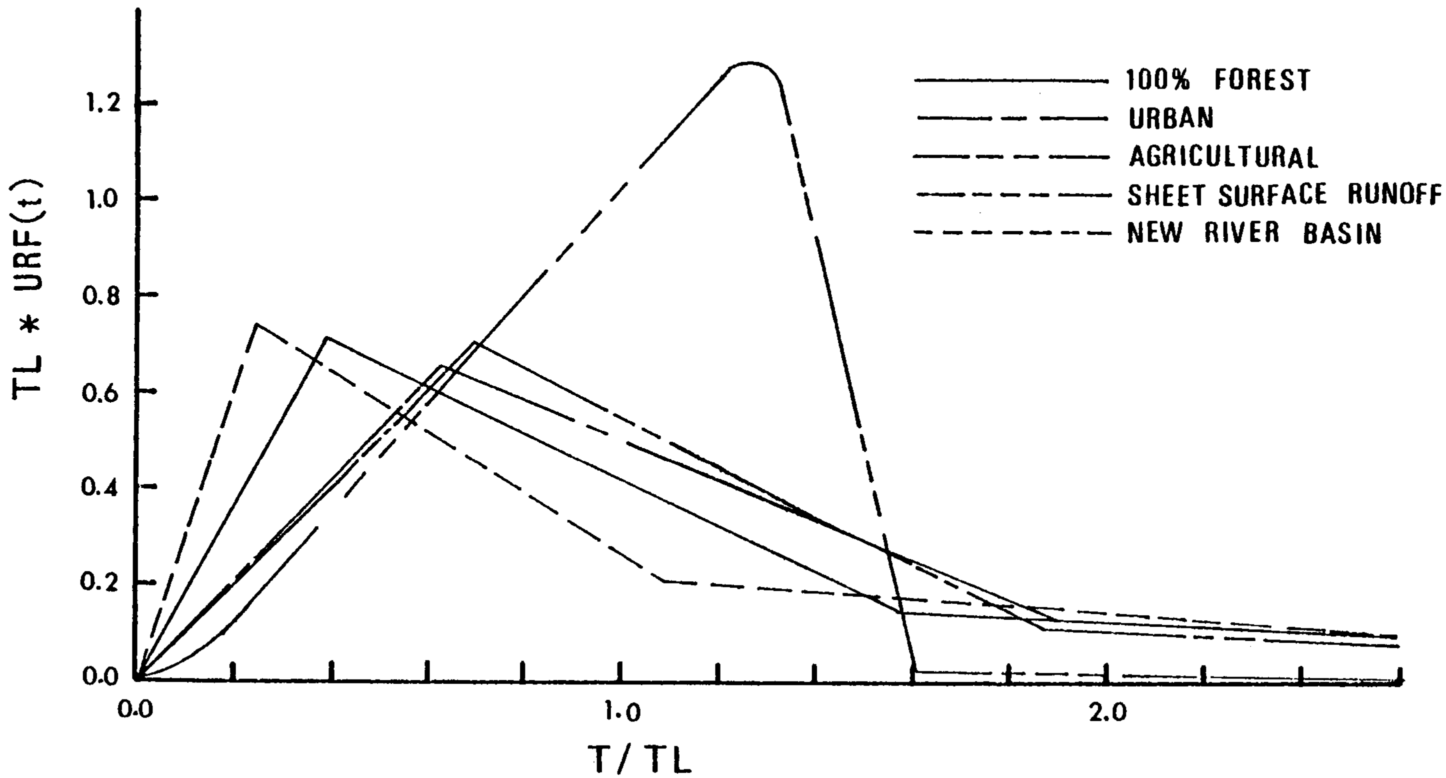

FIGURE 4.5

NURF FOR NEW RIVER BASIN COMPARED TO NURFs FOR OTHER LAND USES

TABLE 4.15

WATERSHED POLICY SPACE VARIATION OF WEIGHTED RAINFALL EXCESS (REI), LAG TIME (TL) AND LAG MODULUS (μ)

Watershed	Anderson Branch	Bill's Branch	Green Branch	Lowe Branch
Mean REI	0.168	0.250	0.177	0.247
CV (%)*	65	66	59	64
Mean TL	6.095	3.411	5.857	5.778
CV (%)*	70	54	54	84
Mean μ	2.738	1.821	2.417	2.738
Minimum μ	0.730	0.271	1.390	0.935
Maximum μ	7.071	3.972	3.840	7.245
CV (%)*	49	57	36	34

*CV is the coefficient of variation

TABLE 4.16

MATRIX FOR WATERSHED LAG MODULUS SIMULATION

Watershed	μ_{AVG}	Mean μ	Area	Percent Forest
Anderson Branch	2.990	2.738	0.81	95
Bill's Branch	1.802	1.821	0.67	88
Green Branch	2.930	2.417	1.38	74
Lowe Branch	3.300	2.738	0.92	98
White Hollow*	3.540	---	2.68	100
Upper Bear Creek*	4.44	---	2.48	100

*Reported by Overton and Troxler [54]

Three different cases were considered in this matrix. Case I was based upon the average lag moduli calculated for the New River Watersheds. Case II used the mean lag moduli determined for the New River Watershed. Case III extended Case I by adding two additional Tennessee Valley watershed lag moduli reported by Troxler and Overton [54]. These two watersheds extend the range of the watershed size. These two watersheds have no mining activity. Results of the optimization of these three cases are shown in Table 4.17. Case III was selected to simulate lag modulus since it has the largest sample size having the highest degree of freedom and represented basins ranging from approximately one-half to three squre miles. A plot of simulated versus observed lag modulus using this regionalization scheme is shown in Figure 4.6.

Storm Hydrograph Simulation

The model TENN-I, described in Chapter III was used to simulate storm watershed hydrographs. Input included the actual accumulative rainfall distribution at equal time intervals. In addition, observed storm hydrographs were provided to allow optimization of Curve Number. This assured that the rainfall excess volume of the simulated hydrograph would equal the runoff volume of the observed hydrograph, and thus establish a basis for comparing the two hydrographs. Rainfall excess intensity was distributed and determined using the SCS Curve Number model described earlier.

The lag modulus simulation model, equation 3.11, incorporated the Case III optimized constants from Table 4.17 to simulate lag modulus. Weighted rainfall excess intensity was calculated from

TABLE 4.17

RESULTS OF OPTIMIZING LAG MODULUS (μ)

Case	Description	C_1	C_2	C_3	Coefficient of Determination
I	New River Watersheds with μ_{AVG}	3.0385	0.0781	-7.0500	0.97
II	New River Watersheds with Mean μ	1.4539	0.0464	-3.0304	0.87
III	All Six Watersheds From Table 4.16 With μ_{AVG}	0.6430	0.0236	0.0251	0.75

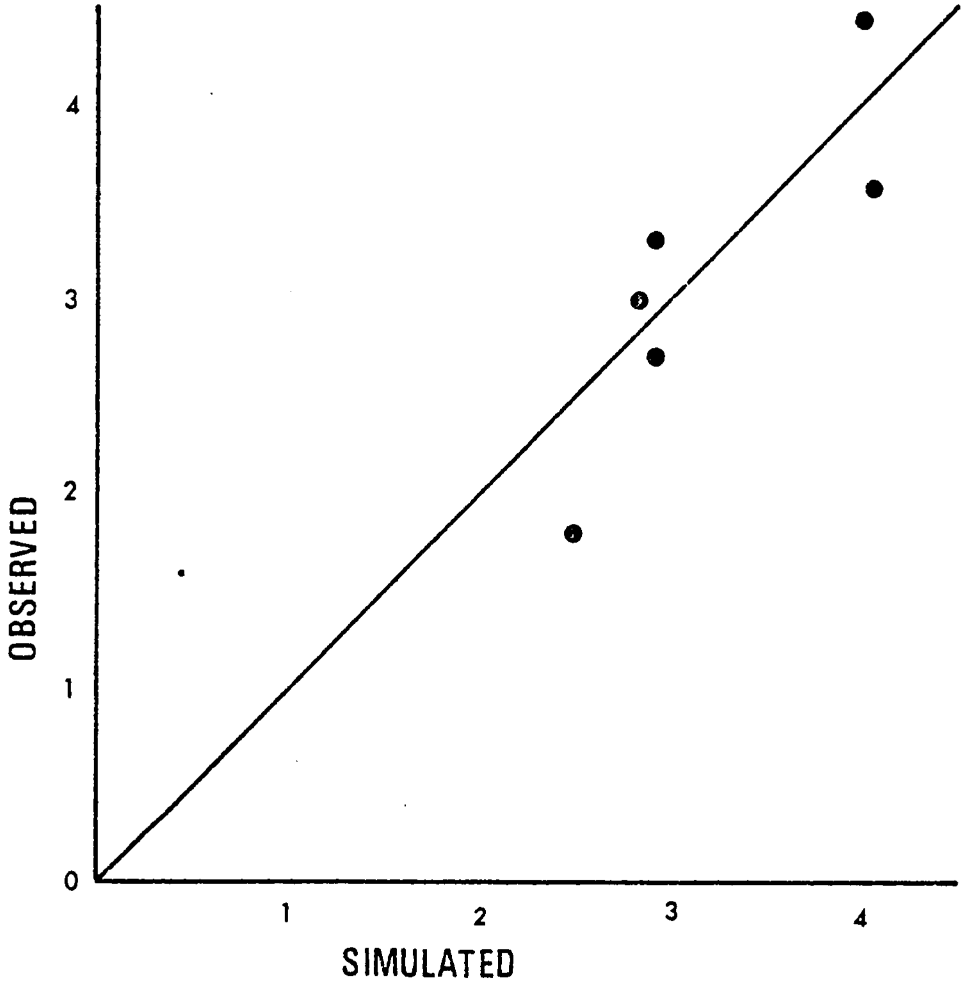

FIGURE 4.6

OBSERVED VERSUS SIMULATED LAG MODULUS

equation 2.11. Lag time for a storm was calculated from equation 3.12.

Once the lag time was established for a storm, a URF was simulated from the NURF constants obtained from all of the New River Basin Watersheds. KUR, KT1, KT2 and KT3 were used to simulate the URF from the Basin NURF. This URF was then convoluted with the rainfall excess time distribution to simulate a storm hydrograph. Storm hydrograph simulation results are tabulated in Tables 4.18 through 4.21. No effort was made to censor these storms. Several of these storms are multiple burst rain storms. Examples of good, fair, and poor fits between observed and simulated hydrographs are shown in Figures 4.7 through 4.11. Figures 4.7 and 4.8 are the result of multiple rainfall burst storms. Figures 4.9 through 4.11 are the result of single burst storms. The effect of changing rainfall abstraction time increments from thirty minutes to fifteen minutes is displayed in Figures 4.12 and 4.13.

Erosion Simulation Model

Evaluation of ERODE-I

The erosion simulator model, ERODE-I, was evaluated on erosion data generated by simulated rainfall of 42 Hawaii sites and 106 storms [124]. Soil loss from the rainfall events was generated for eleven Hawaii soil series on 35 and 75 foot plot lengths with slopes of up to 19 percent. The data included the runoff hydrograph, the soil sedigraph and storm infiltration rates. The detachment, transport and reaction coefficients in the model were obtained through optimization of data grouped by soil type, instead of series. These soils were

TABLE 4.18

ANDERSON BRANCH STORM HYDROGRAPH SIMULATION RESULTS

Date	Total Rain (IN)	REI (IN/HR)	Storm Duration (HR)	Storm Runoff (HR)	Time to Peak		Peak Flow	
					Observed (HR)	Simulated (HR)	Observed (CFS)	Simulated (CFS)
12/25/75	1.47	0.075	15.25	0.63	13.00	12.00	13.87	16.33
12/25/75	1.45	0.102	15.50	0.65	13.50	12.00	13.90	23.74
12/31/75	1.10	0.069	14.00	0.56	16.00	16.50	17.53	17.14
01/18/76	1.49	0.182	9.75	0.66	12.00	12.50	41.67	32.07
05/15/76	1.73	0.104	12.00	0.41	8.50	12.00	11.32	15.45
05/28/76	0.62	0.133	4.00	0.30	3.50	5.00	11.29	14.20
06/28/76	0.54	0.244	1.50	0.15	1.50	2.25	9.12	10.82
11/25/76	1.80	0.143	14.75	1.03	25.25	26.50	43.07	34.67

TABLE 4.19

BILL'S BRANCH STORM HYDROGRAPH SIMULATION RESULTS

Date	Total Rain (IN)	REI (IN/HR)	Storm Duration (HR)	Storm Runoff (HR)	Time to Peak		Peak Flow	
					Observed (HR)	Simulated (HR)	Observed (CFS)	Simulated (CFS)
07/04/75	0.86	0.270	1.00	0.10	0.66	1.83	37.60	6.58
07/08/75	0.66	0.057	2.25	0.03	5.00	7.00	12.24	1.31
08/10/75	0.60	0.024	2.75	0.02	2.50	5.75	4.36	0.43
10/08/75	0.84	0.015	8.00	0.04	7.75	12.00	3.43	0.91
10/17/75	1.81	0.156	13.00	0.73	8.00	13.00	34.52	22.42
11/07/75	0.72	0.033	(5.25)	0.06	5.00	10.25	4.61	1.59
11/12/75	2.13	0.269	11.50	1.55	5.75	6.50	57.17	54.68
11/30/75	0.84	0.068	4.00	0.17	1.75	5.75	16.65	6.14
12/25/75	1.66	0.105	17.50	1.03	16.50	18.00	27.28	26.15
12/25/75	1.68	0.112	20.50	0.52	7.75	11.25	27.42	18.91
12/31/75	1.07	0.100	14.50	0.82	17.00	17.50	24.50	24.02
01/03/76	0.52	0.038	6.50	0.11	6.75	10.25	4.78	3.13

TABLE 4.19 (CONTINUED)

Date	Total Rain (IN)	REI (IN/HR)	Storm Duration (HR)	Storm Runoff (HR)	Time to Peak Observed (HR)	Time to Peak Simulated (HR)	Peak Flow Observed (CFS)	Peak Flow Simulated (CFS)
01/25/76	1.51	0.198	10.25	0.82	13.00	13.50	45.68	32.78
02/18/76	1.50	0.191	10.75	1.06	11.75	12.25	44.25	40.51
02/21/76	0.47	0.034	3.00	0.05	6.75	9.25	6.45	1.45
03/05/76	0.62	0.010	6.25	0.02	5.50	10.00	2.58	0.37
03/09/76	0.52	0.121	5.5	0.25	11.00	12.00	13.43	11.43
03/21/76	1.23	0.264	5.5	0.62	4.50	5.25	50.53	27.88
03/29/76	3.11	0.521	11.25	2.56	12.25	13.00	89.77	78.88
05/15/76	1.66	0.220	11.00	0.92	7.25	8.50	48.39	36.05
05/28/76	2.39	0.377	12.00	0.85	14.25	15.00	51.99	44.02
06/19/76	0.38	0.053	2.53	0.03	2.49	4.90	11.41	0.91
06/20/76	1.09	0.275	1.92	0.22	0.75	2.57	63.91	13.11

TABLE 4.20

GREEN BRANCH STORM HYDROGRAPH SIMULATION RESULTS

Date	Total Rain (IN)	REI (IN/HR)	Storm Duration (HR)	Storm Runoff (HR)	Time to Peak		Peak Flow	
					Observed (HR)	Simulated (HR)	Observed (CFS)	Simulated (CFS)
12/15/75	0.57	0.037	5.25	0.11	2.25	7.00	8.97	6.12
12/15/75	0.57	0.039	6.00	0.14	2.50	7.50	9.00	7.94
12/25/75	1.61	0.071	17.50	0.56	15.50	18.50	26.33	28.31
12/26/75	1.50	0.072	7.25	0.56	15.50	18.50	26.44	32.58
01/11/76	0.68	0.041	4.00	0.07	3.25	6.75	8.65	4.44
01/26/76	1.77	0.102	17.00	0.59	25.31	26.64	42.87	36.34
06/26/76	0.68	0.062	1.25	0.04	1.250	3.25	16.65	3.00

TABLE 4.21

LOWE BRANCH STORM HYDROGRAPH SIMULATION RESULTS

Date	Total Rain (IN)	REI (IN/HR)	Storm Duration (HR)	Storm Runoff (HR)	Time to Peak Observed (HR)	Time to Peak Simulated (HR)	Peak Flow Observed (CFS)	Peak Flow Simulated (CFS)
06/12/75	0.97	0.217	3.00	0.07	1.49	2.32	18.48	5.62
10/17/75	1.25	0.063	10.75	0.30	9.25	12.00	21.28	10.64
05/14/76	1.49	0.073	10.00	0.25	7.75	11.50	5.52	9.60
05/14/76	1.49	0.060	10.50	0.26	7.50	12.00	5.53	9.18
05/28/76	1.28	0.072	4.00	0.23	4.00	5.50	6.02	8.00
05/28/76	1.28	0.062	4.00	0.23	4.00	6.00	5.99	7.43
06/20/76	1.31	0.318	2.50	0.25	1.25	2.75	51.10	19.61
07/03/76	0.72	0.313	1.00	0.15	1.75	2.25	8.51	12.72

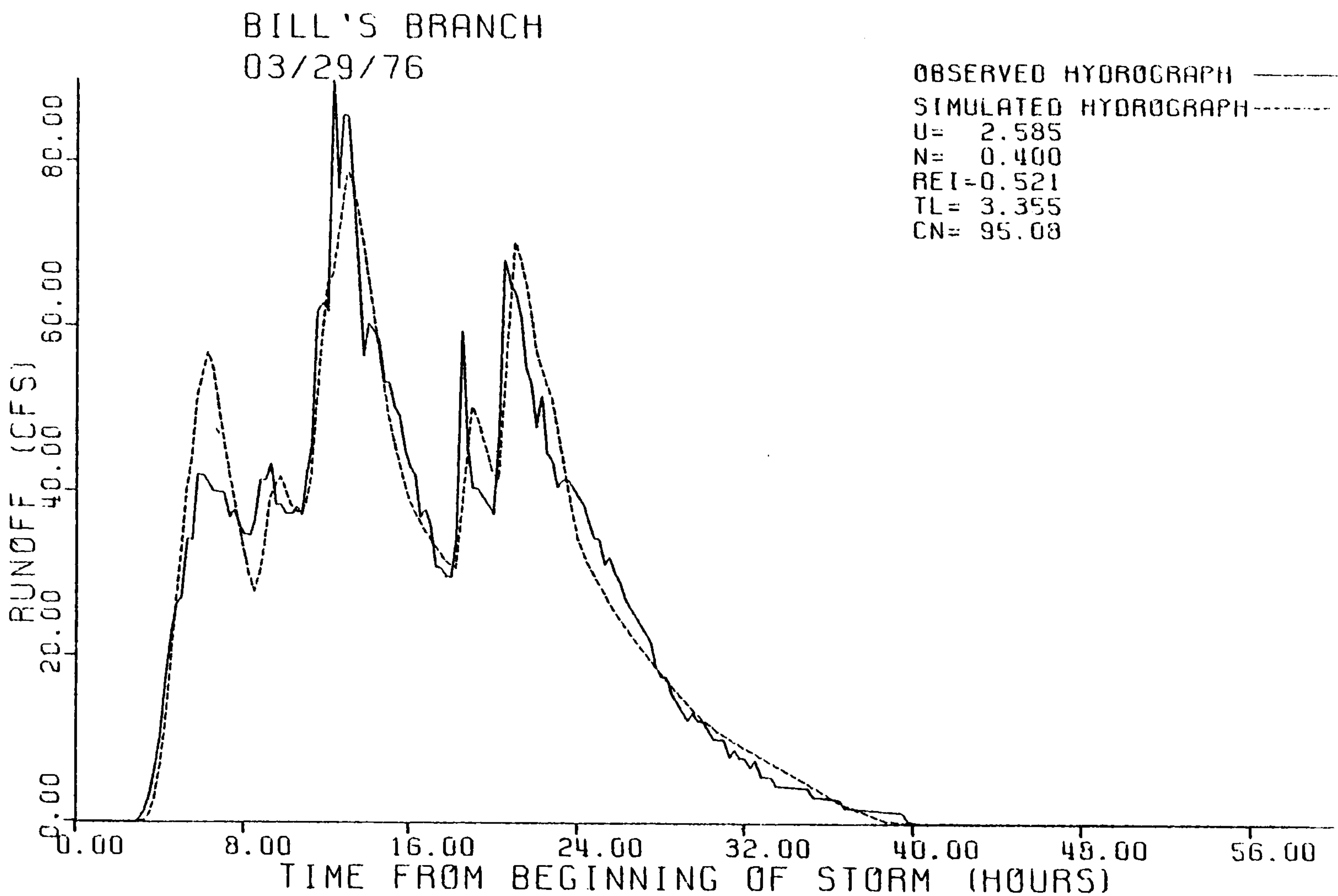

FIGURE 4.7

EXAMPLE OF GOOD FIT BETWEEN OBSERVED AND SIMULATED HYDROGRAPH - 3/29/76

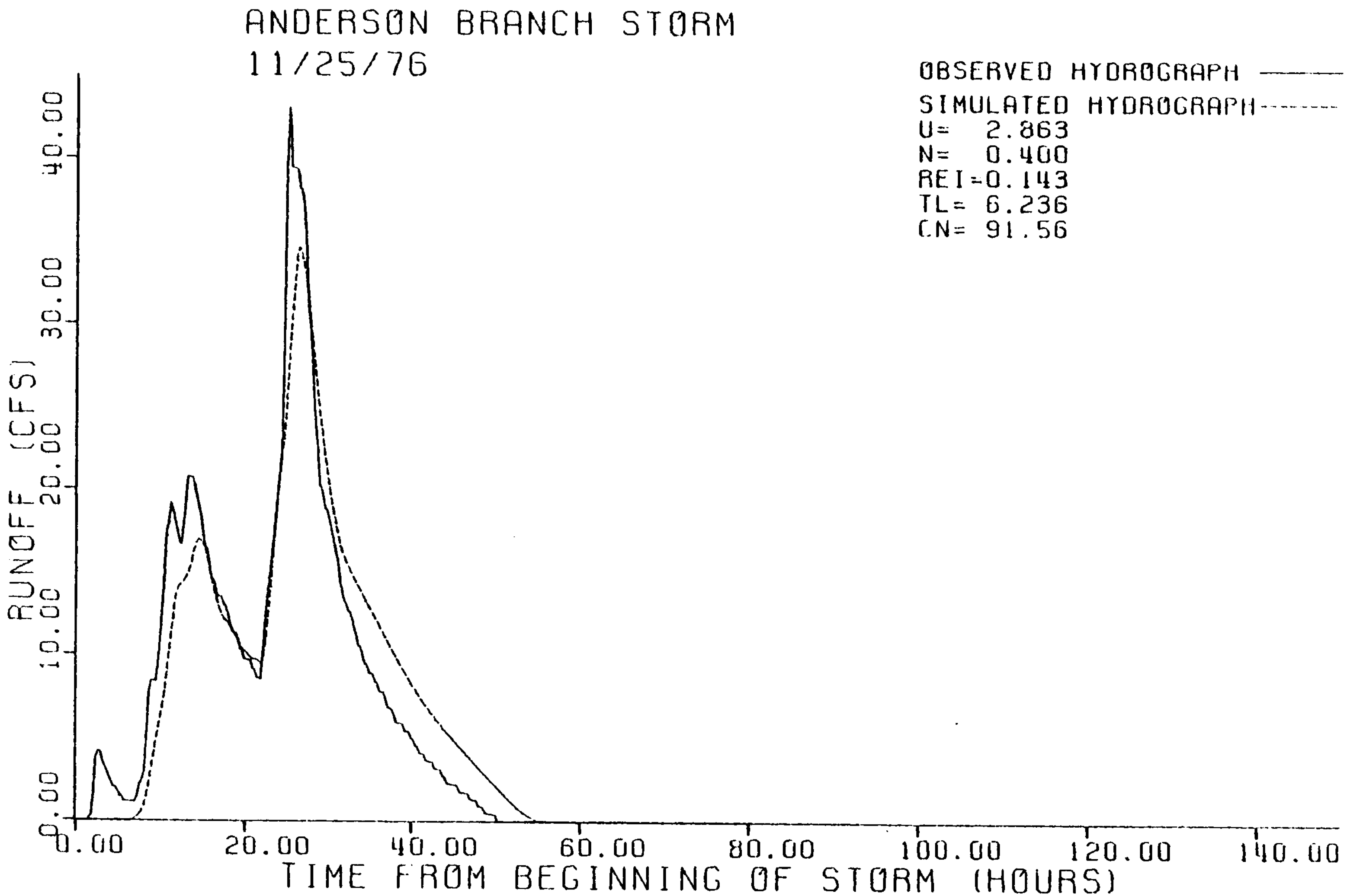

FIGURE 4.8

EXAMPLE OF FAIR FIT BETWEEN OBSERVED AND SIMULATED HYDROGRAPH - 11/25/76

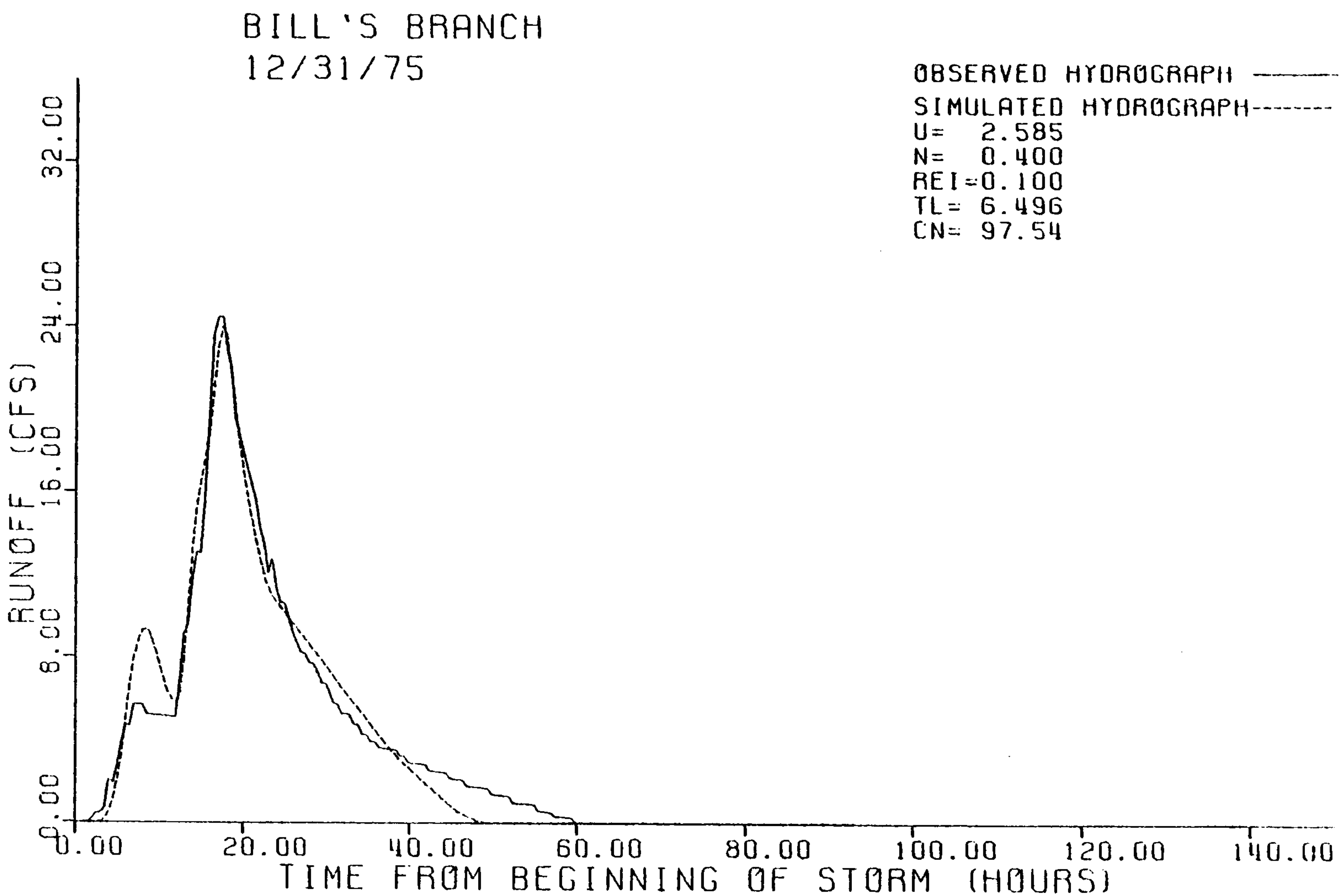

FIGURE 4.9

EXAMPLE OF GOOD FIT BETWEEN OBSERVED AND SIMULATED HYDROGRAPH - 12/31/75

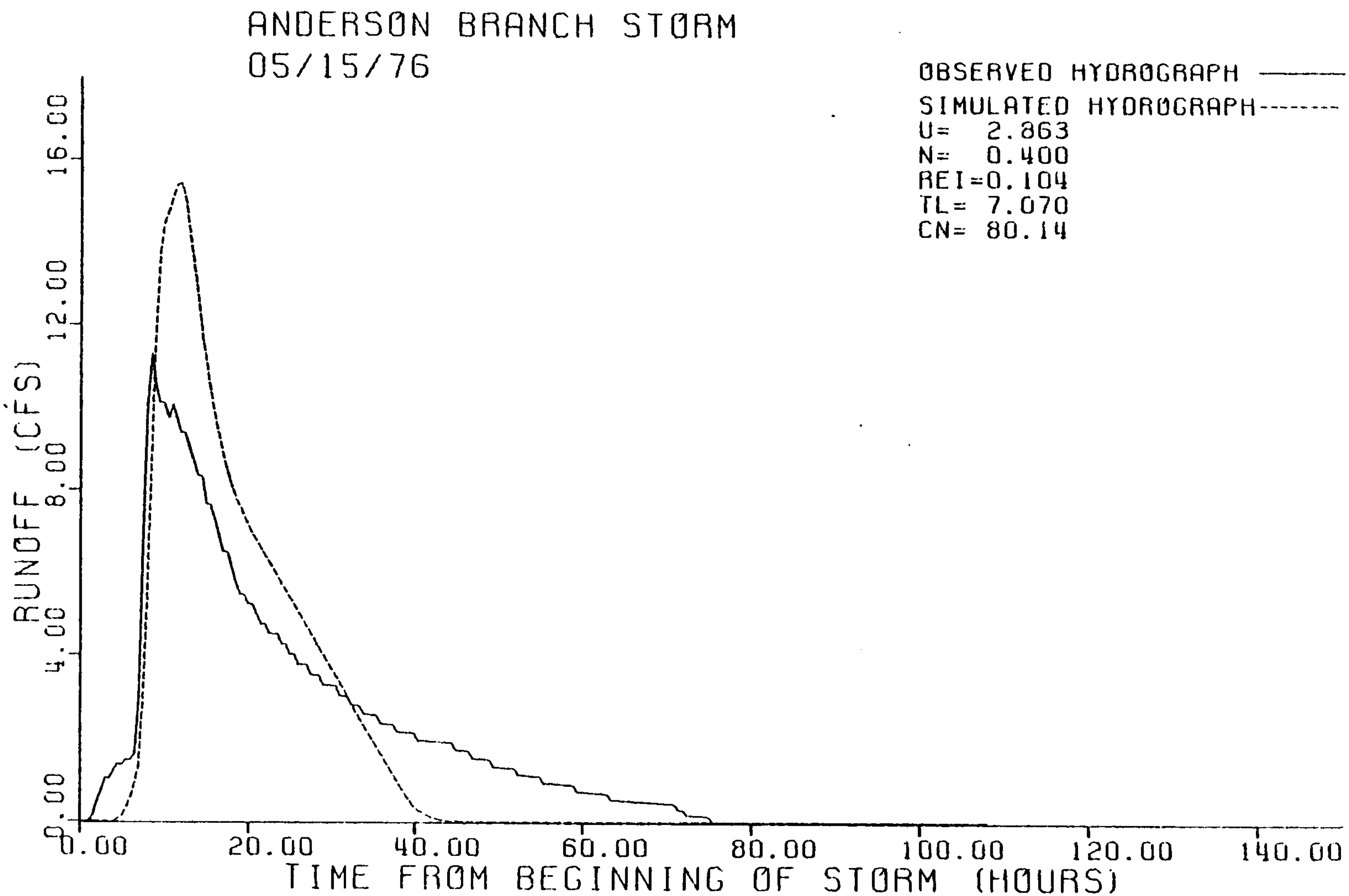

FIGURE 4.10

EXAMPLE OF FAIR FIT BETWEEN OBSERVED AND SIMULATED HYDROGRAPH - 5/15/76

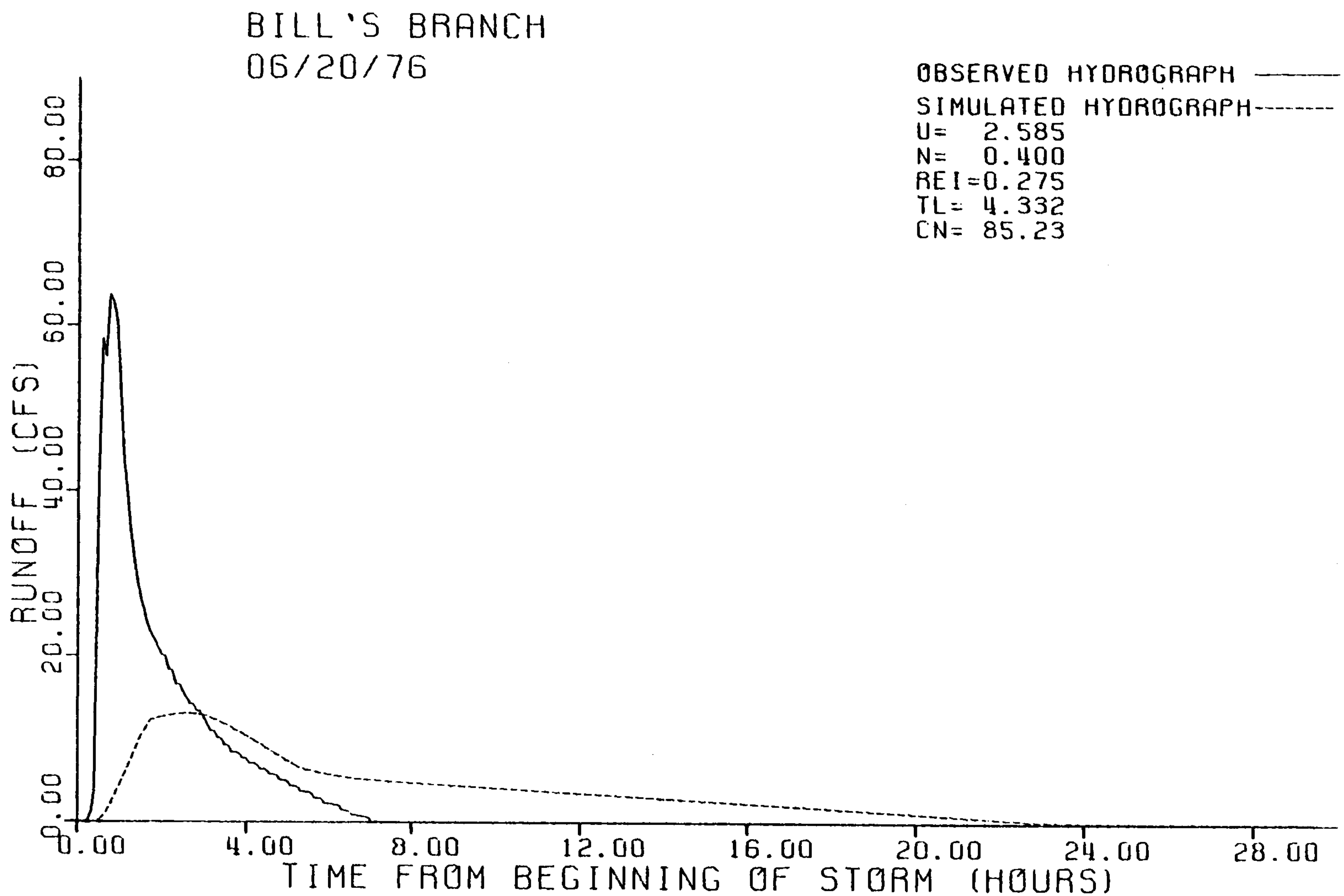

FIGURE 4.11

EXAMPLE OF POOR FIT BETWEEN OBSERVED AND SIMULATED HYDROGRAPH - 6/20/76

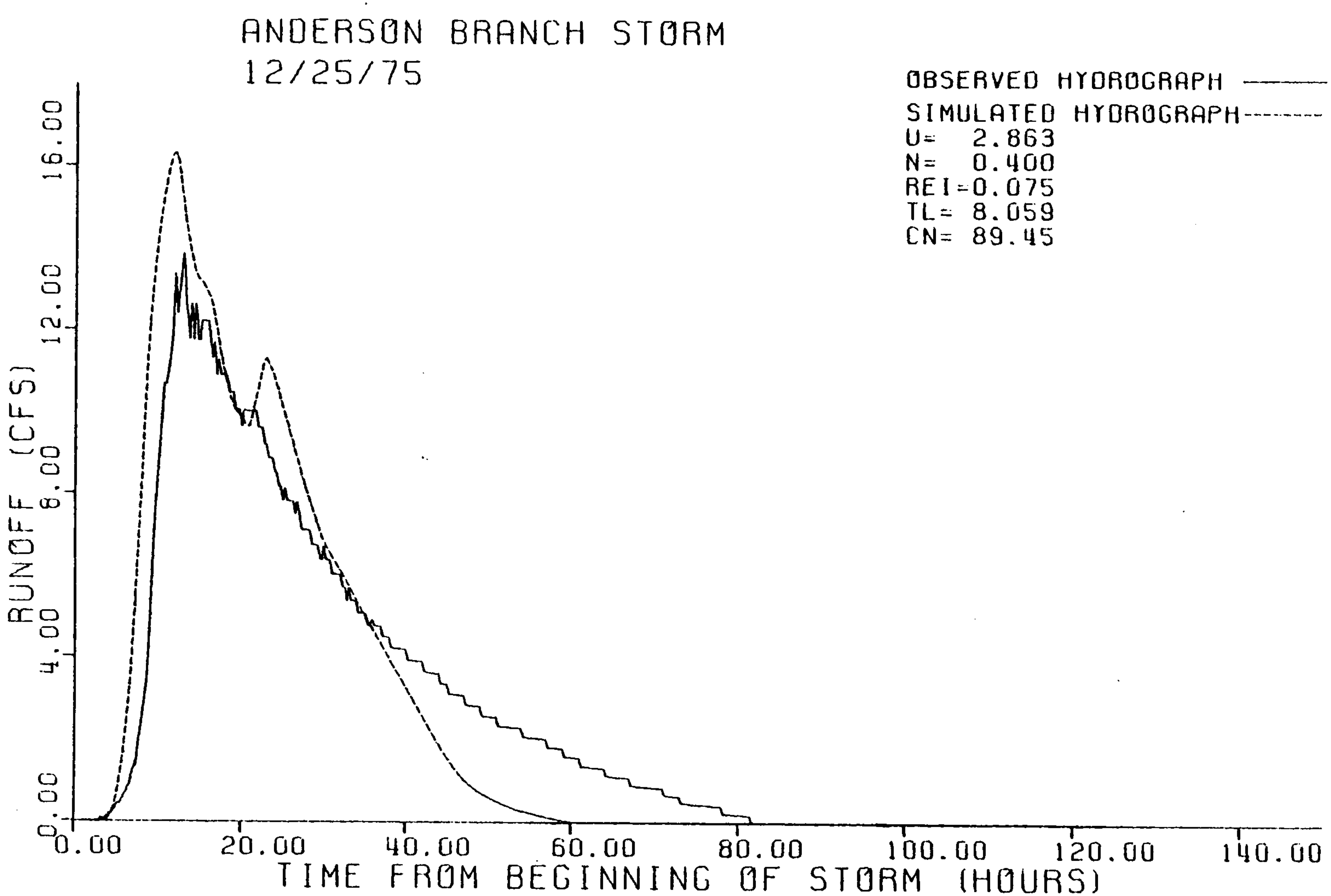

FIGURE 4.12

EXAMPLE STORM WITH RAINFALL ABSTRACTION AT 15 MINUTE INTERVALS

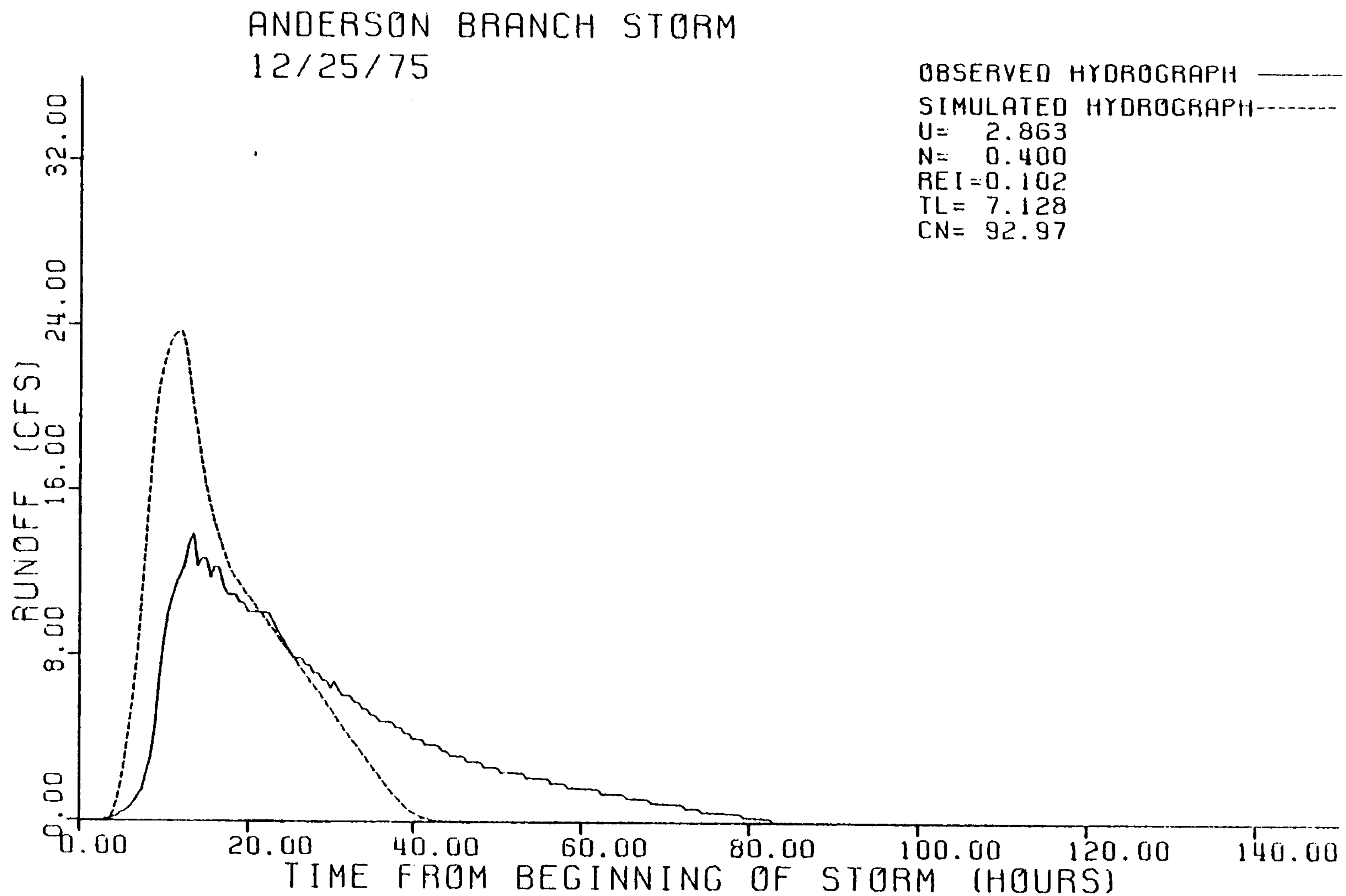

FIGURE 4.13

EXAMPLE STORM WITH RAINFALL ABSTRACTION AT 30 MINUTE INTERVALS grouped into four soil types--silty clay loam, silty clay, stoney fine sandy loam and very fine clay. Each of these soil types was additionally analyzed according to its dry and wet antecedent moisture conditions. A detailed evaluation of ERODE-I on the Hawaii soils is presented in Appendix A. A summary of those results are as follows:

1. The erosion reaction constant (the ratio of the transport to shear detachment) was associated with soil type when plot length was factored out.

2. The transport coefficient was found to be dependent upon soil particle size and density.

3. The rainfall detachment rate coefficient was found to contribute less than 10 percent to the erosion load rates.

4. ERODE-I simulation of accumulative runoff and load compared well with the observed data.

Spoil Bank Erosion Simulation

Since rainfall simulator data were not available for the New River Basin spoil bank sites, the simulation of rainfall erosion events was accomplished by using the model coefficients optimized on the Hawaii data. This transference of information was based on two primary factors. First, the denuded, tilled and graded Hawaii test plots closely resembled the physical characteristics found on steep contour strip mined spoil banks during reclamation. Secondly, the soil in the New River region was classified as a silty clay topsoil, a soil type evaluated from the Hawaii data.

For the spoil bank erosion simulations presented in Tables 4.22 through 4.24, an adjusted reaction coefficient of 2.45 and a transport coefficient of 15.5 were used. In addition, the spoilbank soil was considered to be in a loose, uncompacted and tilled state. The antecedent moisture condition was chosen such that any rainfall occurrence would result in imminent runoff. Thus the rainfall detachment coefficient would be negligible and a SCS Curve Number of 99 was used. These criteria approximate the worst conditions that might occur, be observed, or on which design would be based. Also, for the purpose of the examples herein, the average spoil bank's physical characteristics listed in Table 3.4 (page 65) were used as representative of the different watershed spoil banks.

The rainfall events used herein are those stipulated as minimum design criteria by the Department of Interior, Office of Surface Mining, Reclamation and Enforcement [9]. In the case of overland flow, a temporary design requires a two year storm recurrence interval and a permanent design requires a ten year storm recurrence. Both of these designs must be capable of passing the peak flow resulting from the above respective storms. Since no duration was required on these storms, a thirty minute duration was assumed. This should provide a large peak with reasonably large accompanying volumes that would be of concern. In addition, the minimum storage volume for sedimentation ponds must be based upon the storage required for the runoff from the ten-year, 24-hour precipitation event plus 0.1 acre-foot storage for sediment for each acre of upstream disturbed area. This requirement for sediment storage sets the sediment yield at 0.1 acre-foot for each acre disturbed.

TABLE 4.22

SPOIL BANK EROSION SIMULATION FOR 2 YEAR 30 MINUTE STORM (1.2 INCHES)

Watershed	Peak Flow (IN/HR)	Peak Load Rate (TON/FT WIDTH/HR)	Load (TON/FT WIDTH)	Average Depth of Erosion (IN)	Sediment Storage Required (ACRE-FT/ACRE DISTURBED LAND)
Anderson Branch	2.384	0.2966	0.129	0.09	0.007
Bill's Branch	2.384	0.3369	0.147	0.13	0.011
Bowling Branch	2.384	0.2967	0.129	0.11	0.009
Green Branch	2.384	0.4552	0.198	0.13	0.011
Indian Fork	2.384	0.3345	0.146	0.08	0.007

TABLE 4.23

SPOIL BANK EROSION SIMULATION FOR 10 YEAR 30 MINUTE STORM (1.8 INCHES)

Watershed	Peak Flow (IN/HR)	Peak Load Rate (TON/FT WIDTH/HR)	Load (TON/FT WIDTH)	Average Depth of Erosion (IN)	Sediment Storage Required (ACRE-FT/ACRE DISTURBED LAND)
Anderson Branch	3.589	0.4462	0.198	0.14	0.011
Bill's Branch	3.589	0.5071	0.225	0.20	0.017
Bowling Branch	3.589	0.4467	0.198	0.16	0.014
Green Branch	3.589	0.6853	0.304	0.20	0.016
Indian Fork	3.589	0.5035	0.223	0.12	0.010

TABLE 4.24

SPOIL BANK EROSION SIMULATION FOR 10 YEAR 24 HOUR STORM (5 INCHES)

Watershed	Peak Flow (IN/HR)	Peak Load Rate (TON/FT WIDTH/HR)	Load (TON/FT WIDTH)	Average Depth of Erosion (IN)	Sediment Storage Required (ACRE-FT/ACRE DISTURBED LAND)
Anderson Branch	0.208	0.0259	0.606	0.42	0.035
Bill's Branch	0.208	0.0294	0.689	0.61	0.051
Bowling Branch	0.208	0.0259	0.607	0.50	0.023
Green Branch	0.208	0.0398	0.931	0.43	0.051
Indian Fork	0.208	0.0292	0.684	0.37	0.031

Figures 4.14 through 4.16 show the hydrographs and load rate graphs resulting from the above erosion simulation on Bill's Branch spoil bank.

Table 4.25 shows the spoil bank erosion simulation that could occur if all of the disturbed areas in the watershed displayed the conditions described in the above example at the same instant of time. Since these conditions do not occur uniformly over the entire watershed at any specific time, these values should be considered upper limits of the range of sediment yield magnitudes. Method A in this table was based upon the linear miles of spoil bank in the watershed. Method B is based upon the total number of acres disturbed.

Sediment Yield Model

Load moduli were optimized for all six study watersheds in the New River Basin for both low flow and stormwater conditions. Substantial difference between the two occurred with the storm flow-load moduli being much higher. The watershed suspended sediment load moduli are listed in Table 4.26. These moduli were optimized using equation 3.61 and a data base consisting of stormwater flow and concentrations. Load rates were determined by convoluting the flow concentrations and the flow rate. The data base consisted of 43 storms that occurred in 1976 and 1977.

The regionalization model, equation 3.69, was evaluated by utilizing these optimized watershed moduli. This model asserts that the watershed suspended load is equal to the suspended load produced from the disturbed areas plus the load produced and stored from the last

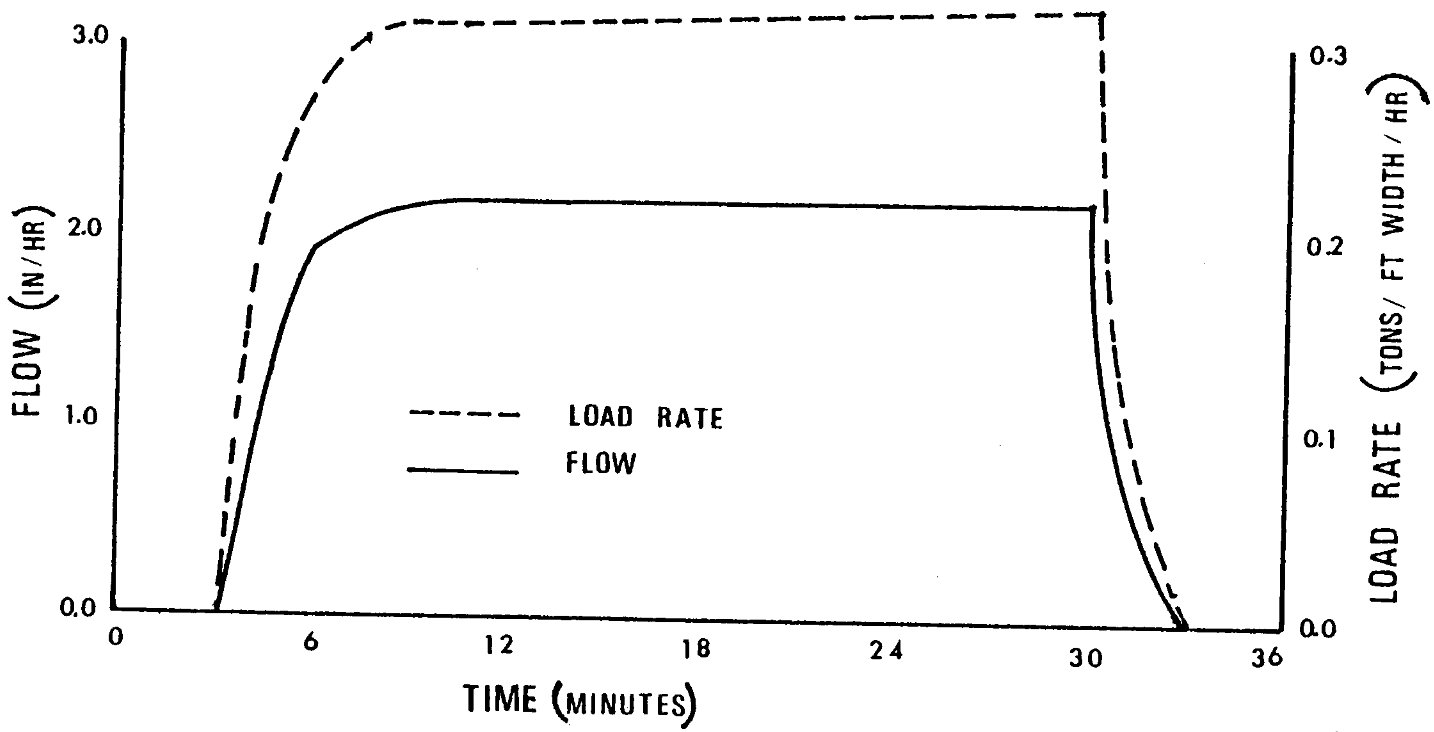

FIGURE 4.14

SPOIL BANK SIMULATION - BILL'S BRANCH 2 YEAR 30 MINUTE STORM

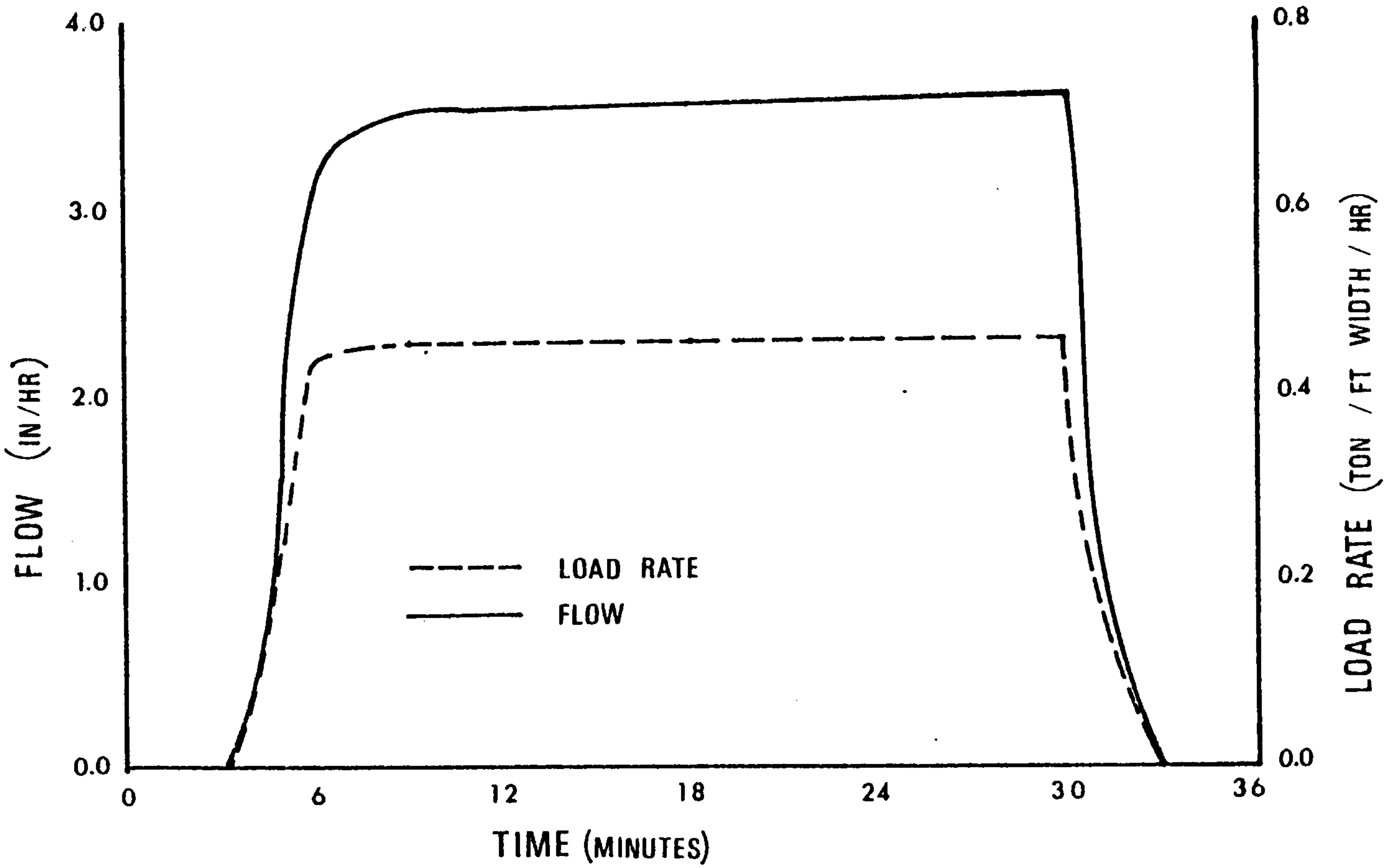

FIGURE 4.15

SPOIL BANK SIMULATION - BILL'S BRANCH 10 YEAR 30 MINUTE STORM

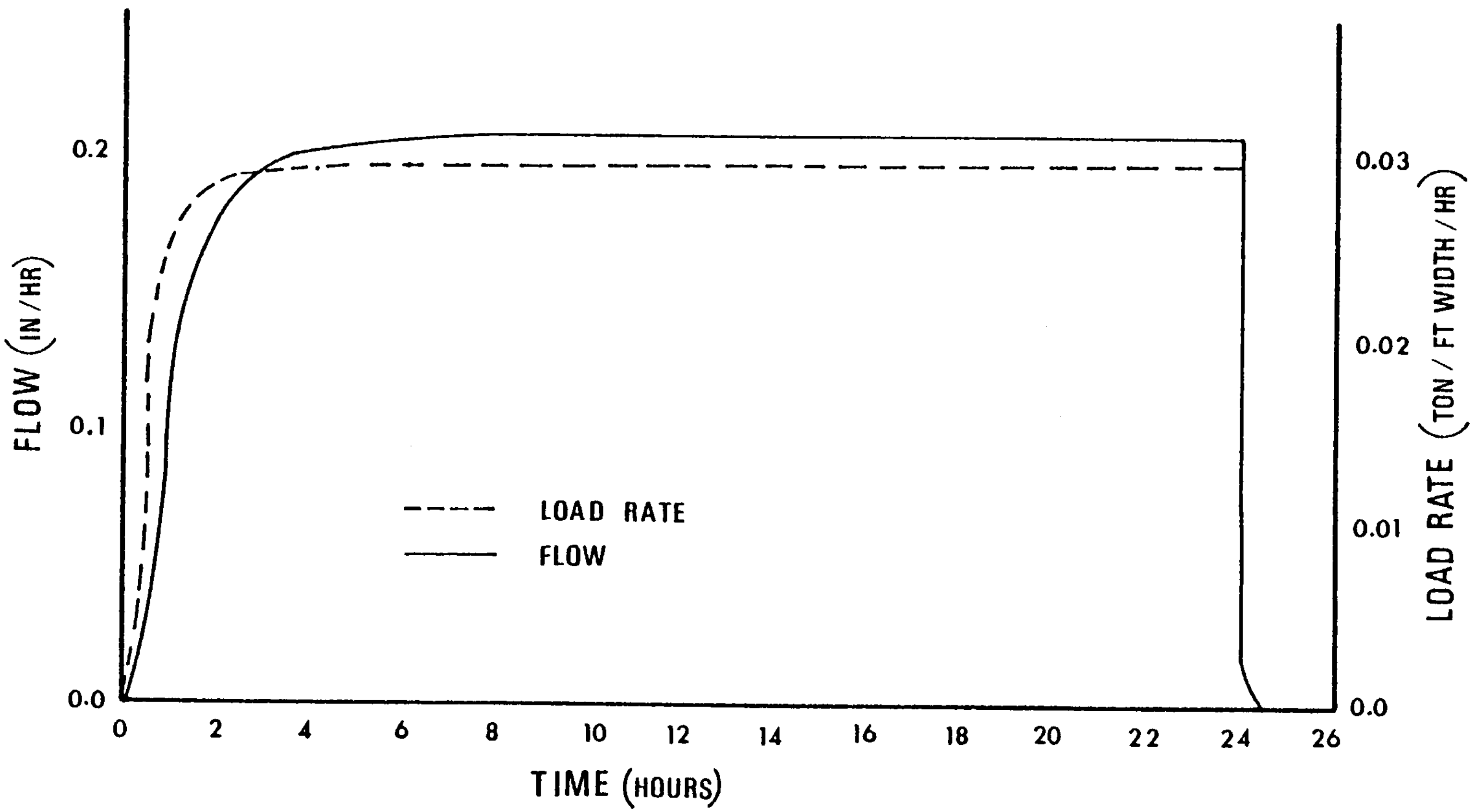

FIGURE 4.16

SPOIL BANK SIMULATION - BILL'S BRANCH 10 YEAR 24 HOUR STORM

TABLE 4.25

TOTAL SPOIL BANK EROSION

Watershed	10 YEAR 24 HOUR		2 YEAR 30 MINUTE		10 YEAR 30 MINUTE	
	Method A* (tons)	Method B** (tons)	Method A* (tons)	Method B** (tons)	Method A* (tons)	Method B** (tons)
Anderson Branch	5861	4192	1246	893	1912	1368
Bill's Branch	6183	6217	1318	1325	2016	2027
Bowling Branch	6920	4846	1081	626	2257	1581
Green Branch	22244	28308	5596	6036	8562	9237
Indian Fork	59509	44447	12686	9478	19421	14507

*Method A is based upon linear miles of spoil bank.

**Method B is based upon acres disturbed.

TABLE 4.26

WATERSHED SUSPENDED SEDIMENT LOAD MODULI

Basin	Load Modulus (LB/ACRE-IN of Runoff)	Number of Observations	Coefficient of Correlation	Standard Error of Estimate
Anderson Branch	3737.69	130	0.79	733.3
Bill's Branch	596.71	144	0.91	130.68
Bowling Branch	352.18	121	0.86	78.4
Green Branch	592.50	83	0.87	594.6
Indian Fork	567.79	125	0.78	715.1
Lowe Branch	4.40	74	0.74	4.4

storm event in the undisturbed areas, minus the load deposited in the watershed between the disturbed areas and the watershed outlet. Using the matrix of information presented in Table 4.27 the coefficients of the model C_1, C_2, and C_3 were optimized using principle components regression so as to filter out the interactive affects of the variables. The results of the optimization are shown in Table 4.28 and are compared with results obtained from an urban study [125].

Two separate optimizations were performed. The first optimization included all the watersheds in the data base. The second optimization was performed with Anderson Branch removed. This segregation was due to the significant difference in land use of the Anderson Branch watershed, i.e. mountain top removal. This censoring greatly improved the optimization results. A plot of the regionalized load moduli versus the observed load moduli using this set of coefficients is shown in Figure 4.17.

Table 4.29 shows the results of simulating individual storm suspended sediment load rates and total loads. These simulations were obtained by convoluting the watershed suspended sediment load modulus with the storm hydrograph. Anderson Branch simulations used the load modulus given in Table 4.26 . The other watershed simulations used the regionalized load modulus model, equation 3.69. Storms that did not have complete hydrographs or rainfall data from which a hydrograph could be produced were not simulated, since total storm loads could not be determined.

TABLE 4.27

MATRIX FOR WATERSHED SUSPENDED LOAD MODULUS MODEL (STORM CONDITIONS)

Basin	Observed Load Modulus (LB/ACRE-IN of Runoff)	Percent Stripped (PS)	Percent Forest (PF)	Lag Modulus (μ) (HRS)	μ * PF
Anderson Branch	3737.69	8.1	91	2.99	272.09
Bill's Branch	569.71	10.8	88	1.80	158.40
Bowling Branch	352.18	3.1	95	2.93	278.35
Green Branch	592.50	24.1	74	3.30	244.20
Indian Fork	567.79	20.0	78	12.33	366.60
Lowe Branch	4.40	0.0	98	7.17	365.54

TABLE 4.28

RESULTS OF OPTIMIZATION OF LOAD MODULUS MODEL (STORM CONDITIONS)

	C_1	C_2	C_3	R^{2*}
All Six Stripped Basins	-5.70	-2.67	1788.59	0.03
Stripped Basins Without Anderson Branch	18.17	1.28	572.67	0.85
5 Urban Basins (4 in Knoxville, Tennessee; 1 in Durham, North Carolina)	16.7	21.5	62.3	0.94

*R^2 is Coefficient of Determination

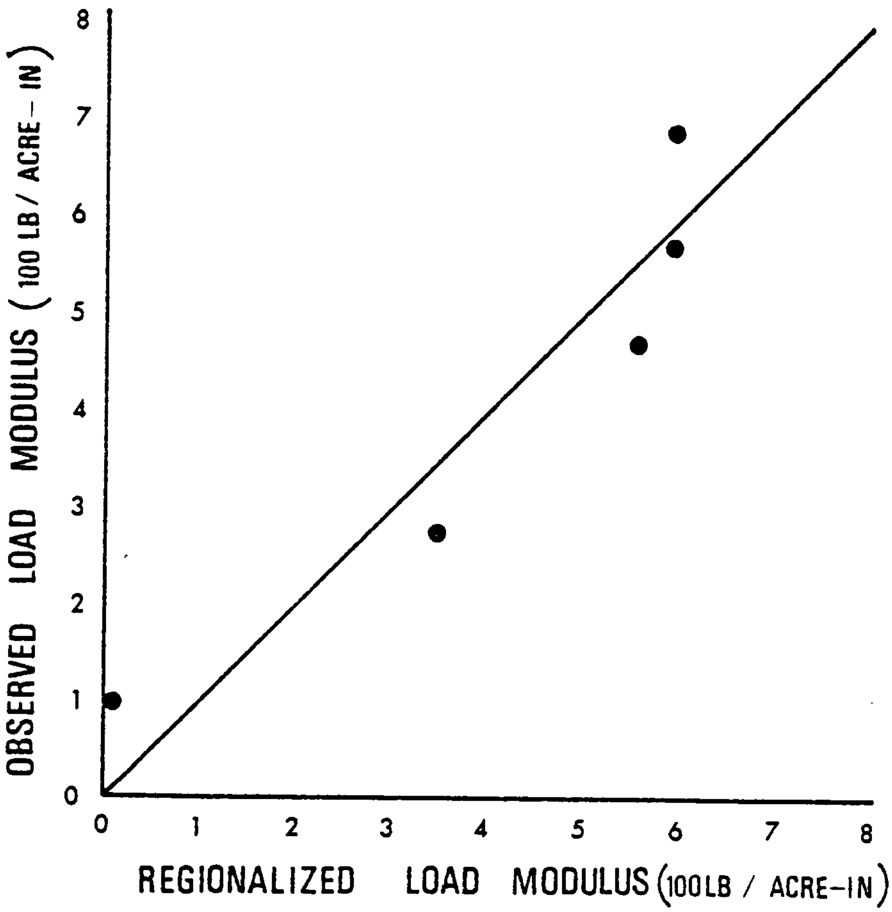

FIGURE 4.17

OBSERVED VERSUS REGIONALIZED LOAD MODULUS

TABLE 4.29

SIMULATED LOAD AND LOAD RATE RESULTS

Basin	Storm Date	Peak Channel Flow (CFS)	Time to Peak		Suspended Solids Peak Load Rate		Total Load	
			Observed (HRS)	Simulated (HRS)	Observed (LBS/S)	Simulated (LBS/S)	Observed (TONS)	Simulated (TONS)
Anderson Branch	05/27/76	0.93	39.00	39.00	0.005	0.17	0.71	0.71
	05/28/76	6.67	14.83	14.83	2.75	2.01	2.27	2.07
	10/06/76	0.41	24.00	24.00	0.09	0.14	0.53	0.50
	06/24/77	8.68	18.91	20.83	22.15	7.89	65.72	64.10
	10/25/77	4.78	41.00	41.00	4.27	4.55	9.95	9.67
Bill's Branch	03/05/76	3.24	16.00	16.00	0.12	0.27	0.42	0.62
	05/28/76	9.45	13.50	13.00	1.13	1.12	2.92	4.12
	10/06/76	2.62	21.25	21.25	0.11	0.25	0.21	0.57
	06/24/77	4.26	19.00	18.75	0.70	0.58	1.12	0.91
	07/29/77	0.82	6.75	6.75	0.05	0.08	0.09	0.20
	09/06/77	8.99	26.25	26.25	0.97	1.17	1.47	1.17
Bowling Branch	03/05/76	2.72	15.50	15.50	0.05	0.05	0.20	0.67
	06/24/77	8.64	20.16	20.16	1.84	0.66	5.69	5.37
	09/06/77	6.53	33.25	27.66	0.12	0.26	1.41	5.40

TABLE 4.29 (CONTINUED)

Basin	Storm Date	Peak Channel Flow (CFS)	Time to Peak		Suspended Solids Peak Load Rate		Total Load	
			Observed (HRS)	Simulated (HRS)	Observed (LBS/S)	Simulated (LBS/S)	Observed (TONS)	Simulated (TONS)
Green Branch	03/05/76	5.01	17.00	17.00	0.31	0.47	1.30	1.67
	05/28/76	22.60	13.00	13.50	7.93	4.00	25.00	23.27
	10/07/76	10.60	21.25	21.25	2.21	2.99	13.33	12.07
Indian Fork	03/05/76	26.90	16.00	17.50	1.53	1.90	6.44	8.51
	09/06/77	65.90	26.50	26.50	22.46	8.50	52.96	50.67
Lowe Branch	03/05/76	1.20	17.25	18.25	0.002	0.02	0.02	0.39
	06/24/77	1.75	23.50	23.50	0.003	0.03	0.03	0.23

Simulated Effects of Strip Mining

The following example simulations are presented to show how the models TENN-I, ERODE-I and LOAD-I may be used to investigate different aspects of contour strip mining on watersheds.

Undisturbed Versus Heavily Mined

A two-hour duration storm with a return period of five years was selected for demonstrating the simulation of the effects of watershed changes caused by mining a previously unmined watershed. Lowe Branch was used since it represents the only undisturbed watershed in the matrix.

Hydrographs and sediment loadographs were simulated for Lowe Branch for the present zero percent disturbance and a projected 24 percent disturbance. These conditions were simulated using TENN-I, the watershed runoff model and LOAD-I, the watershed load modulus model. The results are shown in Figure 4.18.

Design rainfall volume was two and one half inches with a SCS Curve Number of 60. This change in land use doubled the peak flow and increased the runoff volume about 10 percent. With this induced stripping, the sediment load increased from zero to 47 tons of sediment for the storm.

Sediment Delivery Ratio

Using the load modulus model, equation 3.69, a sediment delivery ratio, SDR, can be simulated. Defining the sediment delivery ratio as the ratio between the watershed output load to the total source load leads to the following

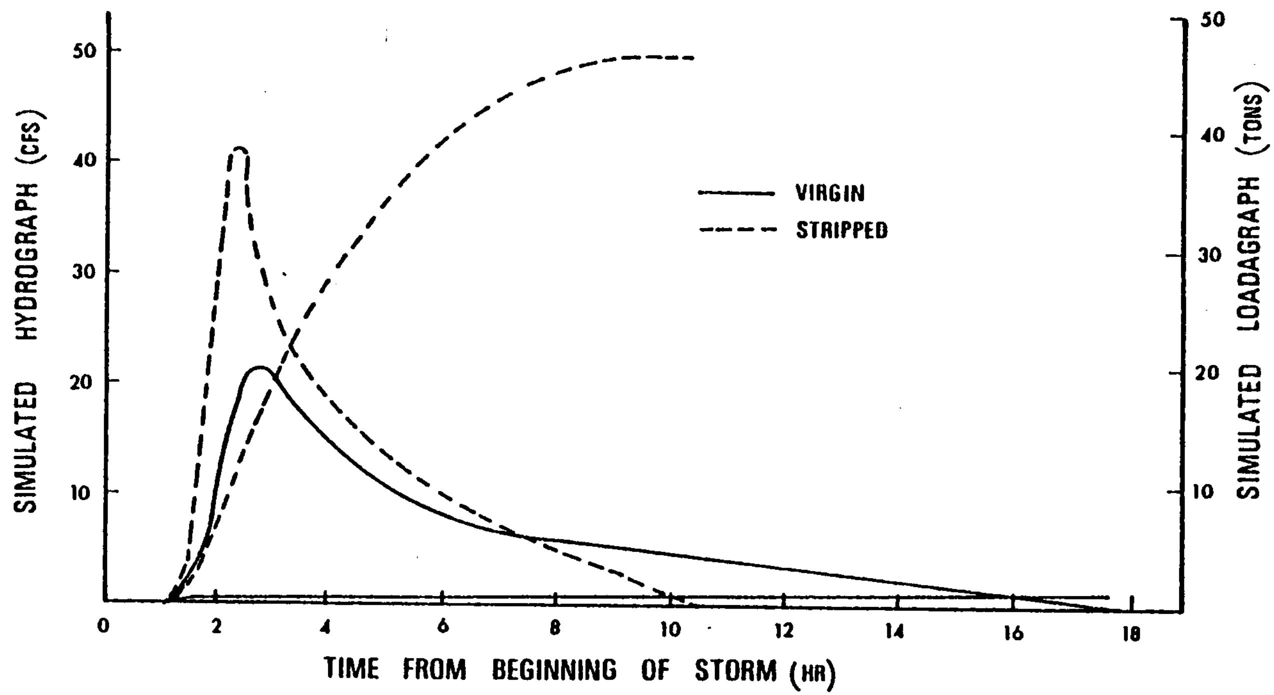

FIGURE 4.18

SIMULATED HYDROGRAPH AND LOADOGRAPH FOR LOWE BRANCH

$$SDR = \frac{\mu_W}{C_1 * PS + C_3} \qquad (4.1)$$

where μ_W is the watershed load modulus, C_1 is index of erosion load generated from equation 3.69, C_3 is index of the watershed stored sediment from equation 3.69, and PS is percent stripped. SDR may be considered a watershed constant if land use remains constant. As stripping activity increases, PS increases and PF, percent forest, decreases. C_1, C_2 and C_3 of the load modulus model remain essentially constant for a given mining method.

The results of using this method are shown in Table 4.30.

Spoil Bank Load Modulus

A comparison of load moduli simulated by the spoil bank erosion model was made with the load moduli derived from watershed suspended sediment loads. Independently, load modulus for the mean spoil banks can be simulated by using equation 3.57 and the same constants used in the earlier erosion simulations.

By comparing equations 3.64, 3.66 and 3.69, the following expression for spoil bank load modulus from the watershed load model can be determined

$$18.17 * \frac{A_B}{A_W} * 100\% = \mu_B * \frac{RD_B * A_B}{RD_W * A_W} \qquad (4.2)$$

Hence, the mean spoil bank load modulus is

$$\mu_B = 18.17 \frac{RD_W}{RD_B} \qquad (4.3)$$

For conditions where the antecedent moisture conditions are saturated, i.e. Curve Number is 100, the ratio of runoff volume of the watershed

TABLE 4.30

SIMULATED SEDIMENT DELIVERY RATIOS

Watershed	SDR * 100%
Anderson Branch	52
Bill's Branch	72
Bowling Branch	43
Green Branch	69
Indian Fork	50
Lowe Branch	18

to that of the spoil bank is approximately equivalent to the ratio of total area to disburbed area. The simulated load moduli for the spoil banks are listed in Table 4.31. Method A in the table calculated load modulus using equation 4.3. Medhod B in the table determined load modulus from equation 3.57. It is interesting to note that, for the time period considered in developing Table 4.31, only Anderson Branch and Bowling Branch were undergoing strip mining activity.

Comparisons with Urbanization

One of the major land uses today, urbanization, produces great impetus to convert more and more land to its use. As such, it is of interest to compare the effects of urbanization on stormwater with the effects of coal strip mining on stormwater. A comparison herein was made between Lowe Branch watershed and West Town Branch of Fourth Creek in Knoxville, Tennessee, an urban watershed. Lowe Branch was undisturbed, where West Town Branch has been converted by development to 45 percent impervious with a remaining 10 percent in forest. West Town is much flatter, as urban areas generally are, and has a long history of farming and use for pasture. The two basins are comparable in size. Lowe Branch is 589 acres or 0.92 square miles, while West Town is 525 acres or 0.82 square miles.

Lag modulus and load modulus were simulated for Lowe Branch for a condition of 24 percent total acreage disturbed. This is generally about the largest area possible to strip mine in the steep mountainous areas of Tennessee. For West Town, lag modulus and load modulus were simulated for the pre-urbanized or rural conditions. These results, as well as the observed load and lag moduli are presented in Table 4.32.

TABLE 4.31

SIMULATED LOAD MODULI FOR SPOIL BANKS

Watershed	Load Modulus (TONS/ACRE-INCH RUNOFF) Method A*	Method B**
Anderson Branch	10.2	13.9
Bill's Branch	8.4	20.0
Bowling Branch	28.9	29.3
Green Branch	3.8	17.6
Indian Fork	4.6	27.0

*Method A is based upon the Watershed Load Modulus Model.

**Method B is based upon the Erosion Model.

TABLE 4.32

COMPARISON OF LAG MODULUS AND LOAD MODULUS AS AFFECTED BY URBANIZATION AND STRIP MINING

	Lag Modulus (HR)			Load Modulus (LB/ACRE-IN RUNOFF)		
Watershed	Before	After	% Decrease	Before	After	% Increase
Lowe Branch	3.30	1.68	51	4	845	21125
West Town	3.50	0.60	83	8	700	8750

The results show that both of the land use changes have a dramatic effect upon the lag modulus. In both cases, the lag modulus decreases. Thus, the lag time decreases and the peak flow of each watershed URF increases. Hence, for a storm occurring on these two watersheds after urbanization and mining have taken place, the time to peak flow would greatly decrease while the peak flow of runoff would considerably increase. Urbanization, here, appears to have more of an effect on lag modulus and thus its watershed runoff peaks than strip mining does on its watershed runoff peaks. By contrast, strip mining of Lowe Branch to 24 percent produces a suspended sediment load per acre-inch of runoff that is only about 20 percent greater than that produced by urbanization of West Town.

CHAPTER V

DISCUSSION

Stormwater Simulation Model

Unit Response Function

The watershed URFs determined in this study showed considerable variability from watershed to watershed and from storm to storm. This variation was explained, to a large extent, by the variation in lag time and resulted in a single curve, NURF, from which all watershed URFs could be simulated.

Other sources of variation observed in the optimized URFs can be explained in terms of natural and artificial inducements. The natural variations are caused by the nonuniformity of rainfall intensity, rainfall distribution and soil moisture conditions within the watershed during a storm event. Sources of artificial variance are twofold. The first source is base flow separation, a problem that has always plagued hydrologic studies. This separation of the storm hydrograph from the total watershed hydrograph can be minimized by observing the hydrograph to its complete recession. This allows the double triangle concept to be more effective. Separation of base flow in this study was accomplished by using a straight line technique. With this method, a straight line is drawn from the first observed storm discharge to the last observed storm discharge on the recession hydrograph. The ordinates of this line represent base flow.

The second source of artificial variance is induced by the abstraction time increment used to optimize a URF from an observed hydrograph. Since the URF time parameters are restricted to integer values of DT, the time increment used in abstracting rainfall values, large values of DT will increase the probability that the "true" time parameters of the URF were not optimized. This variation in URFs caused by different DT values can be observed in Tables 4.1 through 4.4 (pages 69-72).

The URF time to peak parameter was the most critical value affected by this DT increment phenomenon, since it has the smallest time value. Thus, if the ratio of T1/DT is small, large relative errors may be induced. For example, assume the "true" optimum value of T1 was 1.5, but DT was equal to 1. Then the best value for which T1 could be optimized would be either 1.0 or 2.0. This would result in a variance of at least 50 percent of the step size. Introduction of this type of an accuracy error into T1 could cause a chain reaction that would effect the optimization of all other URF parameters.

The individual storm NURFs vary much the same as the URFs, although not to as great a degree. This variation or noise was most likely caused by the variation in the URF.

Peak flows of the unit hydrograph have been widely recognized to be a function of rainfall excess intensity [43, 64] and thus of lag time. Correlations of lag time with URF peak flow were shown to be excellent with coefficients of determination in excess of 0.95. However, the coefficients of determination for T1 were not as good and varied from 0.39 to 0.89. Thus, weaker correlations are most likely the result of natural noise found in flow measurements, and the result of having a T1/DT ratio less than four.

The correlations of lag time with the other URF time defining parameters were much stronger. These stronger correlations are the result of the time parameters to DT ratio being relatively large. Under this condition, the time parameter would not be as influenced by the DT bias. T23 was not optimized but was calculated from the URF optimized parameters T1, T2, T3, UP and UR. The lower, but still good, correlations obtained for T23 are the results of bias present in the other parameters. T3, since it represents the duration of runoff, is obviously biased by the method used to separate base flow.

To a large degree, the confidence that can be placed in the NURF regression coefficients for all four watersheds depends upon the number of data points available. Small samples of data points may be adversely affected by outliers. To minimize this problem, every storm was used in the optimization to determine the regression coefficients that define the basin NURF representative of strip mining. This NURF is shown in Figure 4.5 (page 88). Although this method reduces the influence of an outlier, it increases the influence of Bill's Branch watershed, since it accounts for the largest sample size.

Although the data are scattered to some extent, this analysis has still shown that there is a definite positive relationship between lag time and time scale of its associated unit hydrograph and that flow ordinates are inversely related to lag time. It has also been shown that for the study watersheds there appears to exist a unique relationship between lag time and the URF, i.e. the NURF. Unique NURFs for other land uses within the Tennessee Valley have been reported and are shown in Figure 4.5. It can be clearly seen from this figure that the New River Basin NURF closely approximates that of the completely forested watersheds.

Thus, given a lag time for a watershed with one of the land uses given in Figure 4.5 (page 88), the URF can be simulated from the NURF with that land use. This model results in a slight reduction of URF accuracy, but it does fulfill the objective of simulating URFs for any lag time within the context of the limitations and reliability of the data.

Lag Modulus

Lag modulus simulation is the key to URF simulation using TENN-I. Without it, lag time could not be determined from equation 3.12. Hence, the storm URF and watershed runoff hydrograph could not be simulated.

Lag modulus was formulated assuming that the system was lumped and time invariant. For low intensity, short duration storms, it is questionable whether or not these conditions are met. Hence, the lag modulus formulation responds best to high intensity and/or long duration storms--storms whose watershed responses are of more interest. Under these latter storm conditions, the lumped, time invariant assumptions are realistic. Lumped assumptions were necessitated because of limited data availability. Under these assumptions, the lag modulus considers the land use and rainfall distribution patterns to be uniform across the watershed. Similarly, like the URF variation, the lag modulus variation will be greatest for small storm intensities as a result of nonuniform spacial rainfall distribution.

The time invariant assumption required that during the period of analysis the land use remained constant, the antecedent moisture across the watershed remained constant, and the ongoing mining activities did not change the watershed characteristics, such as drainage area and percent stripped.

The variability of the lag moduli were smaller than the variation of its components, REI and lag time, as can be seen in Table 4.15 (page 89). To equalize the influence of each watershed, only the mean lag modulus from each watershed was used to evaluate the regionalized lag modulus model. This regionalization scheme resulted in good estimation of the mean watershed lag moduli, as can be seen in Figure 4.6 (page 92).

Since lag modulus is a function of rainfall intensity and lag time, and since lag time is a function of storm volume, it might be possible to consider lag modulus on a frequency basis. This was suggested by the plot shown in Figure 5.1. In this figure, the individual storm lag moduli of Bill's Branch were plotted versus the longest storm burst duration that occurred during that storm. Storms with less than 0.05 weighted rainfall excess intensity were omitted. This curve suggests that lag modulus could be a function of storm duration. Only Bill's Branch was considered here because of its larger data base.

Storm Hydrograph Simulations

The storm hydrograph simulation model, TENN-I, used in this study considered the watershed's response to rainfall to be lumped, time invariant and linear within a storm. In addition, it allowed the response to be time variant and nonlinear from storm to storm.

In general, simulations of storms with low weighted rainfall excess intensity and/or small total runoff were poor. These storms are of

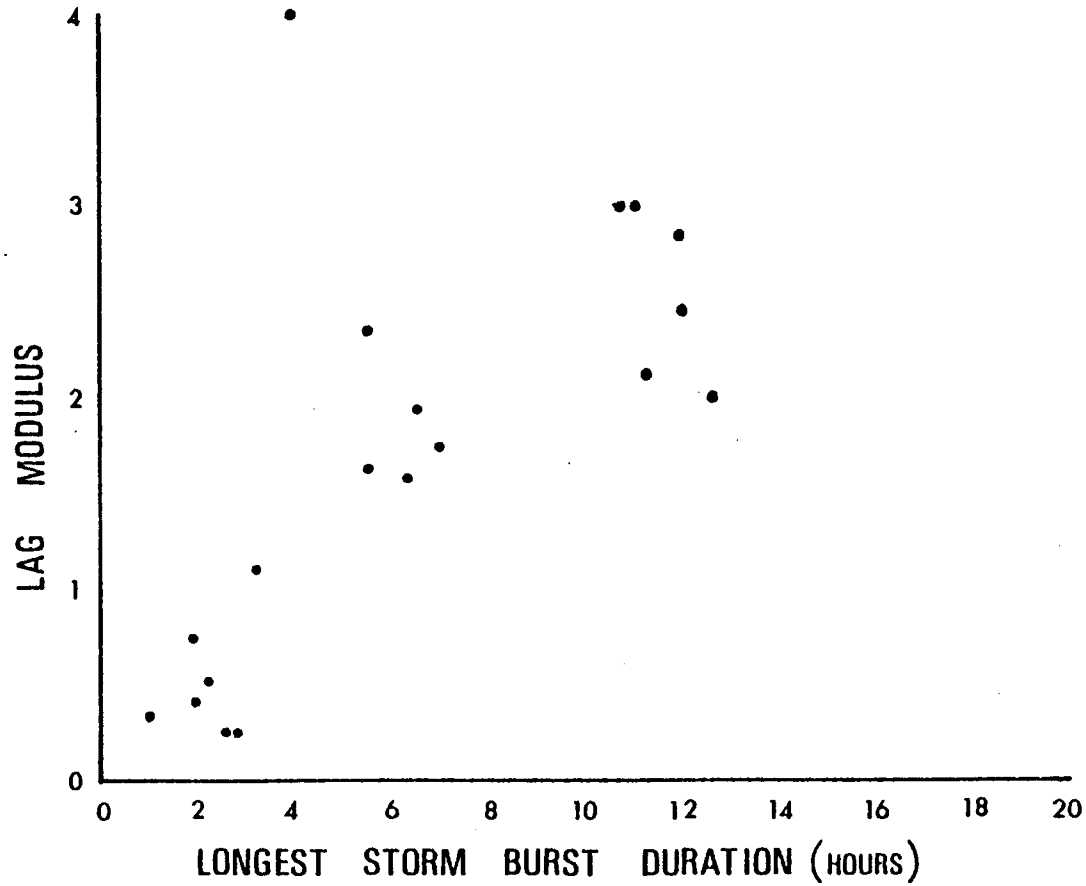

FIGURE 5.1

LAG MODULUS VERSUS LONGEST STORM BURST DURATION little hydraulic significance since hydraulic designs are generally based upon storms having much larger return periods. Small storms were poorly simulated because they often violate the basic assumptions of the lumped system. Uniform rainfall distribution and uniform antecedent moisture conditions over the complete watershed area seldom exist for small storms or isolated thundershowers. As runoff volume and surface area decrease, flow is influenced more by the micromechanics of the basin. Hence, the nonuniformity of the watershed geometry along with the nonuniformity of the land use become more critical. Accounting for the violations of the lumped assumptions would require a model based upon a micromechanic point of view opposed to a macromechanic point of view. Such a model would most likely become mathematically intractable.

The use of the SCS Curve Number method resulted in an accurate volume determination. However, this method often caused the time to peak to be delayed. This resulted from simulating a substantial amount of storage before inception of runoff. The selection of a rainfall abstraction time was extremely critical to the simulation technique. For the storms simulated, a DT in excess of fifteen minutes often gives unreliable results. An example of this is shown in Figures 4.12 and 4.13 (pages 105 and 106). The DT in Figure 4.12 is fifteen minutes while it is thirty minutes in Figure 4.13. The lumping of rainfall caused by larger DT units can change the shape of the simulated hydrograph significantly.

Multiple peak storms were generally well simulated as were relative short duration, intense storms and long duration, intense storms. Since these are the storms that are generally important for design, the model was considered successful in fulfilling the objectives of adequately simulating storms of hydraulic significance.

Erosion Simulation Model

The erosion simulation model, ERODE-I, was evaluated using Hawaii rainfall simulator data. The variation in the reaction, transport and rainfall detachment coefficients was shown to be a function of soil type and soil moisture conditions. Simulation of the Hawaii rain and erosion events was excellent. A detailed discussion of the evaluation of the Hawaii data, the evaluated constants and the storm event simulations can be found in Appendix A.

The reaction, transport and rainfall detachment coefficients are lumped and time invariant. Hence, uniform spacial distribution of soil type, rainfall and soil characteristics over a uniform plane are the prerequisite assumptions. These assumptions are closely approximated for uniform planes or a series of uniform cascading planes where the soil is denuded, tilled and graded, such as the Hawaii test plots and steep contour spoil banks when reclamation is in progress. Under present requirements to save and replace topsoil, the uniform soil characteristics should be more closely approximated than in the past, at least during the reclamation and the early age of the spoil bank. Uniform rainfall over the site cannot be expected to occur for small events, but should occur for storm events of interest.

Since the erosion coefficients were optimized on a time invariant basis, they should not be used to determine the erosion on an aged spoil bank. The spoil bank load moduli found from both ERODE-I and LOAD-I lend credence to this premise. The watershed load moduli obtained by each of these methods displayed similar results when active watershed mining occurred during the period of analysis, i.e. new spoil banks were being created and reclaimed. As the spoil bank ages, vegetation growth increases, the soil settles, soil fines are washed away, armoring occurs, and rills develop that channelize flow. Hence, the soil erosion model should be used only on active mining and reclamation sites until additional erosion model constants are evaluated.

Using three separate design storms, those required by the Office of Surface Mining, the erosion on a newly constructed spoil bank was simulated in Chapter IV for each watershed. It was assumed in these simulations that the spoil bank would have the same physical conditions as the average spoil bank in that watershed. The results from these simulations, Tables 4.22 through 4.24 (pages 109-111), showed that the calculated sediment storage volume required was always a factor of two less than the requirements of the Office of Surface Mining.

Sediment Yield Model

LOAD-I, the sediment yield model was derived from a mass balance of erosion source, deposition and suspended sediment loads. It was evaluated on data collected in the New River Basin. In evaluating the load modulus model, Anderson Branch was removed from the data set because it was shown to be an outlier caused by its similar but distinct land use. After removing Anderson Branch from the sample, LOAD-I results were greatly improved, as can be seen in Table 4.28 (page 120).

Simulation of observed storms using LOAD-I had mixed results. The time to peak and total load simulations were good. These simulations can be observed in Table 4.29 (page 122). The peak load rates were not well simulated in all cases. For extremely high flow rates, the simulated peak load rates were often much lower than the observed.

The variation between simulated and observed peak flow rates has two possible explanations. Since the lag modulus is a lumped system, an outlier in the data could be responsible. It is unlikely that the lumped assumptions of land use, watershed characteristics and/or mining activities could have changed to account for this variation. The more likely explanation is that noise from data collection was responsible.

Data samples were collected as grab samples from the middle of the stream at approximately thirty minute intervals. These samples were not duplicated. For extremely large storm flows it would be difficult to obtain a representative grab sample. In a streamflow discharge of 20 to 60 CFS it would be difficult to obtain a sample that could separate bedload from suspended load. This type of error is also supported by observation that total load simulations were excellent for larger storms with high flows. Since this type of watershed storm is generally considered important for design and the total loads are of more interest than the load rates, the model was considered successful in fulfilling the objectives of adequately simulating loads from storms of hydrologic significance.

Recommendations

The following recommendations are made:

1. Lag modulus should be evaluated to study its within watershed variation.

2. The SCS Curve Number model needs to be extensively evaluated and compared to infiltration observations. The Curve Number method has long been used to distribute rainfall excess, a use for which it was not intended.

3. The models, TENN-I, LOAD-I, and ERODE-I show great potential and should be evaluated on other land uses to expand their usefulness.

4. ERODE-I should be evaluated on actual spoil bank sites to further evaluate its effectiveness.

5. ERODE-I constants should continue to be optimized from rainulator test data collected by the United States Department of Agriculture for various soil types and soil conditions.

6. The erosion simulator reaction constant is a function of length. This relationship needs to be extended and investigated for lengths beyond 75 feet.

7. The erosion simulator rainfall detachment constant should be a function of rainfall intensity. In this study, the rainfall detachment constant was evaluated at a constant rainfall rate. This relationship should be investigated.

8. Simulation of unit suspended sediment graphs should be investigated using a double triangle model approach similar to that used for the hydrologic URF herein.

CHAPTER VI

SUMMARY AND CONCLUSIONS

Study Objective

The goal of this research study was to simulate the effects of steep contour coal strip mining on stormwater response and suspended sediment yield for small watersheds in the New River Basin, Tennessee, using mathematical modeling. To accomplish this objective, three mathematical models were used--a watershed stormwater response model (TENN-I), a soil erosion model (ERODE-I), and a watershed suspended load model (LOAD-I).

Model Development and Evaluation

Watershed Runoff

The watershed stormwater response (hydrograph) simulator, TENN-I, was evaluated using storm data collected mainly from four small watersheds within the New River Basin ranging from 400 to 1400 acres in size. Three of the watersheds were undergoing or had experienced coal strip mining. The fourth was a virgin watershed. Using TENN-I, 54 storm runoff events were simulated using real-time rainfall distribution and measurable basin characteristics. These simulated storms were compared with their associated observed storm hydrographs. The watershed characteristics used in TENN-I were watershed area, percent forest and antecedent moisture conditions. Very good agreement between the simulated and observed stormwater hydrographs was obtained for the storm events having large runoff volumes or long rainfall durations. Hydrographs simulated using TENN-I for runoff events of short duration or low rainfall intensities did not agree with the observed storm hydrographs as well as the previously mentioned simulations.

TENN-I was developed in a series of previous studies [46, 52, 53, 54], from a cumulative total of 26 rural and urban watersheds involving 349 storm events. TENN-I model parameters were simulated by the regionalization scheme developed in the last of the four studies [54].

Watershed Suspended Sediment Yield

The suspended sediment yield model, LOAD-I, was developed and evaluated using storm data collected from six of the New River Basin watersheds. Two of the basins were undergoing active mining. Three of the watersheds had experienced previous mining. The last watershed was virgin. LOAD-I was derived from a mass balance formulation of the watershed erosion sources, deposition sinks and suspended sediment storage. Using the model, 21 suspended sediment storm events were simulated using observed storm runoff, surface drainage area and percent forest as input. For each of these storms, total watershed suspended sediment yield, the peak suspended sediment yield rate and the time to peak yield rate were simulated. Simulations of total suspended sediment yield and time to peak rate agreed well with the observed storms of interest, i.e. those with high runoff volume or long rainfall duration. Simulated peak suspended sediment yield rate did not always show good agreement with the observed for those storms of interest.

Spoil Bank Runoff and Soil Loss

The soil erosion model, ERODE-I, was evaluated using runoff and suspended soil loss data observed on 106 rainulator storm events on 42 Hawaii erosion plots. These plots consisted of 10 soil series which were composed of four basic soil types. These plot sites and soil types included both dry and wet antecedent moisture conditions. ERODE-I was derived from erosion mechanics and overland flow. Runoff response, accumulated runoff volume and total suspended sediment yield simulated by ERODE-I for the Hawaii storms were in excellent agreement with the observed.

Using ERODE-I, soil loss was simulated for strip mined spoil banks undergoing storm events of design magnitude in the New River Basin. These rain storms were the 2 year 30 minute, the 10 year 30 minute and the 10 year 24 hour storms. ERODE-I model coefficients were transferred to the New River Basin, since the Hawaii and New River soil types were similar. Spoil banks were represented by a cascade of planes. The spoil bank surface during formation and reclamation was similar to the Hawaii conditions of disturbance, age and the physical characteristics of the soil to include the denuded, tilled and graded surface conditions. The soil loss from the spoil banks simulated from the above design storms in New River ranged from 0.007 to 0.051 acre-foot per acre of disturbed land. The largest soil loss volume resulted from the 10 year 24 hour storm and was approximately half of the sediment yield value required for design by the Department of Interior, Offices of Surface Mining Reclamation and Enforcement.

Effects of Coal Mining on Runoff and Suspended Sediment Yield

The effects of heavy mining activity were compared to a virgin watershed condition. Using TENN-I and LOAD-I, an undisturbed virgin watershed was considered to be subjected to heavy contour coal strip mining activity amounting to 24 percent of the watershed area. The comparison was performed using a design rain storm of four hours duration with a return period of five years. The effects of the simulation were dramatic. The peak runoff rate was doubled after the occurrence of mining and the time to peak was slightly reduced. Simulated watershed suspended sediment yield increased from less than one ton to 47 tons of sediment for the storm!

Comparison of Effects of Mining with Effects of Urbanization

The effects of urbanization and contour coal strip mining on watersheds of similar size were simulated using TENN-I and LOAD-I. For comparison, an undisturbed virgin watershed was assumed to be subjected to steep contour coal mining amounting to a total disturbance of 24 percent of the watershed area. The urbanized watershed was fully developed and its runoff and sediment response for the rural condition was simulated. For this simulation, the urbanization had a dramatic and profound effect on the stormwater runoff response. Although the strip mining also produced significant effects on its stormwater response, the effects were less of an impact than the impacts of urbanization on its stormwater response. By contrast the watershed subjected to strip mining showed that its sediment yield expressed as pounds per acre-inch of runoff was approximately 20 percent greater than that of the urbanized basin for the same storm.

Application of Simulation Models

Outfall Location

The simulation models, TENN-I, ERODE-I and LOAD-I, provide two alternative outfall locations within a watershed at which simulation can be accomplished (see Figure 6.1). If the simulated event is desired at a location near the disturbed areas, then ERODE-I would be the proper simulator, since its derivation was based on applications for sheet surface runoff and was experimentally verified on plots up to 75 feet in length. If the outfall is to be further away from the disturbed site, such as on a blue line stream, then TENN-I and LOAD-I would be applicable.

Comparisons of simulated spoil bank and observed watershed average suspended sediment yields (see Tables 4.26 and 4.31, pages 117 and 129) indicate that the forested area between the spoil banks and the watershed outlet intervenes and acts as a filter. In addition, the sediment delivery ratios as well as the concentrations of the suspended solids would decrease as the outfall was located farther away from the erosion source, i.e. spoil banks. This was supported by the simulated watershed sediment delivery ratios, shown in Table 4.30 (page 127), which are considerably less than what would be expected at the toe of a spoil bank.

Yet, as the event simulation location of interest moves farther away from the erosion source, the drainage area above the location point

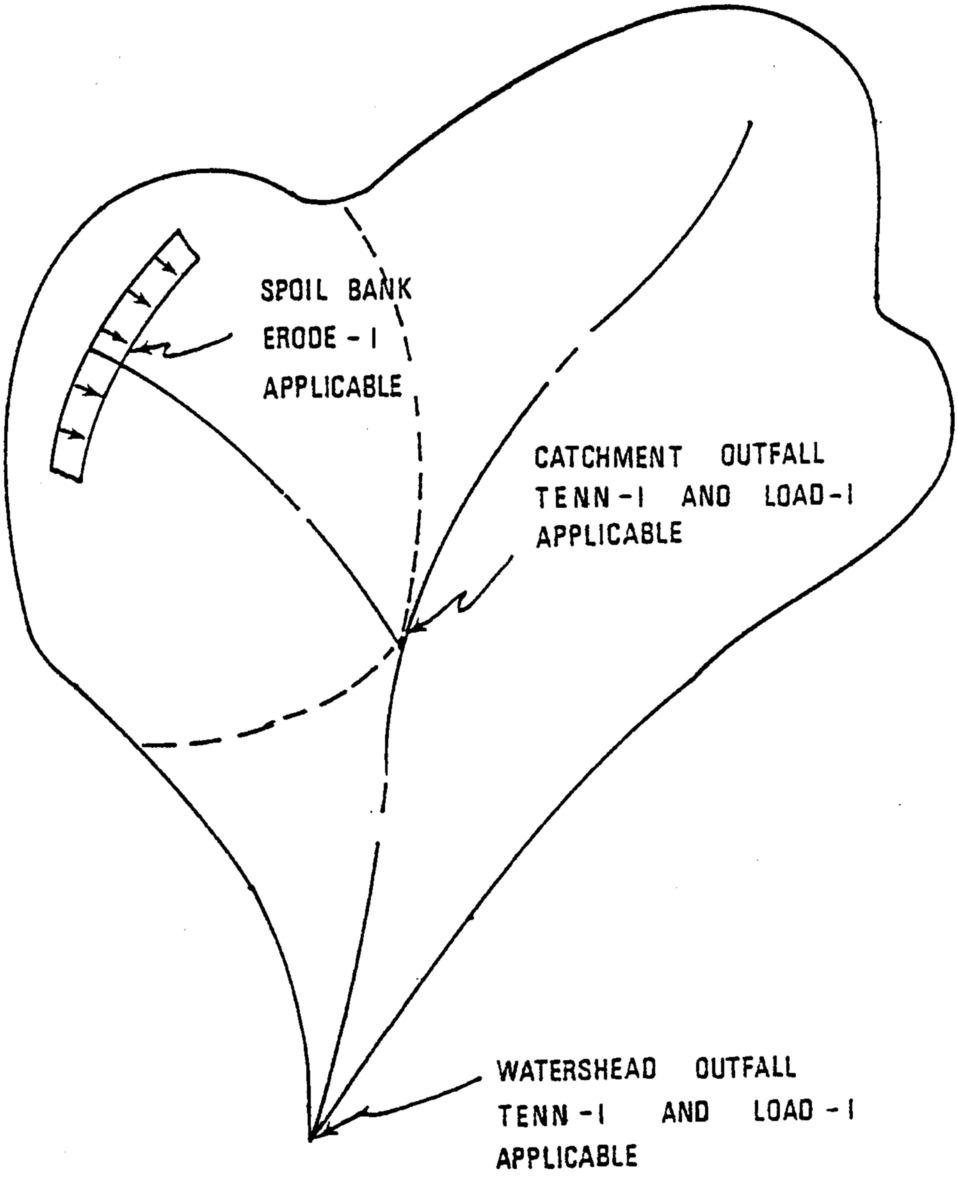

FIGURE 6.1

APPLICATION OF SIMULATION MODELS

will increase. This results in an increased total runoff volume past this outfall. Hence, as the site of the simulation moves closer to the spoil bank or erosion source, the total suspended yield will increase and the runoff volume will decrease. Also, as the watershed area of the LOAD-I and TENN-I simulations approach the disturbed areas used in ERODE-I or vice versa, the results obtained from these models will be similar if all the models are being applied to the same disturbed site.

Ungauged Mining Areas

ERODE-I, TENN-I and LOAD-I may be used to simulate events on ungauged as well as gauged catchments and watersheds. However, the condition under which these models were developed must be similar to the ungauged catchment and watershed conditions. For TENN-I and LOAD-I, this requirement is generally met when the geology, vegetation cover, terrain, mining type (steep contour coal mining), surface drainage and general climate are similar. Hence, if these models are applied to a dry barren mountainous region undergoing mountain top removal, for example, then considerable judgement of the modeler may be required. However, after analyzing a number of events from such a region, TENN-I and LOAD-I could then be used to more reliably simulate events for these conditions.

ERODE-I, on the other hand, could be used on this last example or any other site as long as the soil type and physical soil conditions matched those that have been evaluated to date. Continued evaluation of new soil types and physical soil conditions will greatly extend the applicability and reliability of ERODE-I.

All three of these models can presently be reliably applied throughout the New River Basin and Eastern Tennessee and Kentucky coal region where the mining type is contour stripping. In addition, ERODE-I can be reliably applied in those regions for all known surface mining types.

The ability of these models to simulate stormwater runoff and suspended sediment yield load from measurable, quantifiable and readily available watershed characteristics, provides a powerful tool for evaluating the effects of coal strip mining in planning and design.

BIBLIOGRAPHY

BIBLIOGRAPHY

1. U.S. Department of the Interior, Final Regulatory Analysis OSM-RA-1. U.S. Government Printing Office, Washington, D.C., March 1977.

2. Nielsen, G.F., editor. Keystone Coal Industry Manual. McGraw-Hill, Inc., New York, 1977.

3. The University of Tennessee. Toward a More Beneficial Use of Appalachian Coal. Research Proposal to the National Science Foundation. Department of Civil Engineering, The University of Tennessee, Knoxville, Tennessee, 1971.

4. Westerstorm, L.W. and R.E. Harris. "Coal-Bituminous and Lignite," Bureau of Mines Mineral Yearbook, U.S. Bureau of Mines, 1975.

5. Leamon, A.R. and S.W. Maher. Coal Mining in Tennessee, Information Circular 17, State of Tennessee, Department of Conservation, Division of Geology, Nashville, Tennessee, November 1974.

6. U.S. Department of the Interior, Final Environmental Statement OSM-EIS-1. U.S. Government Printing Office, Washington, D.C., January 1979.

7. Jiram, John. "A Program to Reclaim Orphan Mines," The Tennessee Conservationist, Vol. XVII, No. 9, October 1976.

8. U.S. Congress. "The Surface Mining Control and Reclamation Act of 1977," Public Law 95-87, 30 U.S.C. 1201, Laws of 95th Congress - First Session.

9. U.S. Department of the Interior, Office of Surface Mining Reclamation and Enforcement. "Surface Coal Mining and Reclamation Operations, Permanent Regulatory Program." Federal Register, Book 2 and 3, Vol. 44, No. 50, March 13, 1979.

10. Pomeroy, Maurice. "Don't Let This Happen!" The Tennessee Conservationist, Vol. XLIII, No. 5, June 1976.

11. Onstad, C.A. and G.R. Foster. "Erosion Modeling on a Watershed," ASAE, Transactions, Vol. 18, No. 12, 1975.

12. Overton, Donald E. and Michael E. Meadows. Stormwater Modeling, Academic Press, New York, 1976.

13. Sherman, L.K. "Stream Flow from Rainfall by the Unit-Graph Method." Engineering News Record 108, pp. 501-505, 1932.

14. Sherman, L.K. "The Relation of Hydrographs of Runoff to Size and Character of Drainage-Basins." American Geophysical Union Transactions, Vol. 13, pp. 332-339, 1932.

15. Sherman, L.K. "The Unit Hydrograph Method," In Meinzer, D.E., ed., Physics of the Earth-IX: Hydrology. Ch. XI, McGraw-Hill, Inc., New York, 1942.

16. Dooge, James C.I. Linear Theory of Hydrologic Systems, U.S. Department of Agriculture Technical Bulletin No. 1468, U.S. Government Printing Office, Washington, D.C., October 1973.

17. Haan, C.T. and B.J. Barfield. Hydrology and Sedimentology of Surface Mined Lands, Office of Continuing Education and Extension, College of Engineering, University of Kentucky, Lexington, Kentucky, 1978.

18. Johnstone, D. and W.P. Cross. Elements of Applied Hydrology, McGraw-Hill, Inc., New York, 1949.

19. Prasad, R. "A Non-Linear Hydrologic System Response Model," Journal of the Hydraulics Division, ASCE, Vol. 90, No. HY2, pp. 201-221, July 1967.

20. Nash, J.E. "The Form of the Instantaneous Unit Hydrograph," Proceedings of the General Assembly of Toronto, International Association of Scientific Hydrology, pp. 114-121, 1957.

21. O'Donnell, T. "Instantaneous Unit Hydrograph Derivation by Harmonic Analysis," Commission of Surface Waters, International Association of Scientific Hydrology, Publication 51, pp. 546-557, 1960.

22. Amorocho, J. and G.J. Orlob. "Nonlinear Analysis of Hydrologic Systems," Water Resources Center, University of California, Berkeley, 1961.

23. Amorocho, J. "The Nonlinear Prediction Problem in the Study of the Runoff Cycle," Water Resources Research, Vol. 3, No. 3, pp. 9-17, 1962.

24. Overton, D.E. "Analytical Simulation of Watershed Hydrographs from Rainfall," Proceedings, International Hydrology Symposium, Ft. Collins, Colorado, pp. 9-17, 1967.

25. Heerdegeen, Richard G. "The Unit Hydrograph: A Satisfactory Model of Watershed Response?" Water Resources Bulletin, American Water Resources Association, Vol. 10, No. 6, pp. 1143-1161, December 1974.

26. Morgan, P.E. and S.M. Johnson, "Analysis of Synthetic Unit Graph Methods," Journal of the Hydraulics Division, ASCE, Vol. 88, No. HY5, pp. 199-220, September 1962.

27. Dooge, J.C.I. "A General Theory of the Unit Hydrograph," Journal of Geophysical Research, Vol. 64, No. 2, pp. 241-250, February 1959.

28. Edson, C.G. "Parameters for Relating Unit Hydrographs to Watershed Characteristics," Transactions, American Geophysical Union, Vol. 32, No. 4, pp. 591-596, August 1951.

29. O'Kelly, J.J. "The Employment of Unit Hydrographs to Determine the Flows of Irish Arterial Drainage Channels," Proceedings of the Institute of Civil Engineers, Vol. 4, pp. 365-412, 1955.

30. Snyder, F.F. "Synthetic Unit Graphs," Transactions, American Geophysical Union, Vol. 19, pp. 447-454, 1938.

31. Linsley, R.K. "Application of Synthetic Unit Graphs in Western Mountain States," Transactions, American Geophysical Union, Vol. 24, pp. 580-585, 1943.

32. Eagleson, P.S. "Unit Hydrograph Characteristics for Sewered Areas," Journal of the Hydraulic Division, ASCE, Vol. 18, No. HY2, pp. 1-25, March 1962.

33. Taylor, A.B. and H.E. Schwarz. "Unit Hydrograph Lag and Peak Flow Related to Basin Characteristics," Transactions, American Geophysical Union, Vol. 33, No. 2, pp. 235-246, April 1952.

34. Hudlow, M.D. and R.A. Clark. "Hydrograph Synthesis by Digital Computer," Journal of the Hydraulics Division, ASCE, Vol. 95, No. HY3, pp. 839-861, May 1969.

35. Kent, K.M. "A Method for Estimating Volume and Rate of Runoff in Small Watersheds," U.S. Department of Agriculture, Soil Conservation Service, Washington, D.C., 1968.

36. Commons, G.G. "Flood Hydrographs," Civil Engineering, Vol. 12, pp. 571-572, October 1942.

37. Mitchell, W.D. Unit Hydrographs in Illinois, Illinois Division of Waterways, prepared in cooperation with U.S.G.S., 1948.

38. U.S. Department of Agriculture. Hydrology, Supplement A to Section 4 in Engineering Handbook, Soil Conservation Service, Washington, D.C., 1957.

39. Gray, D.M. "Synthetic Unit Graphs for Small Watershed," Journal of the Hydraulics Division, ASCE, Vol. 87, No. HY4, pp. 33-53, July 1961.

40. Amorocho, J. "Measure of Linearity of Hydrologic Systems," Journal of Geophysical Research, Vol. 68, pp. 2237-2249, April 1963.

41. Morgali, J.R. Hydraulic Behavior of Small Drainage Basins, Technical Report No. 30, Stanford University, 1963.

42. Black, P.E. "Hydrograph Response to Geomorphic Model Watershed Characteristics and Precipitation Variables," Journal of Hydrology, Vol. 17, No. 4, pp. 309-329, 1972.

43. Minshall, N.E. "Predicting Storm Runoff on Small Experimental Watersheds," Journal of the Hydraulics Division, ASCE, Vol. 16, No. HY8, pp. 17-39, August 1960.

44. Singh, K.P. "Nonlinear Instantaneous Unit Hydrograph Theory," Journal of the Hydraulics Division, ASCE, Vol. 94, No. HY2, pp. 53-69, March 1964.

45. Ding, J.Y. "Variable Unit Hydrograph," Journal of Hydrology, Vol. 22, pp. 53069, 1973.

46. Ardis, C.V. "A Storm Hydrograph Model for the Response and Variation of Small Rural Watersheds," Ph.D. Dissertation, Department of Civil Engineering, University of Wisconsin, 1972.

47. Betson, R.P. "What is Watershed Runoff?" Journal of Geophysical Research, Vol. 69, No. 8, pp. 1541-1551, April 1964.

48. Dunne, F. and R.D. Black. "An Experimental Investigation of Runoff Production in Permeable Soils," Water Resources Research, Vol. 6, No. 2, pp. 478-490, April 1970.

49. Betson, R.P. and J.B. Marius. "Source Areas of Storm Runoff," Water Resources Research, Vol. 5, No. 3, pp. 547-581, June 1969.

50. Kirkby, M.J., editor. Hillslope Hydrology, John Wiley and Sons, New York, 1978.

51. Green, R.E. "Optimization by the Pattern Search Method," Research Paper No. 7, Tennessee Valley Authority, January 1970.

52. Betson, R.P. Urban Hydrology: A System Study in Knoxville, Tennessee, TVA, Division of Water Management, Water Systems Development Branch, Knoxville, Tennessee, June 1976.

53. Troxler, William L. "A Stormwater Simulation Model for the Tennessee Valley," M.S. Thesis, Department of Civil Engineering, The University of Tennessee, March 1978.

54. Overton, D.E. and W.L. Troxler. "Regionalization of Stormwater Response," Paper presented at the American Geophysical Union Meeting, Miami, Florida, April 17-21, 1978.

55. Lighthill, M.J. and C.B. Whitham. "On Kinematic Waves: Flood Movement in Long Rivers," Proceedings of the Royal Society of London, Series A, Vol. 229, pp. 281-316, 1955.

56. Henderson, F.M. "Flood Waves in Prismatic Channels," Journal Hydraulics Division, ASCE, HY4, 1963.

57. Woolhiser, D.A. and J.A. Liggett. "Unsteady, One-dimensional Flow Over a Plane--the Rising Hydrograph," Water Resources Research, Vol. 3, No. 3, pp. 753-771, 1967.

58. Henderson, F.M. and R.A. Wooding. "Overland Flow and Groundwater Flow from a Steady Rainfall of Finite Duration," Journal Geophysical Research, Vol. 69, No. 8, pp. 1531-1540, 1964.

59. Wooding, R.A. "A Hydraulic Model for the Catchment-Stream Problem. I Kinematic Wave Theory," Journal of Hydrology, Vol. 3, pp. 254-267, 1965.

60. Wooding, R.A. "A Hydraulic Model for the Catchment-Stream Problem. II Numerical Solutions," Journal of Hydrology, Vol. 3, pp. 268-282, 1965.

61. Wooding, R.A. "A Hydraulic Model for the Catchment-Stream Problem. III Comparison with Runoff Observations," Journal of Hydrology, Vol. 4, pp. 21-37, 1966.

62. Overton, D.E. "Estimation of Surface Water Lag Time from the Kinematic Wave Equations," Water Resources Bulletin, Vol. 4, No. 3, pp. 428-440, June 1971.

63. Overton, D.E. "Kinematic Flow on Long Impermeable Planes," Water Resources Bulletin, pp. 1198-1204, December 1972.

64. Overton, D.E. and D.L. Brakensiek. "A Kinematic Model of Surface Runoff Response," Proceedings of International Symposium on Results from Experimental and Representative Watersheds, Wellington, New Zealand, pp. 100-112, December 1970.

65. Woolhiser, D.A. "Overland Flow on a Converging Surface," Transactions, American Society Agricultural Engineers, Vol. 12, No. 4, pp. 460-462, 1969.

66. Singh, V.P. "A Nonlinear Kinematic Wave Model of Surface Runoff," Ph.D. Dissertation, Colorado State University, Fort Collins, Colorado, 1974.

67. Brakensiek, D.L. "A Simulated Watershed Flow System for Hydrograph Prediction: A Kinematic Application," International Hydrology Symposium Proceedings, Fort Collins, Colorado, pp. 18-24, 1967.

68. Kibler, D.F. and D.A. Woolhiser. "The Kinematic Cascade as a Hydrologic Model," Hydrology Papers, Colorado State University, Fort Collins, Colorado, March 1970.

69. Overton, Donald E. "A Variable Response Overland Flow Model," Ph.D. Dissertation, University of Maryland, College Park, Maryland, 1972.

70. Overton, D.E., W.L. Troxler and J. Bales. A Manual for Simulating Design Hydrographs in Urban Regions Using Kinematic Wave Theory and SCS Curve Numbers, E.P.E., Inc., Knoxville, Tennessee, September 1978.

71. Overton, D.E. "Route or Convolute?" Water Resources Research, Vol. 6, No. 1, pp. 43-52, 1970.

72. Laurenson, E.M. "A Catchment Storage Model for Runoff Routing," Journal of Hydrology, Vol. 2, pp. 141-163, 1964.

73. Askew, A.J. "Derivation of Formula for Variable Lag Time," Journal of Hydrology, Vol. 10, pp. 225-242, 1970.

74. Meyer, L.D. "Overview of the Urban Erosion and Sedimentation Process," Proceedings 1974 National Symposium on Urban Rainfall and Runoff and Sediment Control, UK B4 106, College of Engineering, University of Kentucky, Lexington, Kentucky, pp. 15-23, 1974.

75. Johnson, J.W. "Distribution Graphs of Suspended-Matter Concentrations," Transactions, ASCE, Vol. 108, No. 2199, pp. 941-964, 1943.

76. Rendon-Herrero, D. "A Method for the Prediction of Washload in Certain Small Watersheds," Ph.D. Dissertation, Virginia Polytechnical Institute and State University, Blacksburg, 1972.

77. Rendon-Herrero, D. "Unit Sediment Graph," Water Resources Research, Vol. 14, No. 5, pp. 889-901, 1978.

78. Rendon-Herrero, D. "Estimation of Washload Produced on Certain Small Watersheds," Journal Hydraulics Division, ASCE, Vol. 100, No. HY7, pp. 835-848, 1974.

79. Rendon-Herrero, D. "Closure: Estimation of Washload Produced on Certain Small Watersheds," Journal Hydraulics Division, ASCE, Vol. 101, No. HY7, pp. 1061-1064, 1976.

80. Zingg, A.W. "Degree and Length of Land Slope as it Affects Soil Loss in Runoff," Agricultural Engineering, Vol. 21, No. 2, pp. 59-64, February 1940.

81. Smith, D.D. "Interpretation of Soil Conservation Data for Field Use." Agricultural Engineering, Vol. 22, pp. 173-175, 1941.

82. Musgrave, G.W. "The Quantitative Evaluation of Factors in Water Erosion, A First Approximation," Journal of Soil and Water Conservation, Vol. 2, No. 3, pp. 133-138, 1947.

83. Wischmeier, W.H. and D.D. Smith. "A Universal Soil-Loss Equation to Guide Conservation Farm Planning," Transactions 7th International Congress of Soil Science, Madison, Wisconsin, 1960.

84. Wischmeier, W.H. and D.D. Smith. "Predicting Rainfall-Erosion Losses from Cropland East of the Rocky Mountains," Agriculture Handbook No. 282, U.S. Department of Agriculture, 1965.

85. Wischmeier, W.H. and D.D. Smith. "Predicting Rainfall Erosion Losses," Agriculture Handbook No. 537, U.S. Department of Agriculture, December 1978.

86. Renfro, G.W. "Use of Erosion Equations and Sediment-Delivery Ratios for Predicting Sediment Yield," Proceedings of the Sediment-Yield Workshop 1972, Agricultural Research Service, pp. 33-45, June 1975.

87. Young, R.A. and C.K. Mutchler. "Effect of Slope Shape on Erosion and Runoff," Transactions of the American Society of Agricultural Engineers, pp. 231-239, 1969.

88. Fogel, M.M., L.H. Herkman and L. Duckstein. "A Stochastic Sediment Yield Model Using the Modified Universal Soil Loss Equation," Soil Erosion Prediction and Control, Soil Conservation Society of America, Ankey, Iowa, pp. 226-233, 1977.

89. Onstad, C.A. and G.R. Foster. "Erosion Modeling on a Watershed," Transactions of American Society of Agricultural Engineers, Vol. 18, No. 2, pp. 288-292, 1975.

90. Foster, G.R. and W.H. Wischmeier. "Evaluating Irregular Slopes for Soil Loss Prediction," Transactions of the American Society of Agricultural Engineers, Vol. 17, No. 2, pp. 305-309, 1974.

91. Foster, G.R., L.D. Meyer and C.A. Onstad. "A Runoff Erosivity Factor and Variable Slope Length Exponent for Soil Loss Estimates," Transactions of the American Society of Agricultural Engineers, pp. 683-687, 1977.

92. Cook, H.L. "The Nature and Controling Variables of the Water Erosion Process," Soil Science Society of America, Proceedings, Vol. 1, pp. 487-494, 1936.

93. Ellison, W.D. "Soil Erosion Studies," Agricultural Engineering, Vol. 28, pp. 145-146, 197-201, 245-248, 297-300, 349-351, 402-405, 442-444, 1947.

94. Stallings J.H. "Mechanics of Water Erosion," U.S. Department of Agriculture, Soil Conservation Service TP-118, 1953.

95. Smith, D.D. and W.H. Wischmeier. "Rainfall Erosion," Advances in Agronomy, Vol. 14, pp. 109-148, 1962.

96. Robins, J.J. and E.L. Neff. "Principles of the Erosion Process," Forest Watershed Management Symposium, Oregon State University, pp. 127-139, 1963.

97. Meyer, L.P. and E.J. Monke. "Mechanics of Soil Erosion by Rainfall and Overland Flow," Transactions of the American Society of Agricultural Engineers, pp. 572-580, 1965.

98. Meyer, L.D. and W.H. Wischmeier. "Mathematical Simulation of the Process of Soil Erosion by Water," Transactions of the American Society of Agricultural Engineering, pp. 754-762, 1969.

99. Kilinic, M. and E.V. Richardson. "Mechanics of Soil Erosion from Overland Flow Generated by Simulated Rainfall," Hydrology Papers, Colorado State University, Fort Collins, Colorado, No. 63, 1973.

100. Bennett, James P. "Concepts of Mathematical Modeling of Sediment Yield," Water Resources Research, Vol. 10, No. 3, pp. 485-492, 1974.

101. Foster, G.R. and L.D. Meyer. "Mathematical Simulation of Upland Erosion by Fundamental Erosion Mechanics," ARS-S-40, U.S. Department of Agriculture, Washington, D.C., pp. 190-197, 1975.

102. Foster, G.R. and L.D. Meyer. "A Closed-Form Soil Erosion Equation for Upland Areas," Sedimentation, Ft. Collins, Colorado, 1972.

103. Foster, G.R., L.D. Meyer and C.A. Onstad. "An Erosion Equation from Basic Erosion Principles," Transactions of the American Society of Agricultural Engineers, pp. 678-682, 1977.

104. Simons, D.B., E.V. Richardson and C.F. Nordin. "Bedload Equations for Ripples and Dunes," U.S. Geological Survey Professional Paper 462-H, 1975.

105. Meyer, L.D., G.R. Foster and M.J.M. Romkens. "Source of Soil Eroded by Water from Upland Slopes," Proceedings Sediment-Yield Workshop, U.S. Agriculture Research Service, ARS-S-40, pp. 177-189, 1972.

106. Willis, J.C. "Erosion by Concentrated Flow," U.S. Department of Agriculture, Agricultural Research Paper 41-179, 1971.

107. Foster, G.R. and L.R. Meyer. "Transport of Soil Particles by Shallow Flow," Transactions of American Society of Agricultural Engineers, Vol. 15, No. 1, pp. 99-102, 1972.

108. Yalin, Y.S. "An Expression for Bed-Load Transportation," Hydraulics Division, ASCE, Vol. 89, No. HY3, pp. 221-250, 1963.

109. Bagnold, R.A. "An Approach to the Sediment Transport Problem for General Physics," U.S. Geological Survey Professional Paper 422-I, 1966.

110. Yang, C.T. "Unit Stream Power and Sediment Transport," Journal Hydraulic Division, ASCE, Vol. 98, No. HY10, pp. 1805-1827, 1972.

111. Threadgill, E.B. and Ronald E. Henderson. "Effect of Rainfall on the Velocity Distribution and Tractive Force in a Triangular Open Channel," Transactions of the American Society of Agricultural Engineers, pp. 352-355, 1969.

112. Strand, R.I. "Bureau of Reclamation Procedures for Predicting Sediment Yield," Present and Prospective Technology for Predicting Sediment Yields and Sources, U.S. Department of Agriculture, pp. 10-15, June 1975.

113. Livesey, R.H. "Corps of Engineers Methods for Predicting Sediment Yields," Present and Prospective Technology for Predicting Sediment Yields and Sources, U.S. Department of Agriculture, pp. 16-32, June 1975.

114. Flaxmen, E.M. "The Use of Suspended-Sediment Load Measurements and Equations for Evaluation of Sediment Yield in the West," Present and Prospective Technology for Predicting Sediment Yields and Sources, U.S. Department of Agriculture, pp. 46-56, June 1975.

115. Renard, Kenneth G. "Sediment Rating Curve in Ephemeral Streams," Transactions of the American Society of Agricultural Engineering, pp. 80-85, 1969.

116. Ward, Nancy A. "A Parametric Model of Suspended Solids Concentration for Two Strip Mined Watersheds," M.S. Thesis, Department of Civil Engineering, The University of Tennessee, Knoxville, Tennessee, March 1977.

117. Baird, Ralph W. "Sediment Yields from Backland Watersheds," Transactions of the American Society of Agricultural Engineers, pp. 454-456, 1964.

118. Rogers, J.S., A.P. Barnett and Carlisle Cobb, Jr. "An Evaluation of Factors Affecting Runoff and Soil Loss from Simulated Rainfall," Transactions of the American Society of Agricultural Engineers, pp. 457-459, 1964.

119. U.S. Department of Agriculture. "Sediment Sources, Yields and Delivery Ratios," National Engineering Handbook, Section 3, Sedimentation, U.S. Department of Agriculture, 1971.

120. Boyce, Robert C. "Sediment Routing with Sediment-Delivery Ratios," Proceedings of the Sediment-Yield Workshop 1972, Agricultural Research Service, pp. 61-65, June 1975.

121. Overton, D.E., R.A. Minear and E.C. Crosby. "Load Modulus for Urban Sediment Production," International Symposium on Urban Storm Water Management, University of Kentucky, Lexington, Kentucky, pp. 283-287, July 24-27, 1978.

122. Foster, G.R., L.F. Huggins, and L.D. Meyer. "Simulations of Overland Flow on Short Field Plots," Water Resources Research, Vol. 4, No. 6, pp. 1179-1187, 1968.

123. Tung, Hong-Shoung. "Impacts of Contour Coal Mining on Streamflow, A Case Study of the New River Watershed, Tennessee," Ph.D. Dissertation, The University of Tennessee, August 1975.

124. Dangler, E.W., S.A. El-Swaify, L.R. Ahuja and A.P. Barnett. Erodibility of Selected Hawaii Soils by Rainfall Simulation, Agricultural Research Service, U.S. Department of Agriculture, Washington, D.C., May 1976.

125. Minear, R.A., Bruce A. Tschantz, G.L. Vaughan, D.E. Overton and G. Briggs. Environmental Aspects of Coal Production in Appalachian Region, Progress Report, June 1, 1977 - May 31, 1978, U.S. Department of Energy Contract No. EY-76-S-05-4946, May 1978.

126. Cheek, J.B., N. Radhakiishnan and F.T. Tracy. Application of Spline Integration Methods to Engineering Problems, U.S. Army Engineer Waterways Experiment Station, Vicksburg, Mississippi, July 1971.

127. Halstead, Robert G. Erosion and Sediment Control in Urbanizing Areas of Colorado, U.S. Department of Agriculture, Soil Conservation Service, Denver, Colorado, 1978.

128. Rogers S.S., A.P. Barnett and Carlisle Colb. "An Evaluation of Factors Affecting Runoff and Soil Loss from Simulated Rainfall," Transactions of the American Society of Agricultural Engineering, pp. 457-459, 1964.

APPENDICES

APPENDIX A

EVALUATION OF ERODE-I ON HAWAII SOILS

Introduction

The erosion simulation model, ERODE-I, was evaluated using soil loss data collected by the U.S. Department of Agriculture on Hawaiian soil using a rainfall simulator. The data, which has slopes up to 19 percent, permitted continuing refinement and verification of the model as well as allowing the determination of detachment, transport and deposition coefficients as a function of soil type.

In addition, integration of the erosion model produced a derivation of load modulus for each plot site.

Derivation of ERODE-I

The one-dimensional conservation of mass equation for sediment transport is

$$\frac{\partial(h\delta)}{\partial t} + (1-\lambda)\frac{\partial y}{\partial t} + \frac{\partial(hU_p\delta)}{\partial x} = \frac{\partial}{\partial x} hE_p(\frac{\partial \delta}{\partial x}) \qquad (A.1)$$

where δ is sediment concentration, h is depth of flow, λ is porosity of deposited sediment, t is time, y is local bed elevation, U_p is average velocity of sediment, x is distance positive in direction of flow, E_p is sediment particle mass transfer coefficient, u is flow velocity, and S_0 is local bed slope. The quantities above are illustrated in Figure A.1.

Equation A.1 is completely general for a rectangular cross-section and differs from the conservation of mass equation for a dissolved

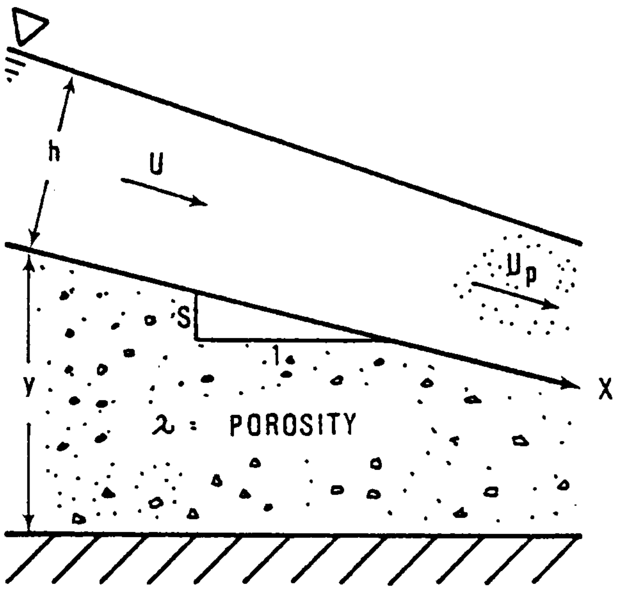

FIGURE A.1

FLOW TRANSPORT SYSTEM

substance in that the second term on the left accounts for deposition or erosion of the bed. It is assumed that the sediment velocity equals the flow velocity. In addition, the term on the right hand side of equation A.1 accounts for the dispersion of the material while it is suspended. This term is normally small by comparison to the other terms in the equation and is thus considered negligible.

For steady state conditions, equation A.1 may be expressed as follows

$$D_F + R_{DT} = \frac{\partial E_B}{\partial x} \tag{A.2}$$

where

$$E_B = \gamma_s \; \mu \delta h \tag{A.3}$$

E_B is the sediment weight transport rate per unit of width, γ_s is the specific gravity of sediment particles, D_F is the net soil particle weight detachment rate per unit area resulting from shear caused by flow, and R_{DT} is the net soil particle weight detachment rate per unit area resulting from rainfall impact.

For unsteady flow, comparisons of A.1, A.2 and A.3 reveal that the following equation controls

$$D_F + R_{DT} = \frac{\partial E_B}{\partial x} - \gamma_s \frac{\partial \delta h}{\partial x} \tag{A.4}$$

Shear detachment rate (D_F) is related to transport capacity (T_c) and sediment load (E_B) in the following form

$$D_F = C(T_c - E_B) \tag{A.5}$$

where C is a reaction rate coefficient or diffusion coefficient which is a function of both transport, detachment and slope length [101].

Further, transport capacity (T_c) may be expressed using stream sediment transport mechanics in the following form

$$T_c = C_T S_o q \tag{A.6}$$

where C_T is a coefficient of transport that is a function of soil material properties, i.e. particle size and density and is expressed in units of lbs/cu. ft.; q is overland flow per unit width; and S_o is slope of land profile.

Combining A.4, A.5 and A.6 results in the following differential equation

$$\frac{\partial E_B}{\partial x} + C E_B = \gamma_s \delta \frac{\partial h}{\partial t} + C C_T S_o q + R_{DT} \tag{A.7}$$

Under the assumptions of kinematic overland flow and for the case of the rising hydrograph, equation A.7 can be integrated to obtain the following for a single plane

$$E_B(X,t) = (1-e^{-cx}) \frac{R_{DT}}{C} + C_T S_o q + \frac{\gamma_s}{c} \delta I_e \tag{A.8}$$

where I_e is the rainfall excess and is equal to $\partial h/\partial t$ from kinematic flow theory.

The data used to evaluate ERODE-I is not presented herein because of its voluminous nature. It is available from the Agricultural Research Service, U.S. Department of Agriculture [124]. This data was obtained from situs rainulator tests conducted on several different denuded soil types. Each soil plot test was 12 feet wide and either 35 or 75 feet long with slopes ranging from 3 to 19 percent. Available data included soil type, plot length, total rain, accumulated runoff distribution, accumulated soil loss distribution, storm (rainfall) distribution and infiltration rate distribution analysis. Tables A.1 and A.2 are representative of data available.

Because only accumulated runoff and soil loss data was available, soil erosion rates and flow rates were determined by using a cubic spline curve-fitting technique [126] to produce the rates necessary to evaluate the equation [127]. This method allowed all data points to be used, provided fast and accurate visual observation of the hydrograph, produced continuous derivatives at all points and allowed quick interpolation of any desired time. This method is easily modified to satisfy new or additional data and can indicate possible data errors readily through visual inspection of both accumulated and rate graphs representations. Figures A.2, A.3 and A.4 are typical examples of erosion and runoff rate determinations of this method.

Soil Constants from ERODE-I

Soil properties which influence erosion by rainfall and runoff are those factors which affect infiltration capacity of a soil and those which affect the resistance of the soil to detachment and transport by falling or flowing water. The evaluation of these factors; average rainfall detachment, transport coefficient and reaction coefficient, from optimization of the erosion model are presented in Table A.3. Differing conditions of soil structure, particle size and gradation, organic content and soil permeability as well as physical site

TABLE A.1

EROSION RUNOFF DATA OBTAINED FROM RAINFALL SIMULATION EXPERIMENTS

Site	Plot	Length	Slope	Total rain	Runoff after--					Soil loss after--					Storm duration
					30 min	60 min	90 min	120 min	Final	30 min	60 min	90 min	120 min	Final	
MOLOKAI-A SERIES															
		Feet	Percent	Inches	Inches					Tons per acre					Minutes
1	1	35	18.4	4.73	0.02	0.33	0.92	1.57	1.59	0.010	1.360	5.270	8.360	8.440	
	2	75	15.8	4.74	.04	.49	1.19	2.01	2.05	.083	4.330	11.03	20.89	21.28	
2	1	35	5.5	5.00	.01	.50	1.26	2.05	2.07	.004	.300	.850	1.440	1.470	
	2	75	6.8	5.03	.03	.56	1.35	2.24	2.32	.029	.990	3.260	5.590	5.780	
3	1	35	14.9	4.62	.02	.37	1.01	1.70	1.73	.024	1.450	5.940	10.63	10.75	
	2	75	15.4	4.83	0	.12	.49	1.04	1.07	0	1.260	6.760	12.41	12.70	
3 wet	1	35	14.9	5.02	.88	1.92	3.00	---	4.09	6.684	13.36	18.64	---	22.89	119.5
	2	75	15.4	4.34	.78	1.84	2.84	---	3.89	10.91	23.60	31.94	---	39.15	119.5

Source: Dangler, El-Swaify, Ahuja and Barnett [124]

TABLE A.2

INFILTRATION RATE AS A FUNCTION OF TIME

MOLOKAI-A SOIL			
Site 1 Plot 1-Dry		Site 1 Plot 2-Dry	
TIME (MIN)	INFILT. RATE (IN/HR)	TIME (MIN)	INFILT. RATE (IN/HR)
27.0	2.31	23.0	2.29
28.0	2.30	24.0	2.28
30.0	2.27	26.0	2.23
32.0	2.24	27.0	2.18
33.0	2.22	28.0	2.15
34.0	2.17	30.0	2.06
35.0	2.11	32.0	2.01
36.0	2.08	33.0	1.81
37.0	2.03	36.0	1.70
38.0	1.97	38.0	1.69
39.0	2.06	39.0	1.65
40.0	2.02	42.0	1.49
43.0	1.81	43.0	1.42
46.0	1.58	45.0	1.38
48.0	1.56	48.0	1.32
49.0	1.53	50.0	1.27
52.0	1.40	53.0	1.18
57.0	1.43	54.5	1.13
66.0	1.09	58.0	1.15
67.0	1.12	63.0	1.12
72.0	1.22	65.5	1.10
73.0	1.24	68.0	1.05
77.0	1.06	70.5	1.00
87.0	1.33	73.0	0.95
97.0	0.97	75.5	0.88
107.0	0.97	81.0	0.94
117.0	0.89	83.0	0.92
		87.0	0.89
		92.5	0.81
		93.0	0.82
		94.0	0.83
		95.5	0.86
		98.5	0.63
		99.5	0.65
		103.0	0.67
		104.5	0.68
		105.5	0.64
		110.5	0.84
		111.5	0.63
		114.0	0.64
		115.5	0.74
		119.0	0.93

Source: Dangler, El-Swaify, Ahuja and Barnett [124]

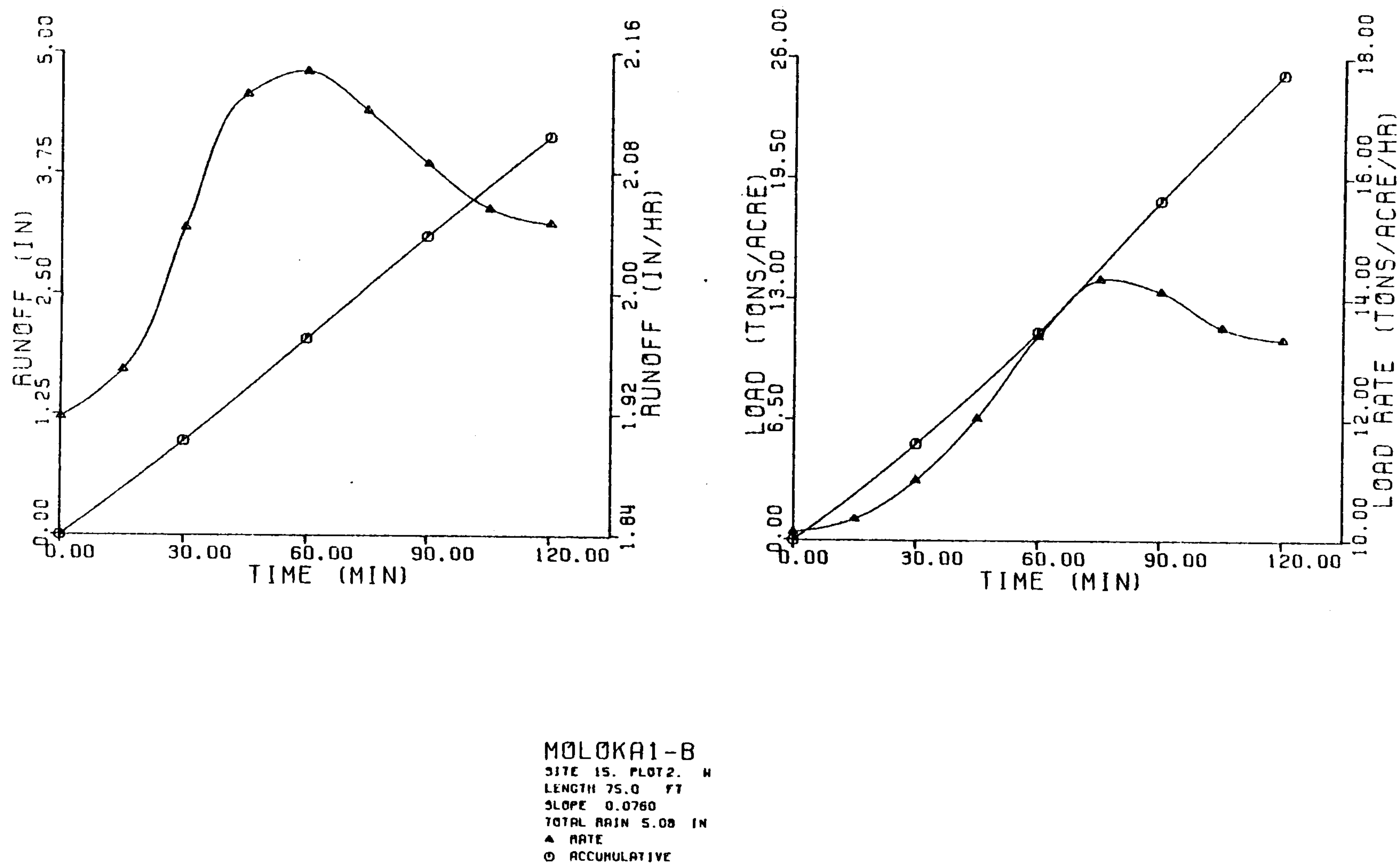

FIGURE A.2

SILTY CLAY LOAM SOIL (DRY)

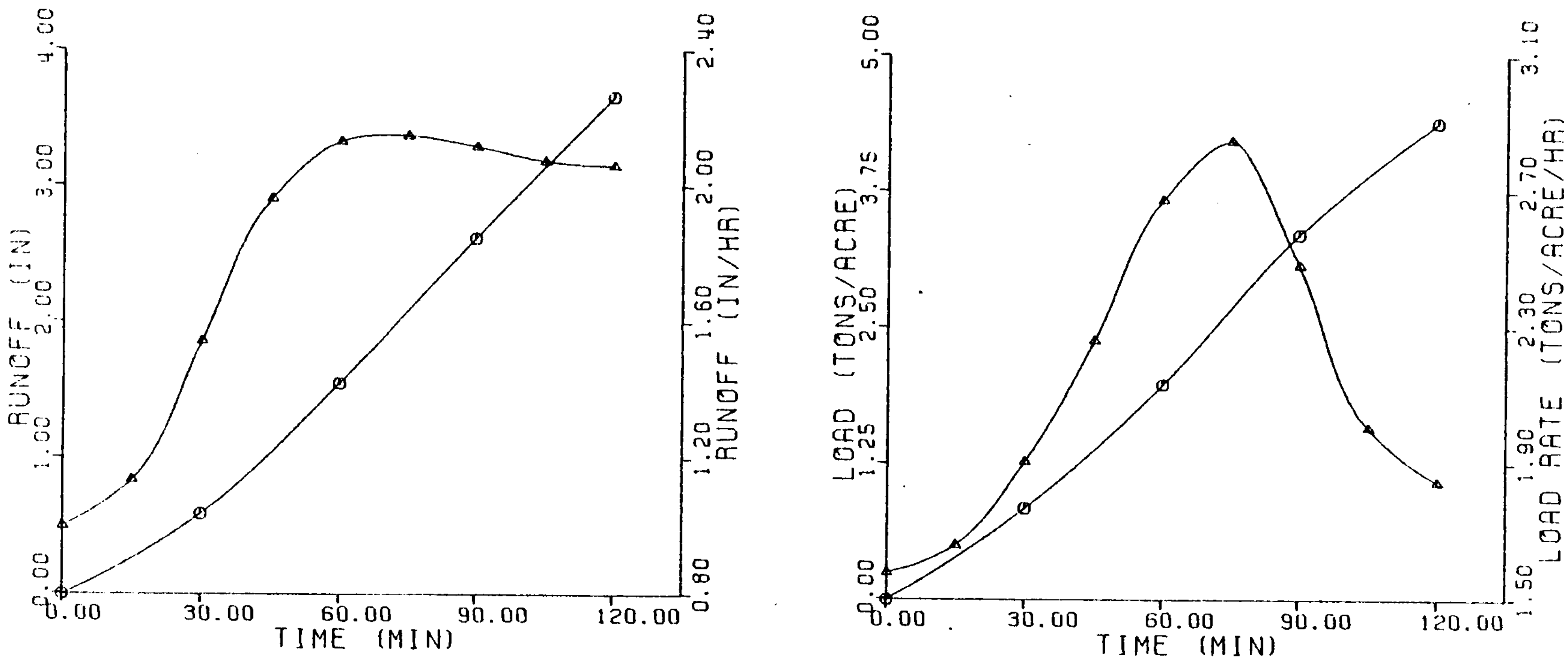

LUALUALE1
SITE 21, PLOT1, W
LENGTH 35.0 FT
SLOPE 0.0353
TOTAL RAIN 5.12 IN
△ RATE
⊘ ACCUMULATIVE

FIGURE A.3

SILTY CLAY LOAM (WET)

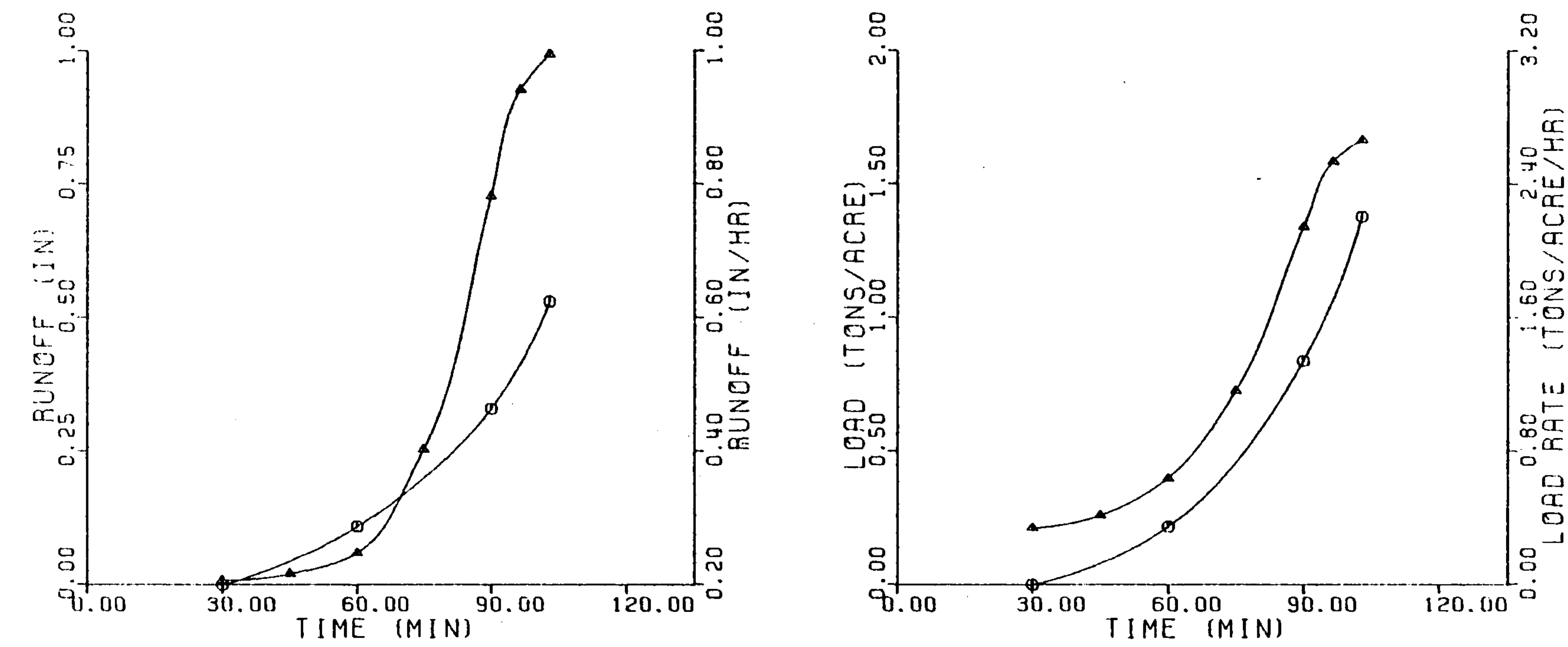

MOLOKA1-B
SITE 12. PLOT2.
LENGTH 75.0 FT
SLOPE 0.0460
TOTAL RAIN 4.37 IN
▲ RATE
⊕ ACCUMULATIVE

FIGURE A.4

VERY FINE CLAY SOIL (WET)

TABLE A.3

OPTIMIZED PARAMETERS IN ERODE-I

	Moisture Condition	Plot Length (FT)	Coefficient of Determination	C (1/FT)	C_T (LB/FT^3)	R_{DT} (LB/FT^2-HR)
Silty Clay Loam (Kaolinite)	Dry	35	0.82	0.0428	7.91	0.00558
		75	0.87	0.0128	12.71	0.0298
	Wet	35	0.69	0.685	14.31	0.0104
		75	0.82	0.0334	16.62	-0.0136
Silty Clay (Kaolinite)	Dry	35	0.95	0.0291	3.64	0.00572
		75	0.21	0.0141	8.79	0.0136
	Wet	35	0.36	*	14.68	*
		75	0.75	0.0280	13.07	-0.0251
Stoney Fine Sandy Loam	Dry	35	0.80	0.0483	12.88	0.00625
	Wet	35	0.89	0.0390	6.27	0.0185
Very Fine Clay (Montmorillonite)	Dry	35	0.99	0.0616	16.23	0.00414
		75	0.99	0.0173	3.63	-0.000189

*Values not available

characteristics are grouped and indicated by soil type classification, initial moisture conditions and plot length.

Table A.3 displays the evaluated reaction coefficient, C, the ratio of the soil detachment constant, C_D, to the soil transport coefficient, C_T. These figures indicate that for the soils considered and conditions observed, these soils are more transportable than they are detachable. These observations are reasonable in light of the soil make up, since erodibility of soils decrease as the percentage of clay or organic matter (loam) content increases. Clay acts as a binder between particles and tends to limit detachment. Most soils with high clay content are relatively resistent to detachment by rainfall and runoff. Once eroded, however, clays are easily transmitted and settle out slowly [127].

An increase in organic matter (loam) reduces erodibility in a different manner by maintaining a favorable structure which improves its stability and permeability [127]. This increases infiltration capacity and delays the start as well as reducing the amount of runoff. All of the soils under investigation were reported to be well drained. After the start of a rainfall event, loam soils averaged a longer time to the beginning of runoff than did the fine clay soils.

Well-drained and well-graded gravels and gravel sands with little or no silt are not easily erodible (detached). Coarse granular soils also have high permeabilities and good infiltration capacities which can either prevent or delay runoff [127].

Clayey soils are known to have higher water holding capacities and poorer infiltration characteristics relative to sands and gravels.

In this report, clayey soils are more vulnerable to erosion because they tend to increase the amount of runoff [127]. This can be observed in Table A.3 by the increase in C values under wet conditions compared to C values under dry conditions for soils containing clay, i.e. the ratio of detachment to transport potential increases. The sandy soil on the other hand has a slight decrease or possibly no significant change from dry to wet conditions.

The erosion reaction constant, C, is formulated in terms of unit slope length. Conversion of this constant to eliminate the slope length relation results in remarkably similar constants for soils having different slope length. These are tabulated in Table A.4. These figures suggest the possibility of producing a reaction constant for a soil type as a function of its initial moisture content, independent of slope length.

Optimized values for the transport coefficient, C_T, are presented in Table A.3. C_T is dependent upon particle size and density and differences in the observed values can be explained in this light. The silty clay is slightly less transportable than the silty clay loam for both the wet and dry conditions. However, both of these soils are considerably less transportable under dry conditions. This can be attributed to clay losing or reducing its binding qualities under wet conditions and releasing smaller silt, loam and clay particles to be transported.

The stoney fine sandy loam has just the opposite effect. The well-drained material is more easily transported when dry rather than wet conditions prevail. Under high moisture conditions, this well-drained

TABLE A.4

C ADJUSTED FOR LENGTH

			C Adjusted	Avg C
Silty Clay Loam	Dry	35	1.4	1.2
		75	1.0	
	Wet	35	2.4	2.45
		75	2.5	
Silty Clay	Dry	35	1.0	1.0
		75	1.0	
	Wet	35		2.1
		75	2.1	
Stoney Fine Sandy Loam	Dry	35	1.7	1.7
	Wet	35	1.4	1.4
Very Fine Clay	Dry	35	2.1	1.7
		75	1.3	

soil allows the extremely fine material to either pass deeper into the soil with infiltration or be transported away first leaving a layer of larger particles on the surface. This creates an armoring effect and decreases the transportability of soil under wet conditions for flows less than that previously encountered.

The dry fine soil, according to Table A.3, displays the potential to be as transportable as the silty clay soils are when wet.

R_{DT}, shown in Table A.3 (page 173), is the average rainfall detachment rate over the storm duration. Although some patterns and conclusions can be drawn from these optimized values, they are not strongly persuasive and require a larger data base to ascertain their true worth. The most pertinent observation is that in all cases the rainfall detachment term of the erosion model contributed less than 10 percent of the significant load rates.

The soils R_{DT} values indicate that rainfall detachment increases due to plot length for dry conditions and increases for wet conditions where plot length is under 35 feet. Several of the wet soil conditions are negative. These could be attributable either to noise in the data since the rainfall detachment contribution is so low or possibly represent the effect of slowing down surface flow by the beating action of the raindrops. This latter phenomenon has been recognized to occur in sheet or overland flow [128]. The implications of this is that the rainfall detachment term reacts as a deposition term as well as an erosion term.

Load Modulus

The erosion model, A.8, when integrated over the duration of the storm results in the following load equation

$$L = \frac{1-e^{-cx}}{c} R_{DT} T + C_T S \nabla w + \frac{\gamma\delta}{c} R\phi \qquad (A.9)$$

where L is load per unit width, T is storm duration, $R\phi$ is total excess rainfall, and ∇w is volume of runoff per unit width. Since the load modulus is a representation of the sediment concentrations generated for significant flows and is defined as

$$\mu = \frac{L}{xR\phi} = \gamma\delta \qquad (A.10)$$

where μ is the load modulus, x is the plane length, γ is the unit weight of soil, and δ is the volume concentration of soil to water; then equation A.9 can be transformed into the following load modulus simulator

$$\mu = \frac{1-e^{-cx}}{(cx-1)} R_{DT} \frac{T}{R\phi} + C \left\{\frac{C_T \; Sx}{(cx-1)}\right\} \qquad (A.11)$$

Equation A.11 was optimized using the Hawaiian data to obtain coefficients that would represent the terms $\frac{1-e^{-cx}}{cx-1} R_{DT}$ and $\frac{C \; C_T}{cx-1}$. Once the coefficients were obtained values for R_{DT} and C_T were used from Table A.3 (page 173) to obtain values of C. The results of this technique are listed in Table A.5.

The similarity of the C values between the erosion model and the load modulus model are good. Discrepancies between the C values appear to be caused by variations in the ability to measure the runoff and erosion, i.e. noise in the raw data. This load modulus simulator allows the erosion model to be used since the concentration factor can be simulated.

TABLE A.5

REACTION CONSTANT COMPARISON

			Load Modulus Coefficient of Determination	C from Load Modulus Model	C from Erosion Model
Silty Clay Loam	Dry	35	0.75	0.0371	0.0428
		75	0.82	0.0167	0.0128
	Wet	35	0.85	0.0557	0.0685
		75	0.99	0.0243	0.0334
Silty Clay	Dry	35	0.88	0.0332	0.0291
		75	0.95	0.0171	0.0141
	Wet	35	0.90	0.0715	*
		75	0.97	0.0187	0.0280
Stoney Fine Sandy Loam	Dry	35	0.89	0.0528	0.0483
	Wet	35	0.95	0.0489	0.0390
Very Fine Clay	Dry	35	0.93	0.0614	0.0616
		75	*	*	0.0173

*Indicates value is missing.

ERODE-I Simulation

The erosion model, ERODE-I, is capable of simulating the time distribution of erosion mass transport rate as well as determining the total load at the end of a specific site slope per unit width for any real time storm or design storm rainfall distribution. This model has been developed into a Fortran computer program for the IBM 360. Input requirements are minimal and consist of the rainfall time distribution, the slope, slope length, Manning-n value, SCS curve number, C, C_T and load modulus. A comparison of actual and simulated events using this model are presented in Figures A.5 and A.6.

The event simulated in Figures A.5 and A.6 is for an average rainfall intensity of 2.4 inches per hour on a dry silty clay loam for a storm duration of two hours. The accumulated runoff in Figure A.5 compares well. The observed total runoff being 1.59 inches as compared to 1.58 inches predicted by ERODE-I. The runoff rate produced by ERODE-I lags the runoff rate curve produced by the spline fitting technique. This difference is considered to occur due to the necessity of selecting what were felt to be reasonable values for certain hydrologic inputs, such as Manning-n values, that are not available in the Hawaiian published data.

The soil loss events for this storm are shown in Figure A.6. The accumulated load compares well with the observed loads. The observed total soil loss was 8.44 tons per acre and the predicted loss was 8.70 tons per acre. Differences in load rates are the results of mathematical anomalies experienced because of small errors in data collection.

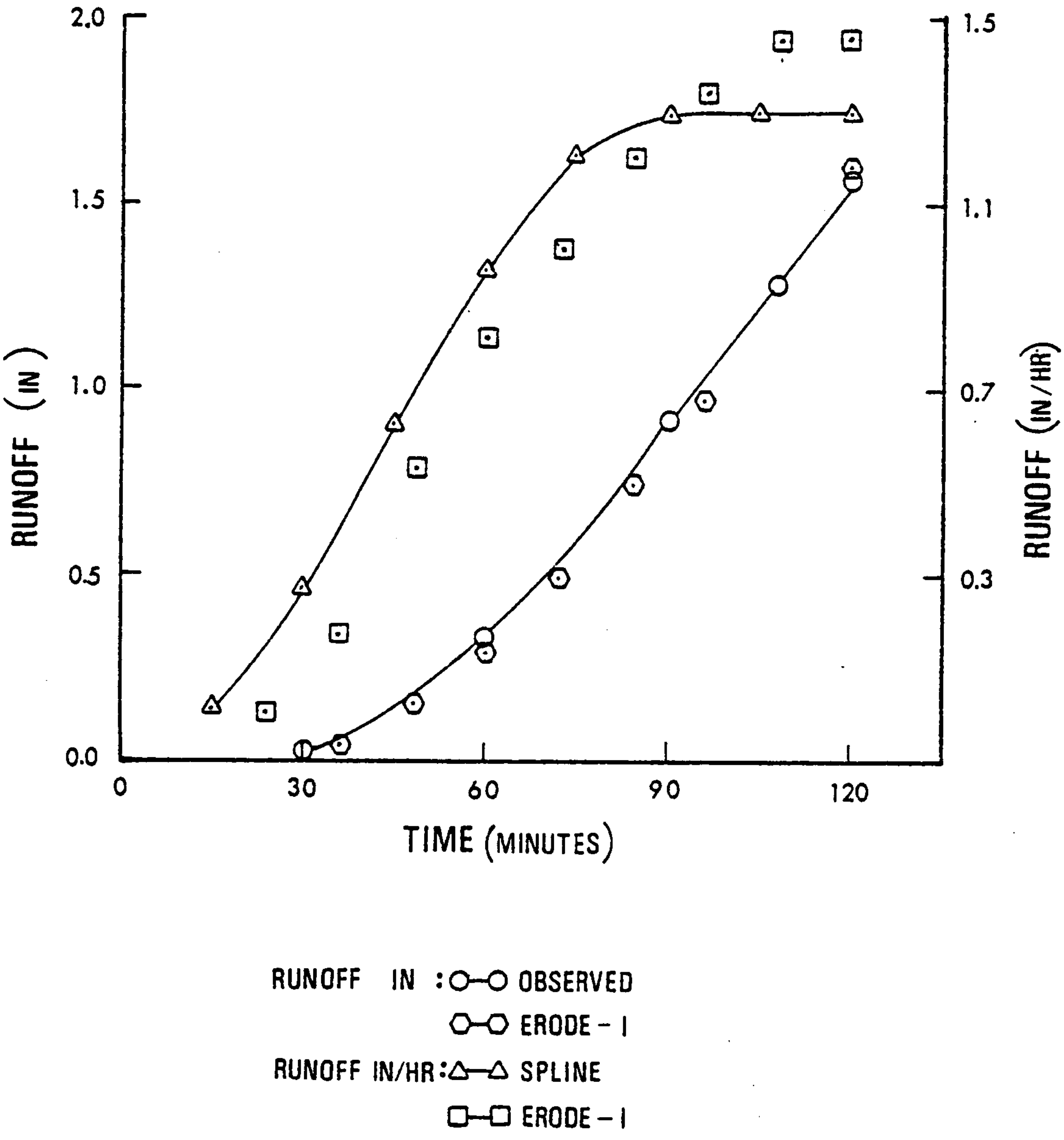

FIGURE A.5

OBSERVED AND SIMULATED RUNOFF (SITE 1, PLOT 1, DRY)

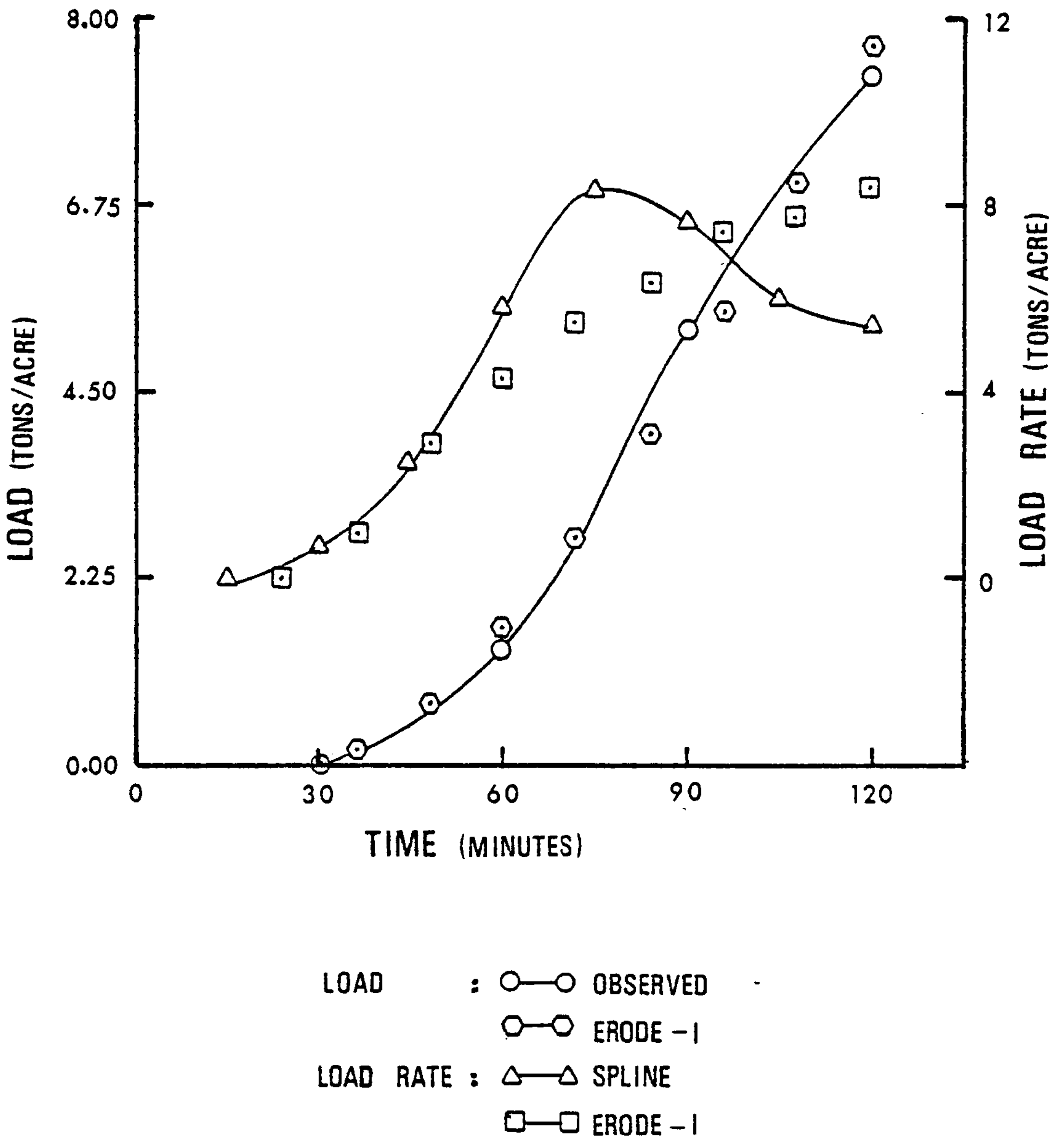

FIGURE A.6

OBSERVED AND SIMULATED LOAD AND LOAD RATE (SITE 1, PLOT 1, DRY)

If the accumulated load of the 90 minute observation had been slightly lower, say 5.1 tons per acre instead of 5.3 tons per acre, the inflection point of the accumulated load would have moved to the right. This would cause the spline routine to simulate load rates that are more comparable to those produced by ERODE-I.

The above example is representative of all simulations run on the Hawaiian data. The load curves, total loads and accumulated runoff show good approximations, while the rate curves ranged from fair to good. In comparing the rate curves, it must be remembered that the comparison is not between observed and predicted rate curves, but between two different techniques of simulation.

The ERODE-I model and Lag Modulus model are functions of measurable site values and the constants in Table A.3 (page 173). The continued determination of the constants C, C_T and R_{DT} will allow these models to be applied to ungaged sites.

APPENDIX B

REGRESSION OF URF PARAMETERS

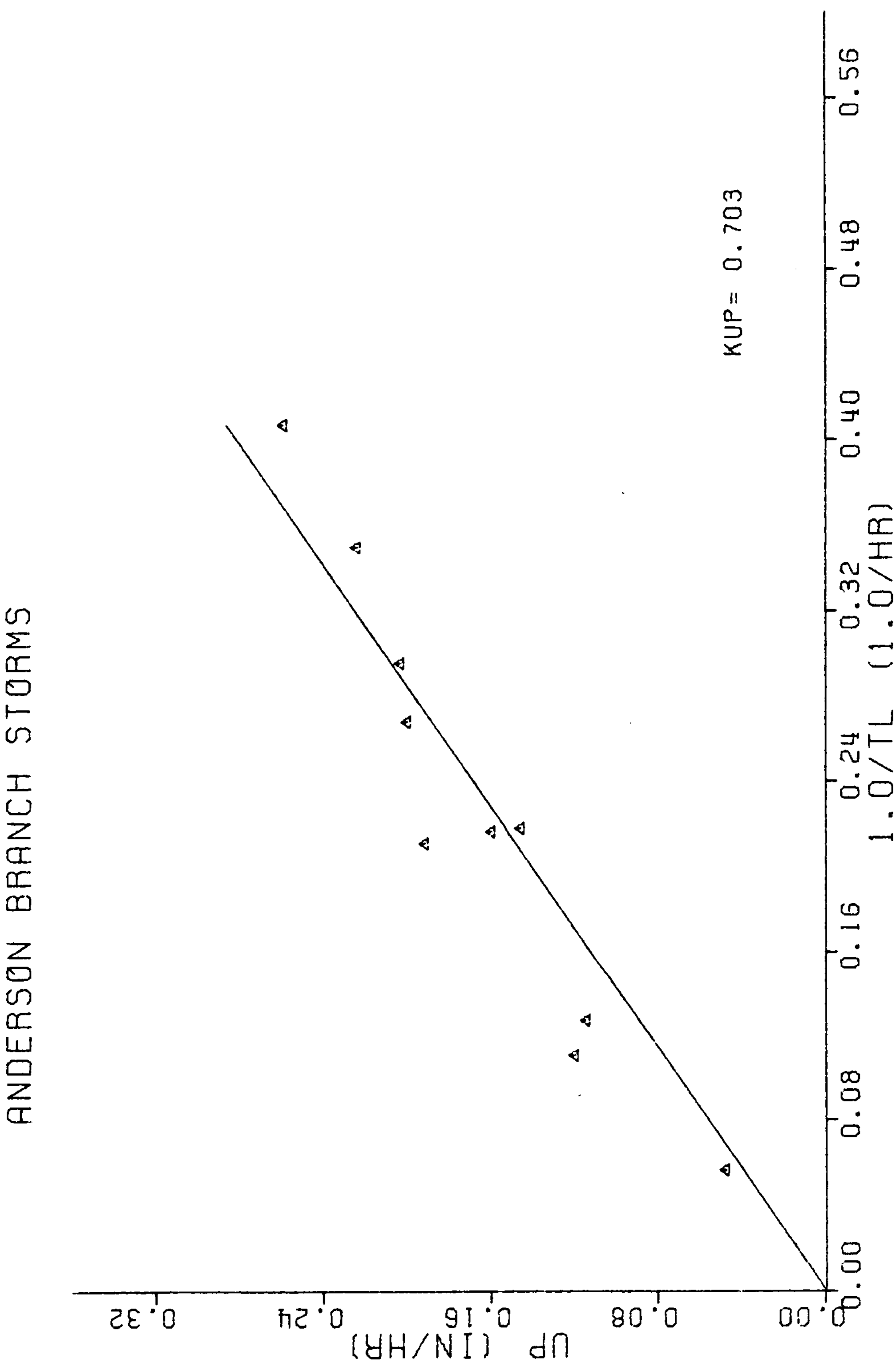

FIGURE B.1

REGRESSION OF UP VERSUS 1/TL - ANDERSON BRANCH

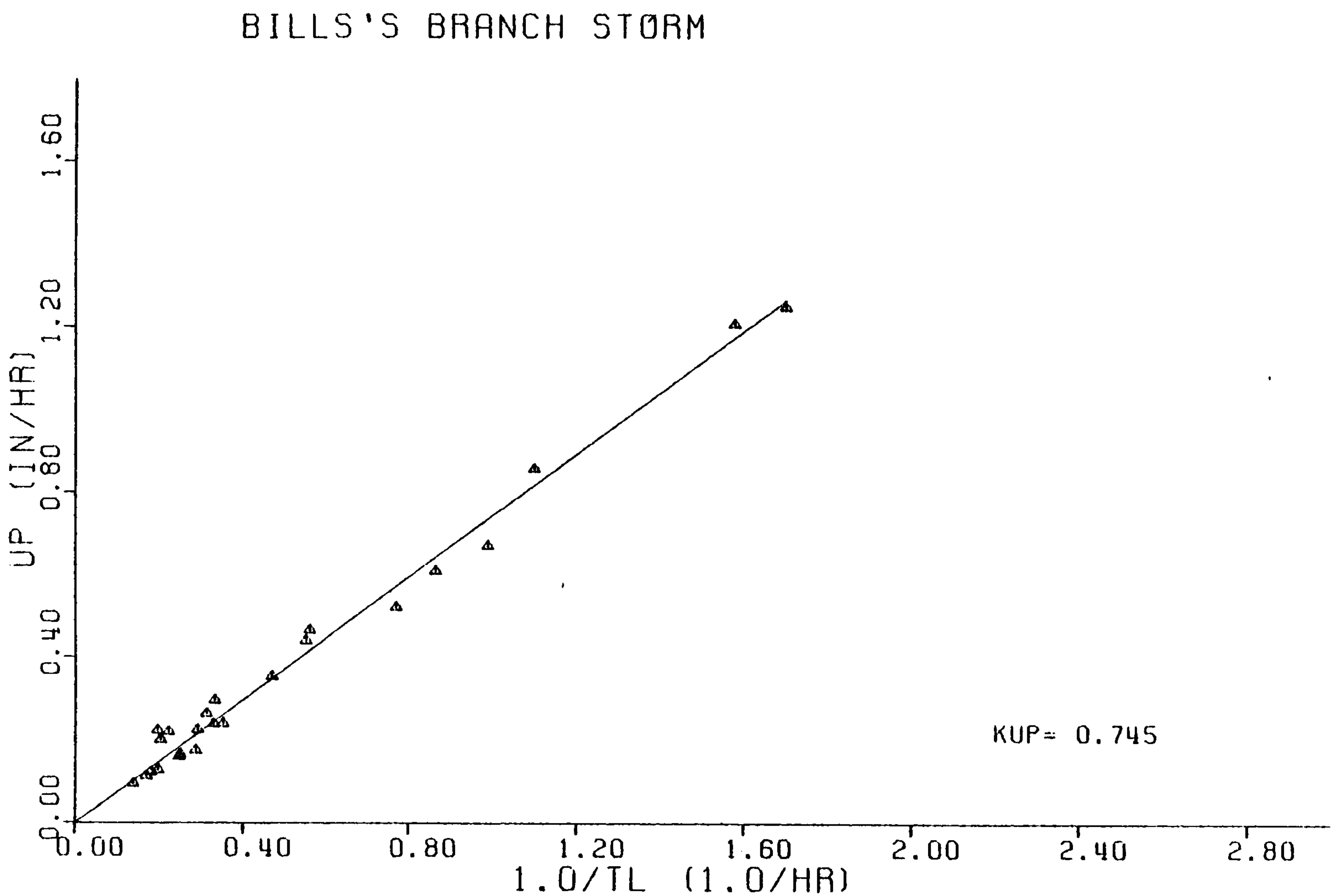

FIGURE B.2

REGRESSION OF UP VERSUS 1/TL - BILL'S BRANCH

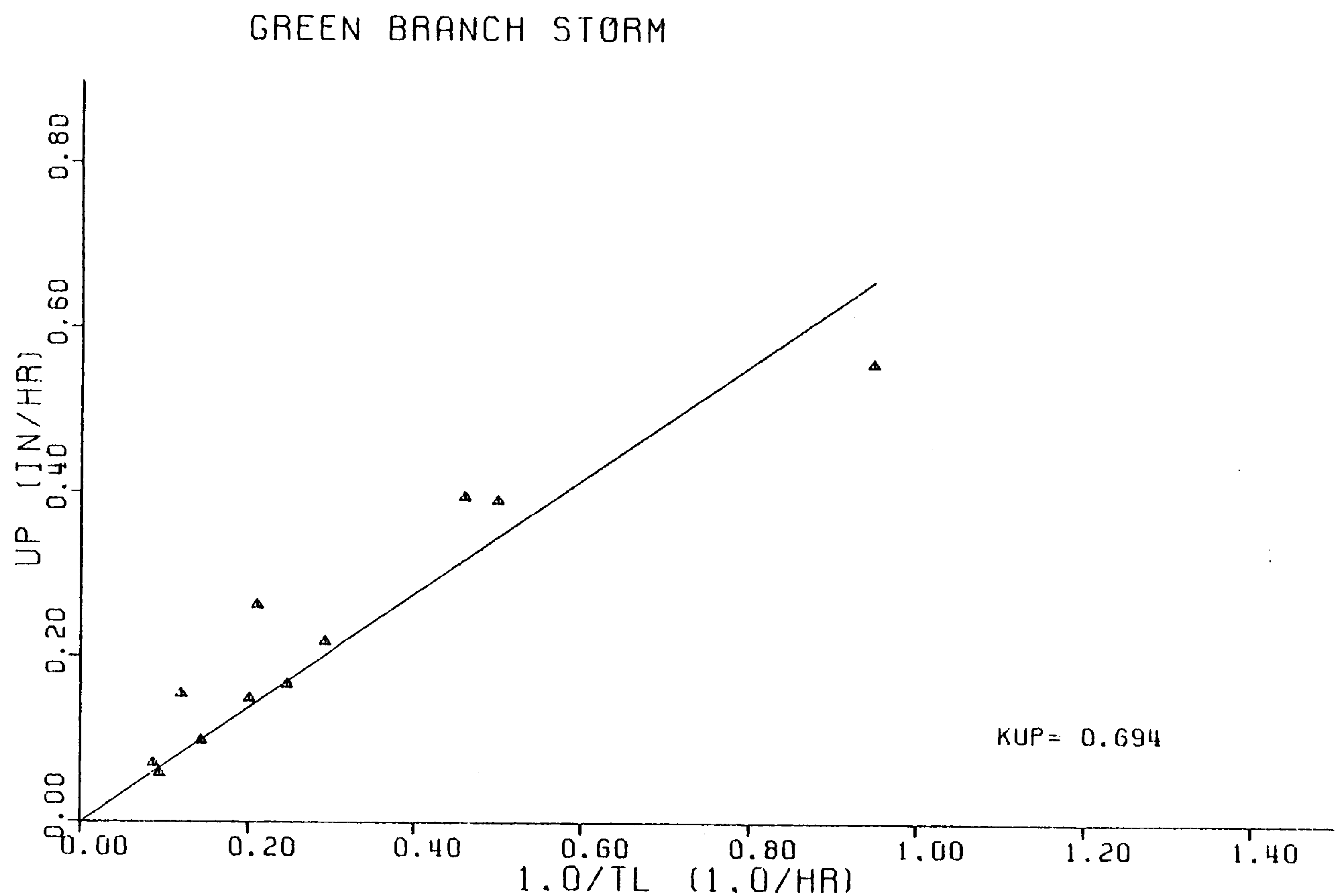

FIGURE B.3

REGRESSION OF UP VERSUS 1/TL - GREEN BRANCH

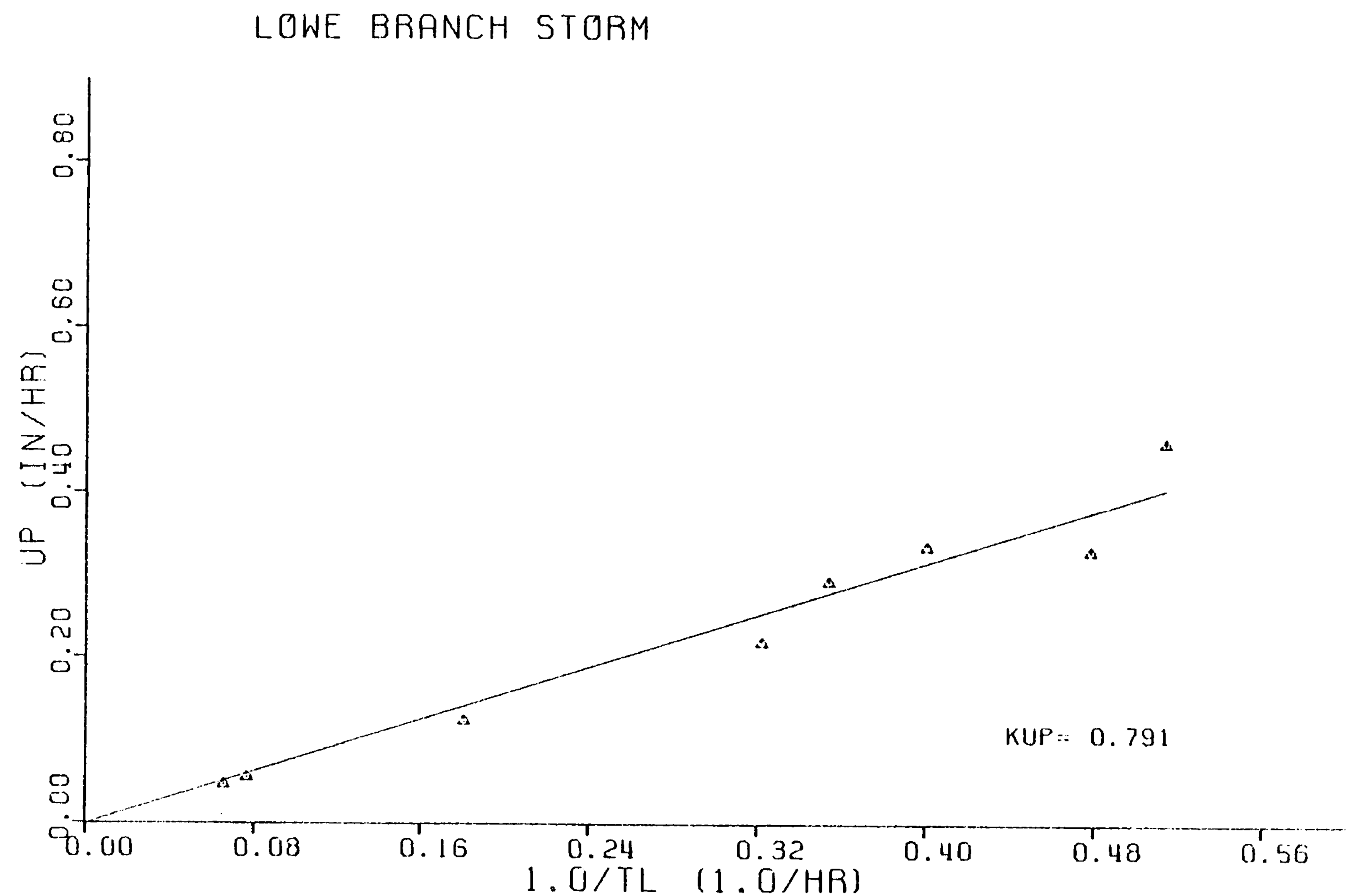

FIGURE B.4

REGRESSION OF UP VERSUS 1/TL - LOWE BRANCH

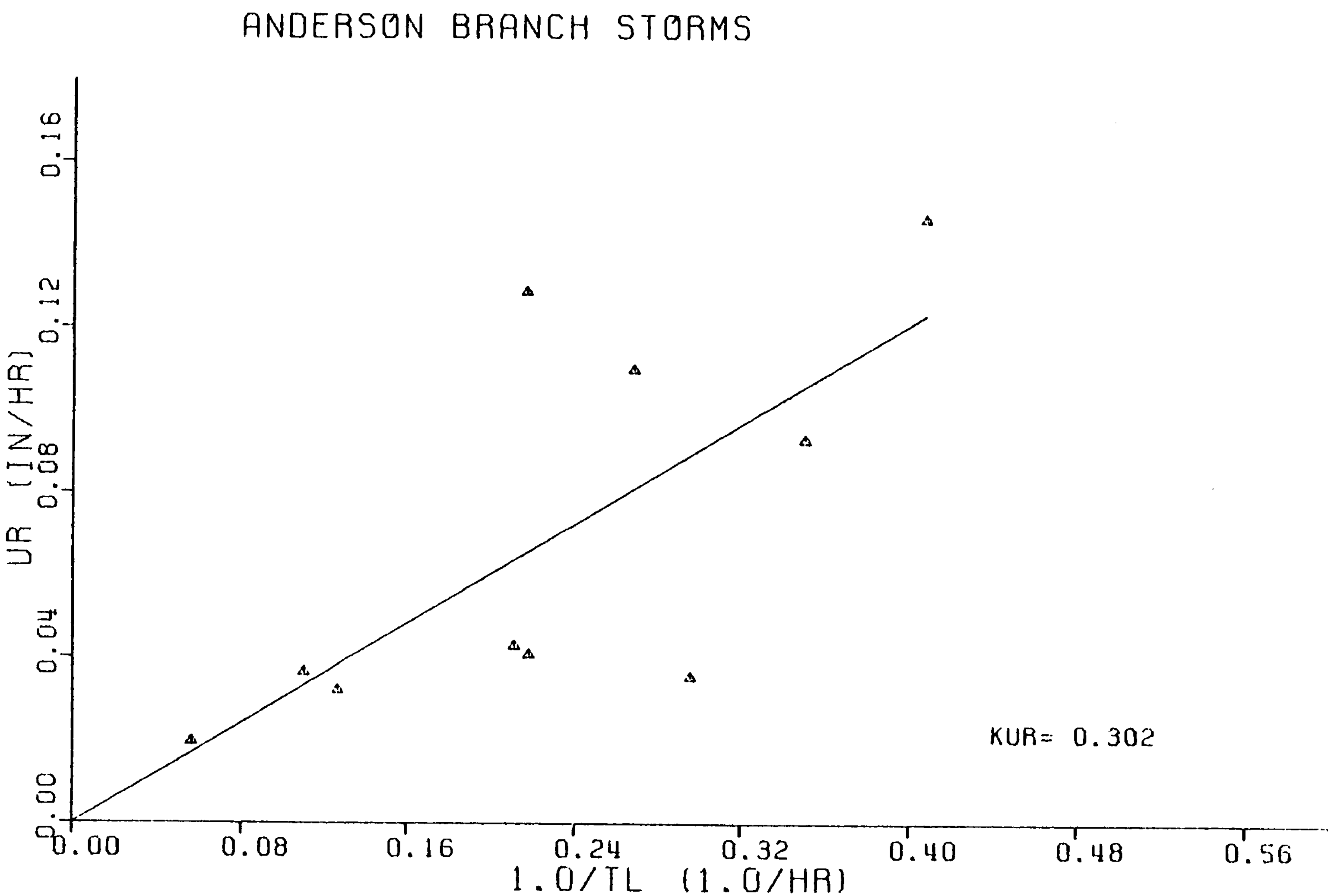

FIGURE B.5

REGRESSION OF UR VERSUS 1/TL - ANDERSON BRANCH

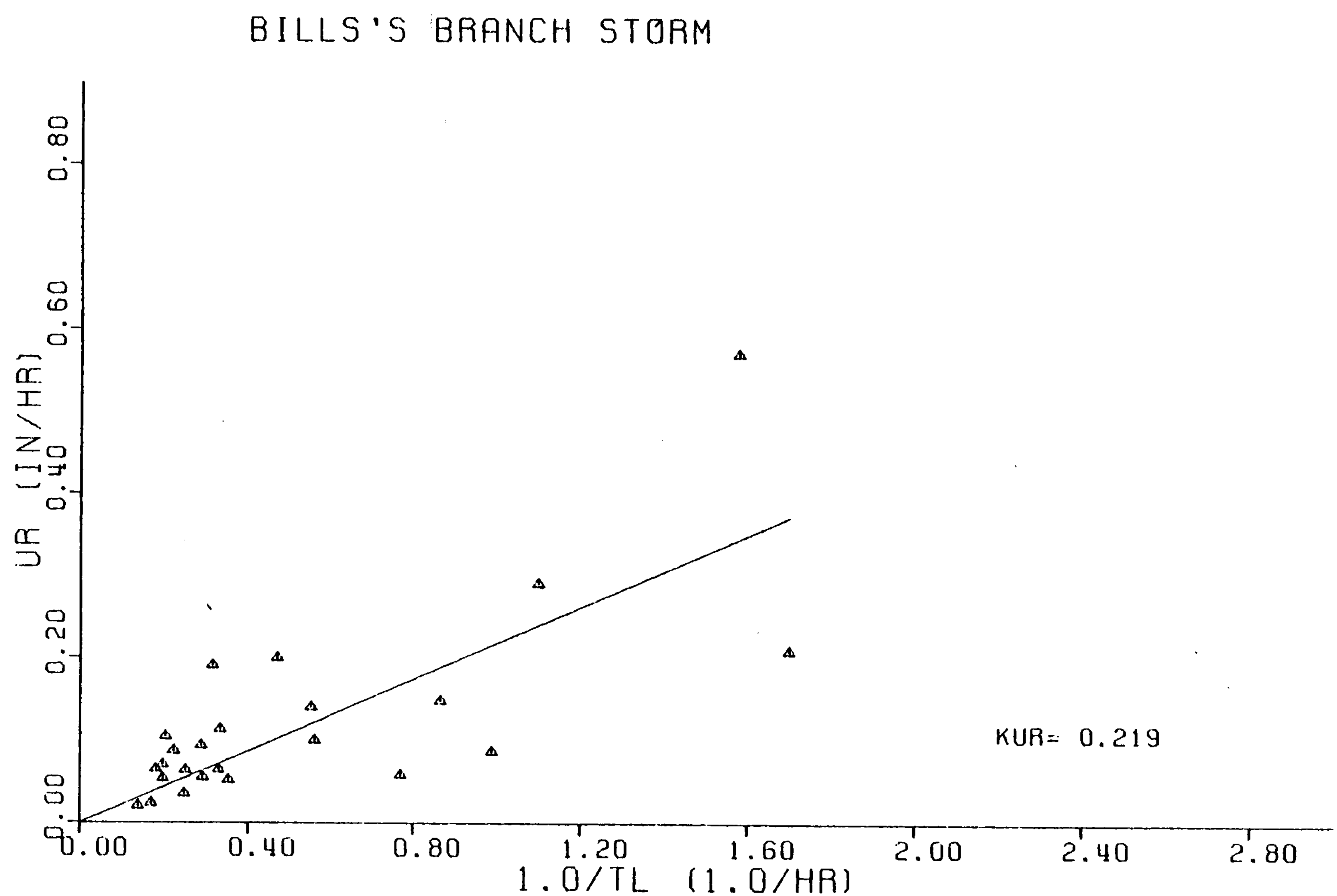

FIGURE B.6

REGRESSION OF UR VERSUS 1/TL - BILL'S BRANCH

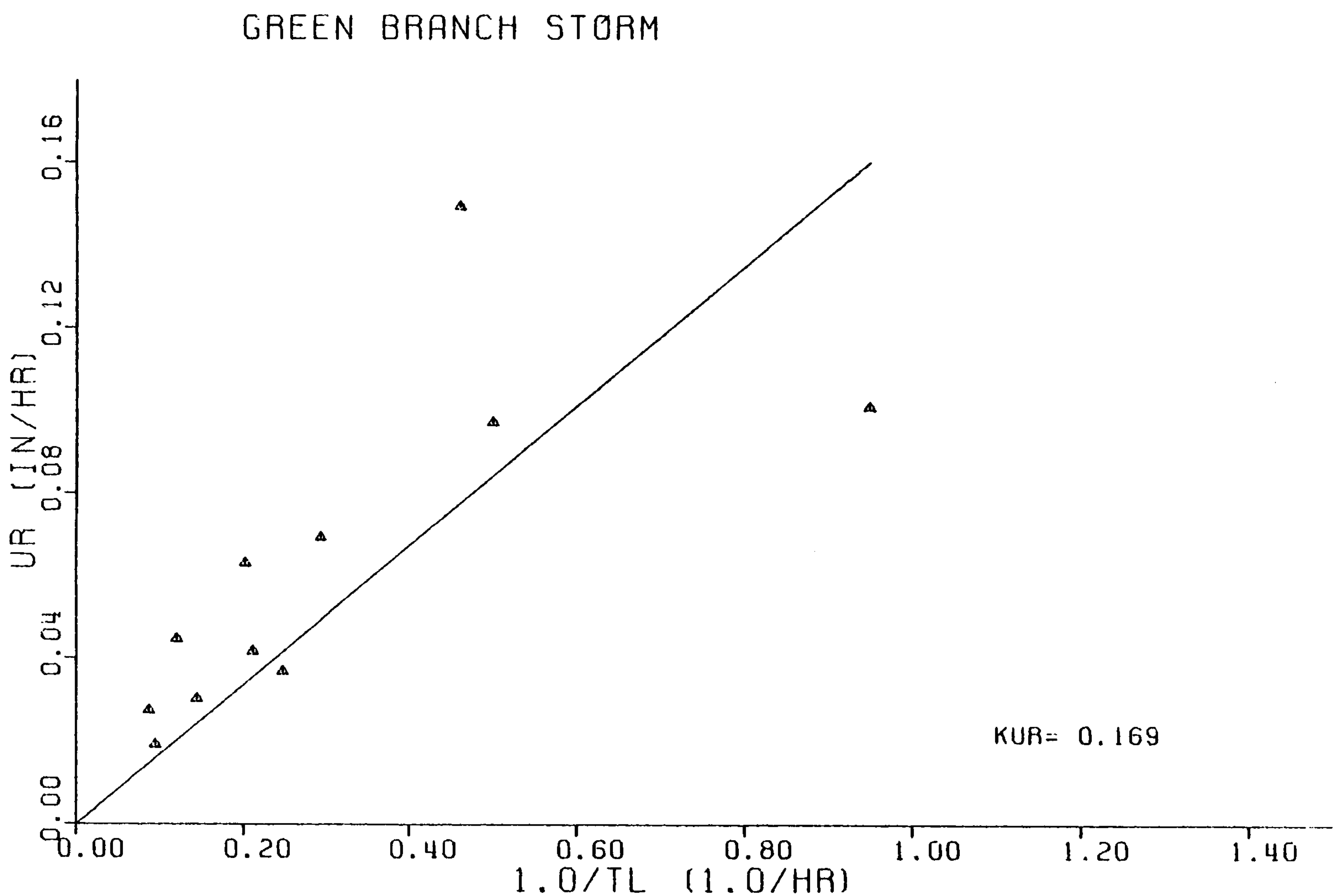

FIGURE B.7

REGRESSION OF UR VERSUS 1/TL - GREEN BRANCH

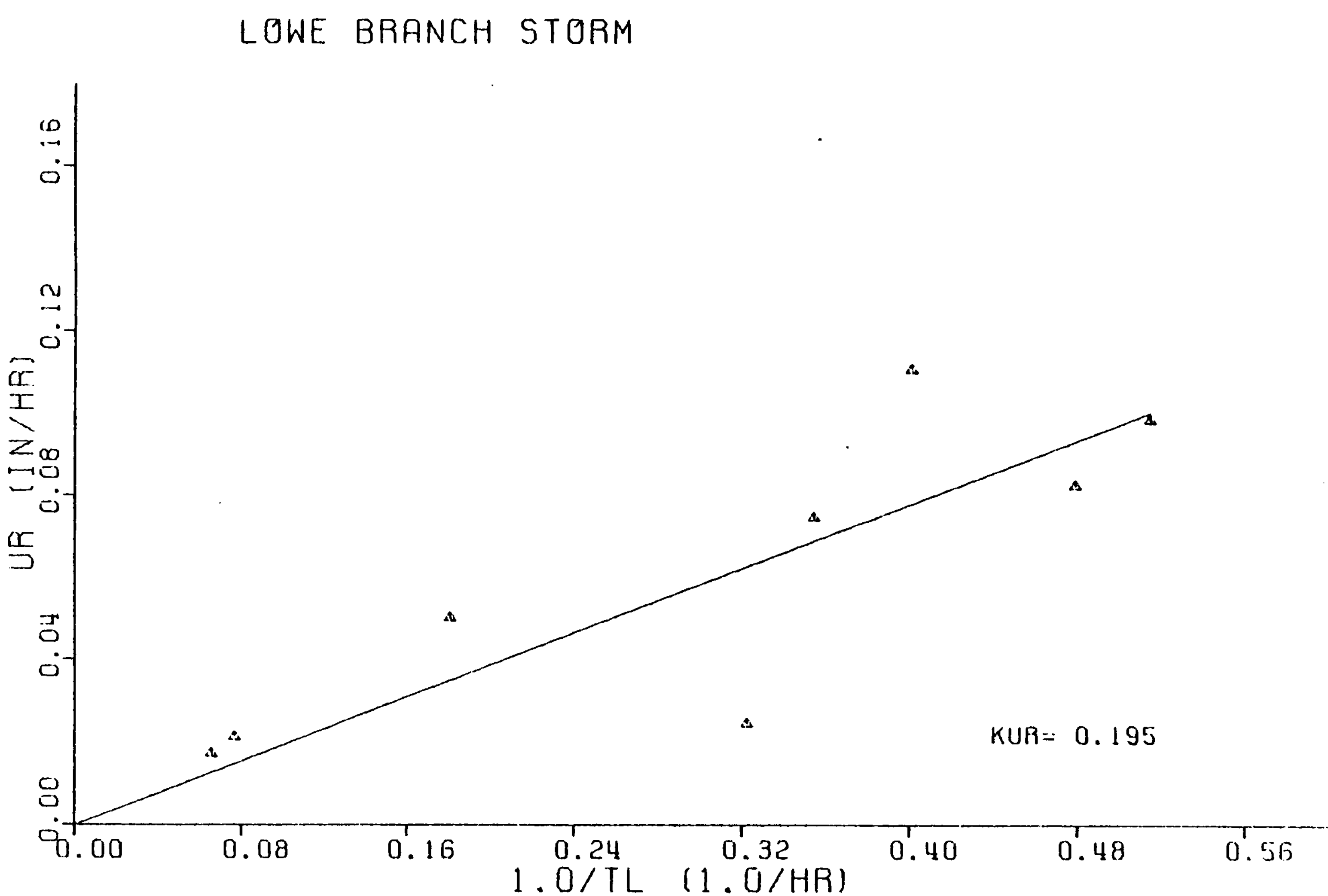

FIGURE B.8

REGRESSION OF UR VERSUS 1/TL - LOWE BRANCH

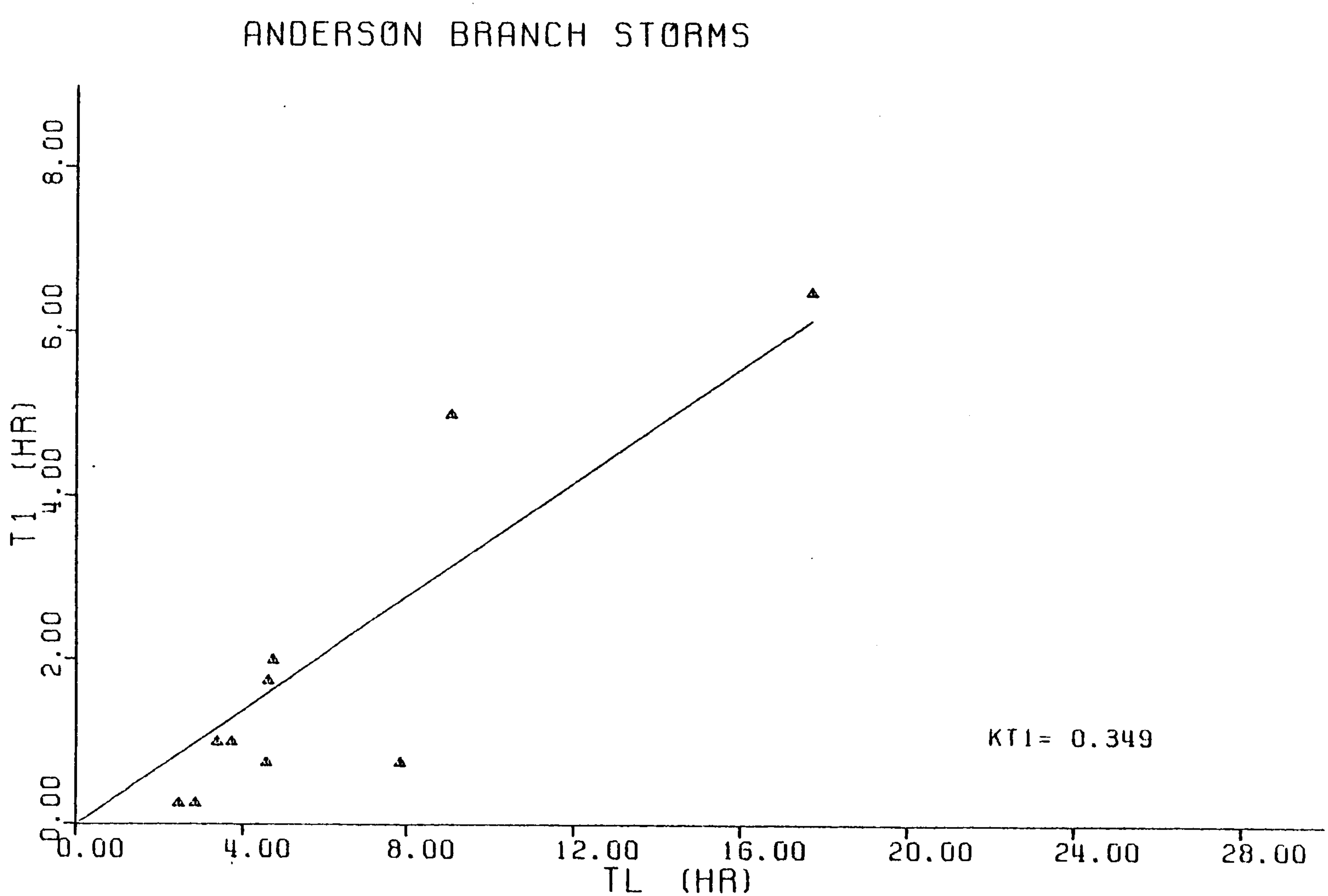

FIGURE B.9

REGRESSION OF T1 VERSUS TL - ANDERSON BRANCH

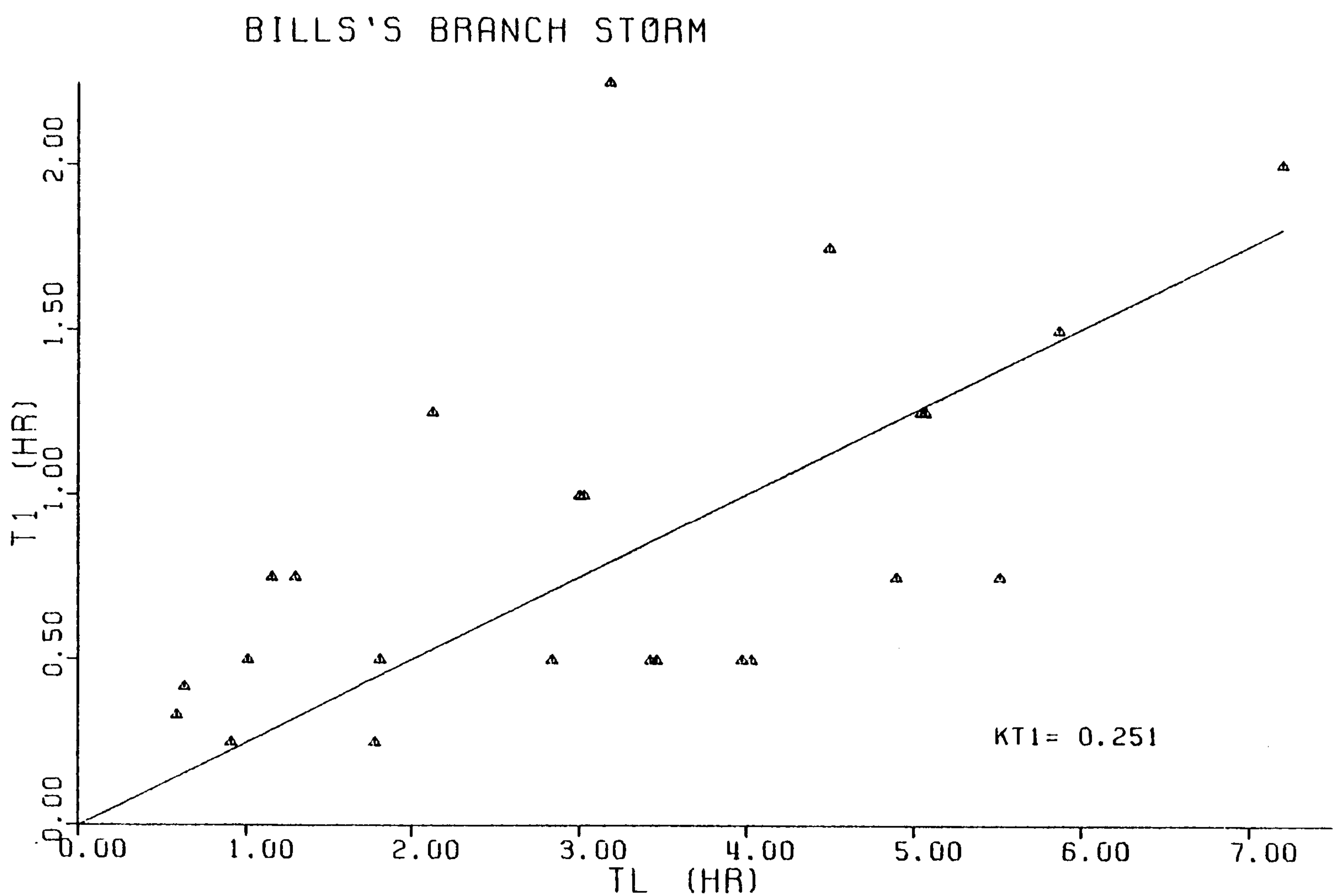

FIGURE B.10

REGRESSION OF T1 VERSUS TL - BILL'S BRANCH

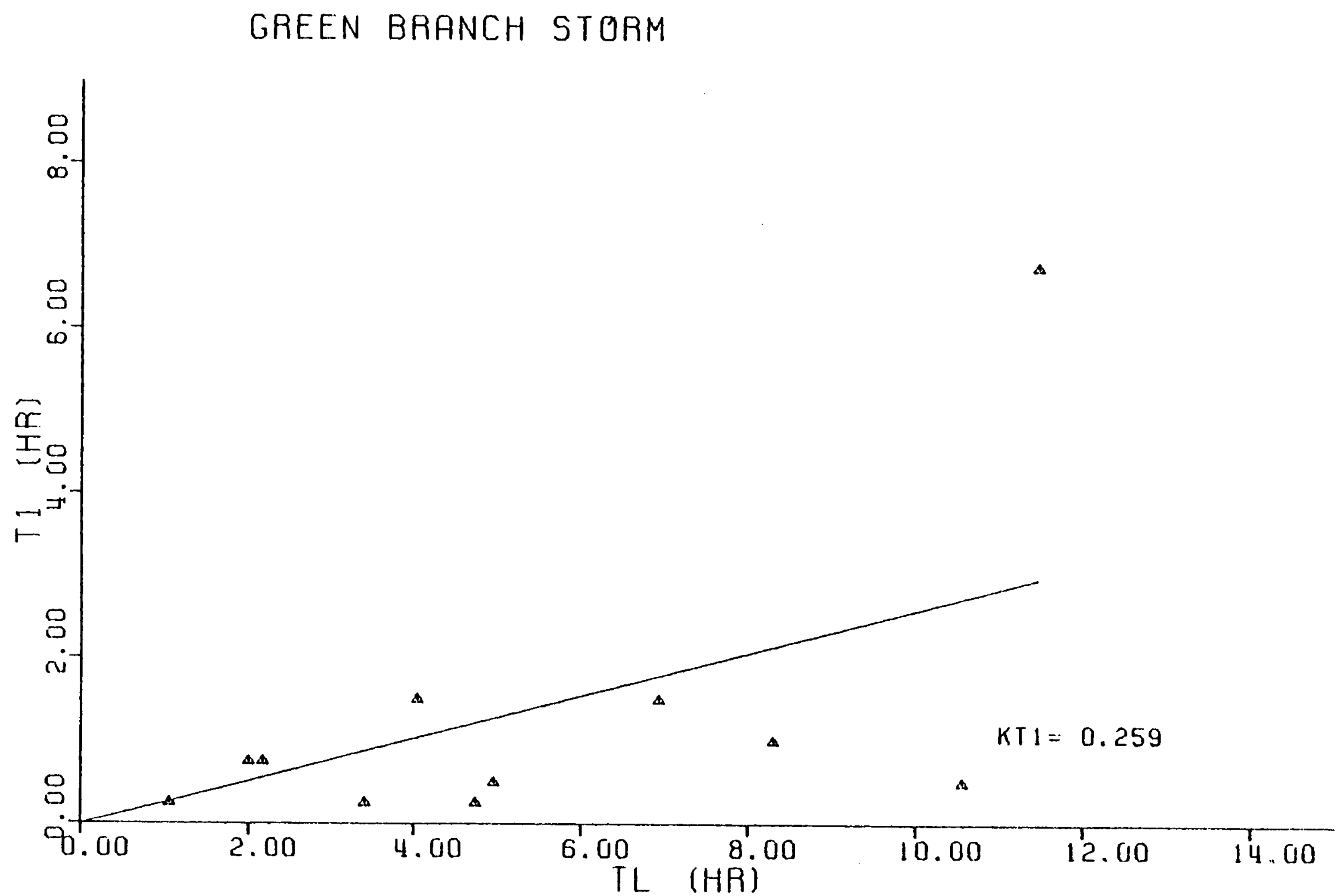

FIGURE B.11

REGRESSION OF T1 VERSUS TL - GREEN BRANCH

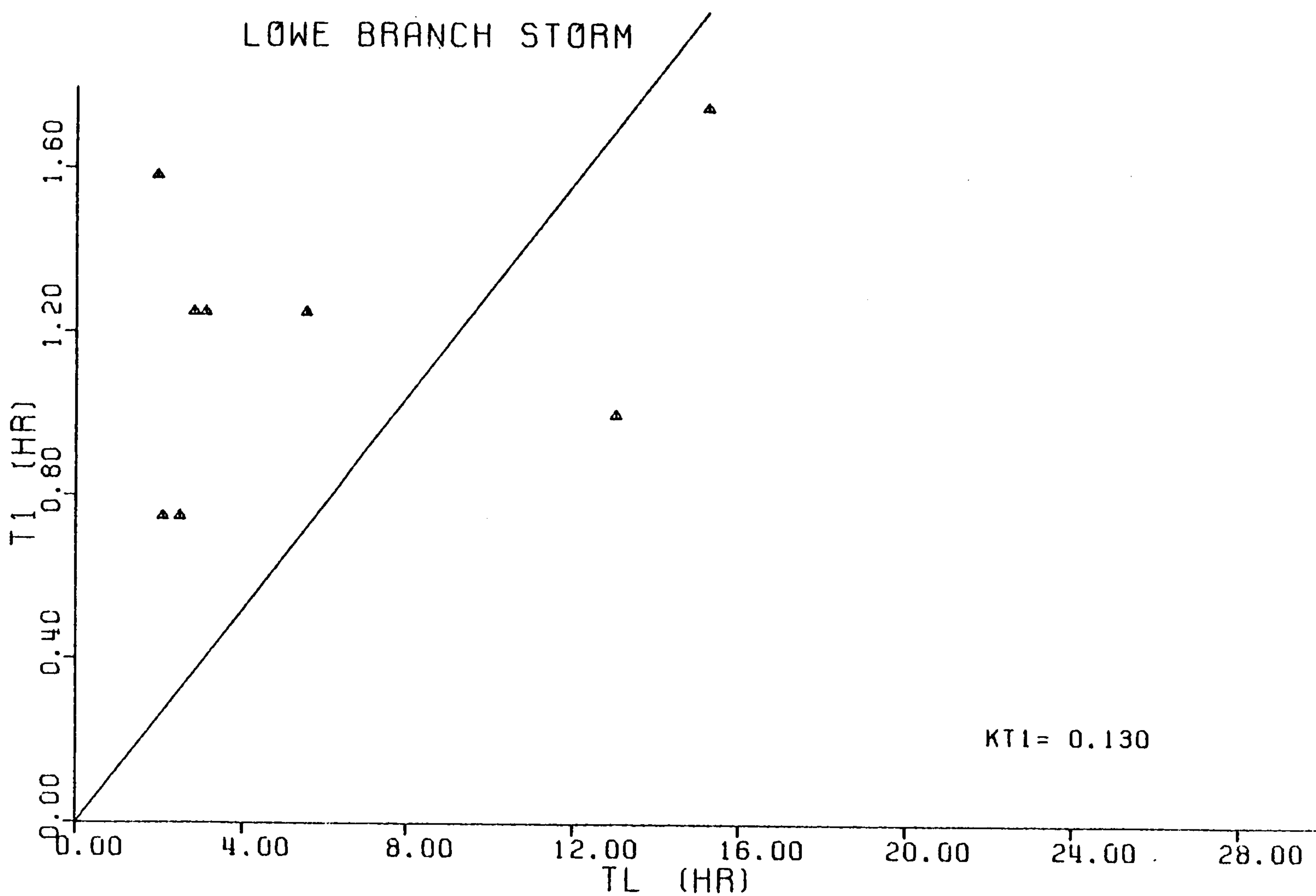

FIGURE B.12

REGRESSION OF T1 VERSUS TL - LOWE BRANCH

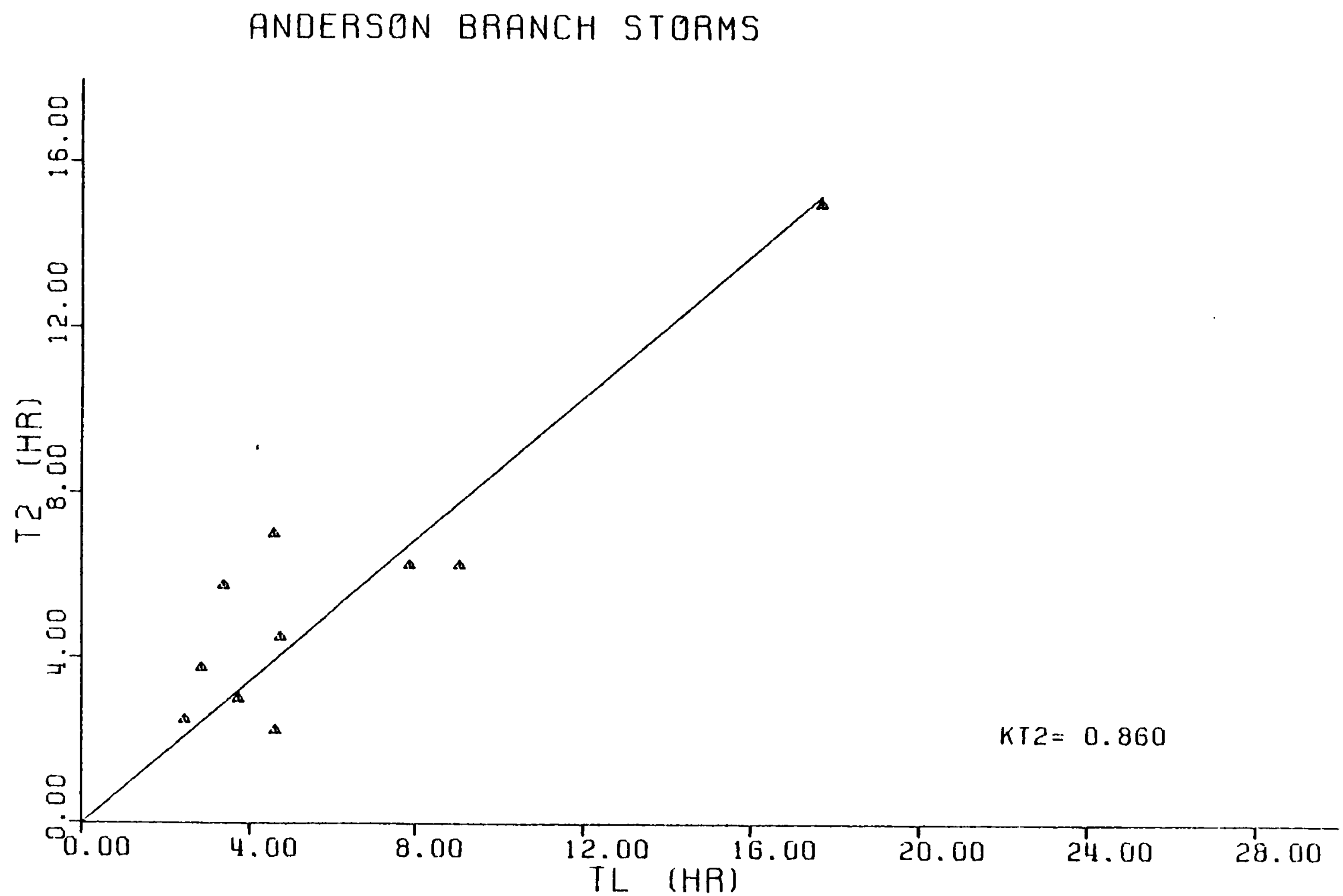

FIGURE B.13

REGRESSION OF T2 VERSUS TL - ANDERSON BRANCH

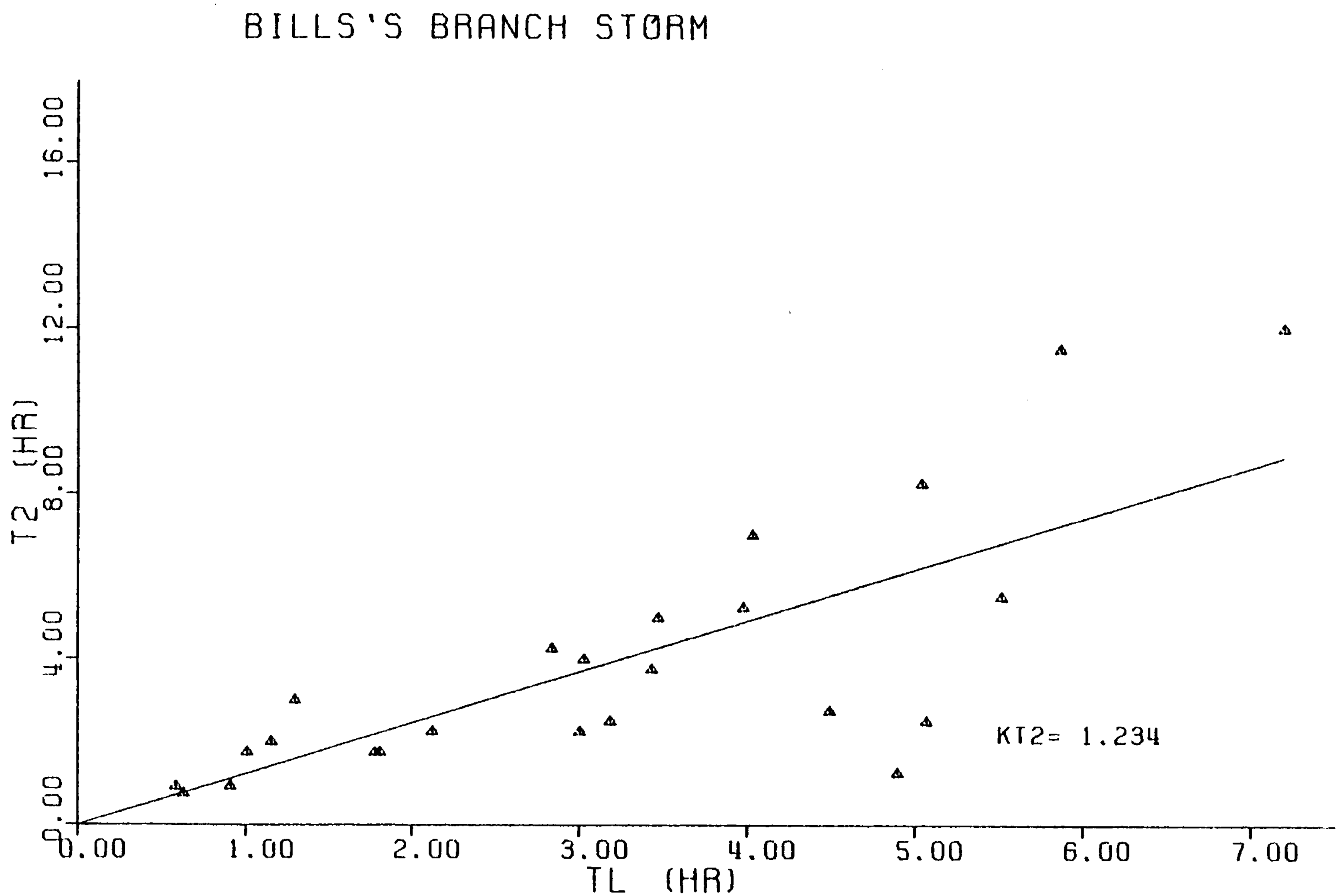

FIGURE B.14

REGRESSION OF T2 VERSUS TL - BILL'S BRANCH

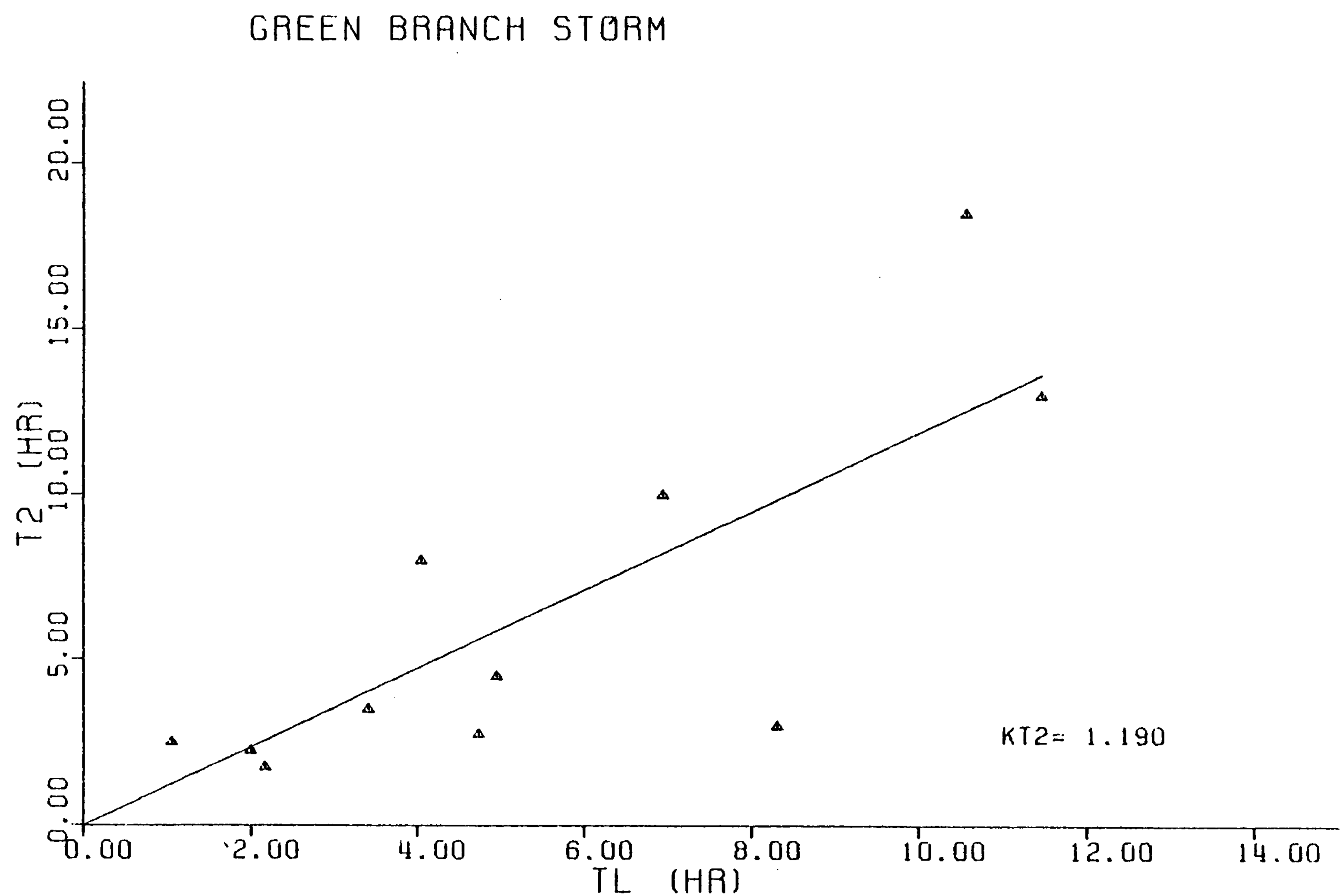

FIGURE B.15

REGRESSION OF T2 VERSUS TL - GREEN BRANCH

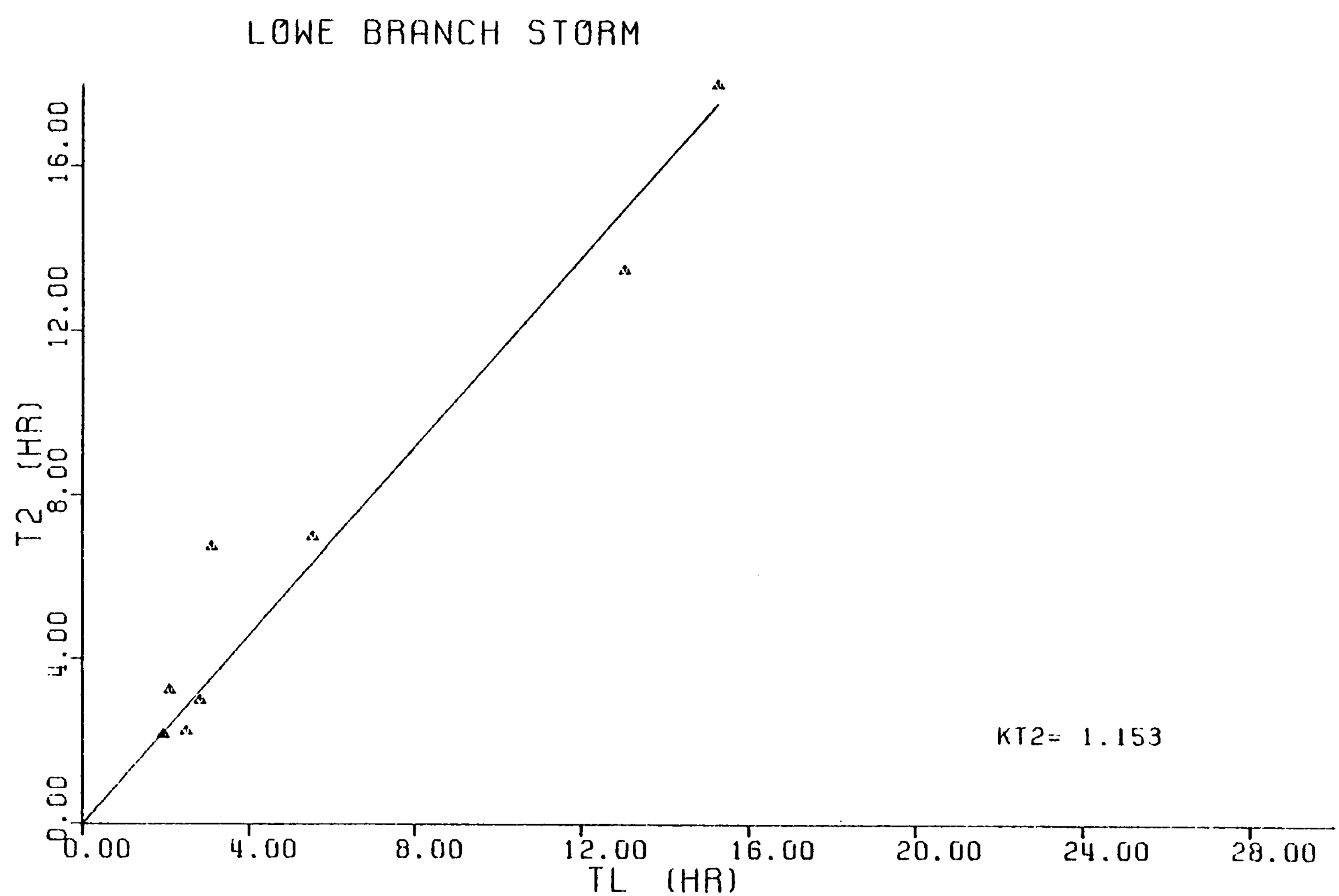

FIGURE B.16

REGRESSION OF T2 VERSUS TL - LOWE BRANCH

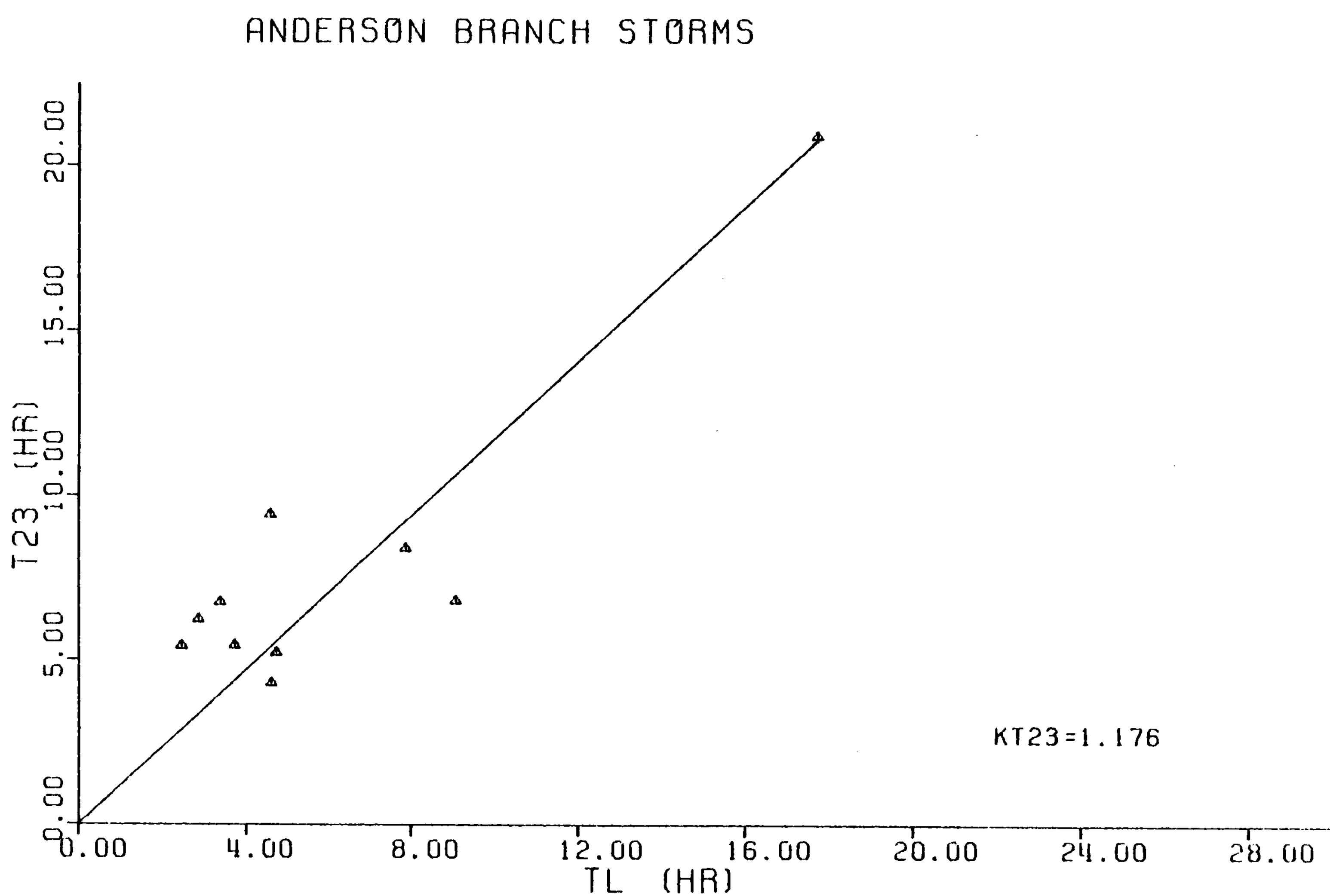

FIGURE B.17

REGRESSION OF T23 VERSUS TL - ANDERSON BRANCH

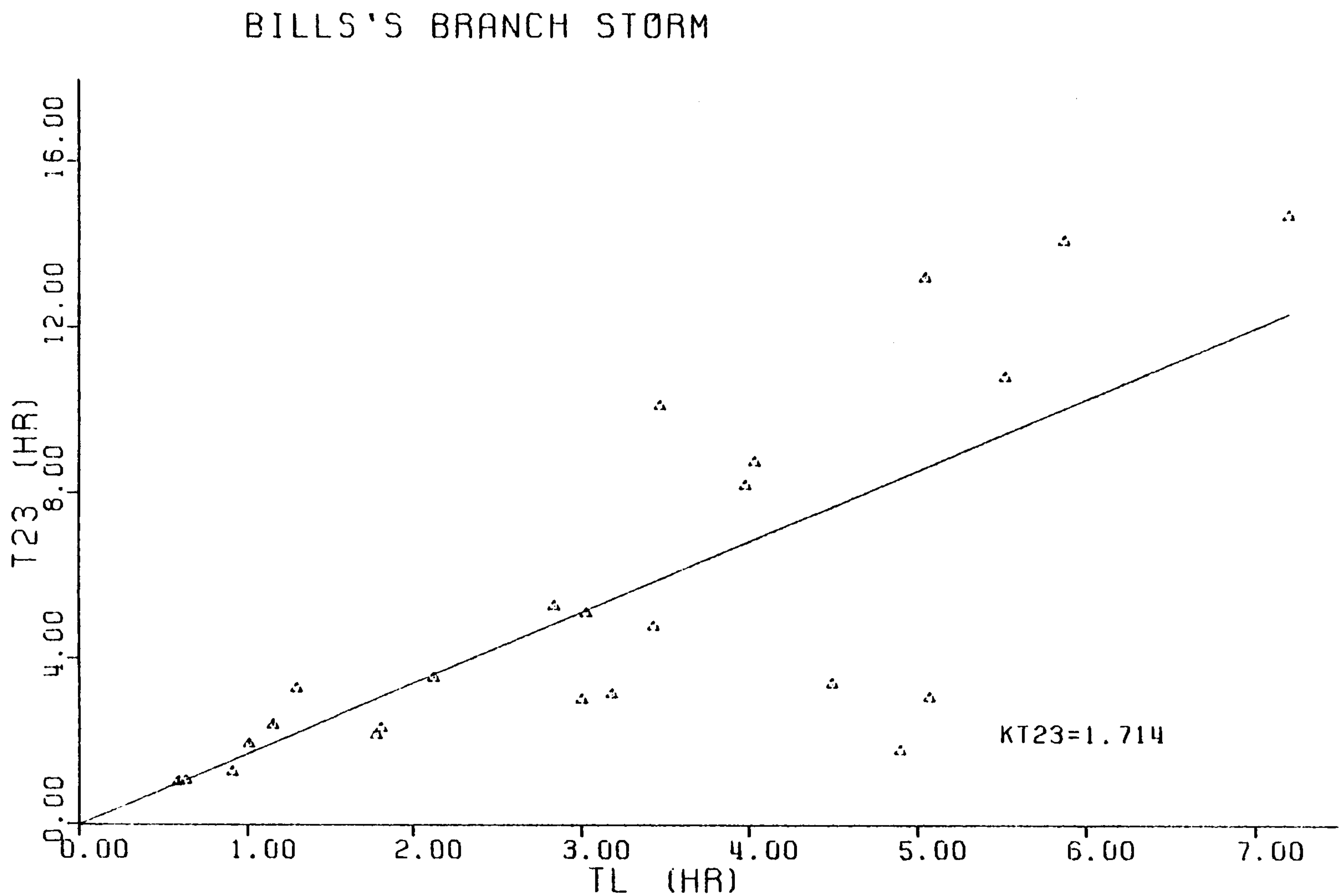

FIGURE B.18

REGRESSION OF T23 VERSUS TL - BILL'S BRANCH

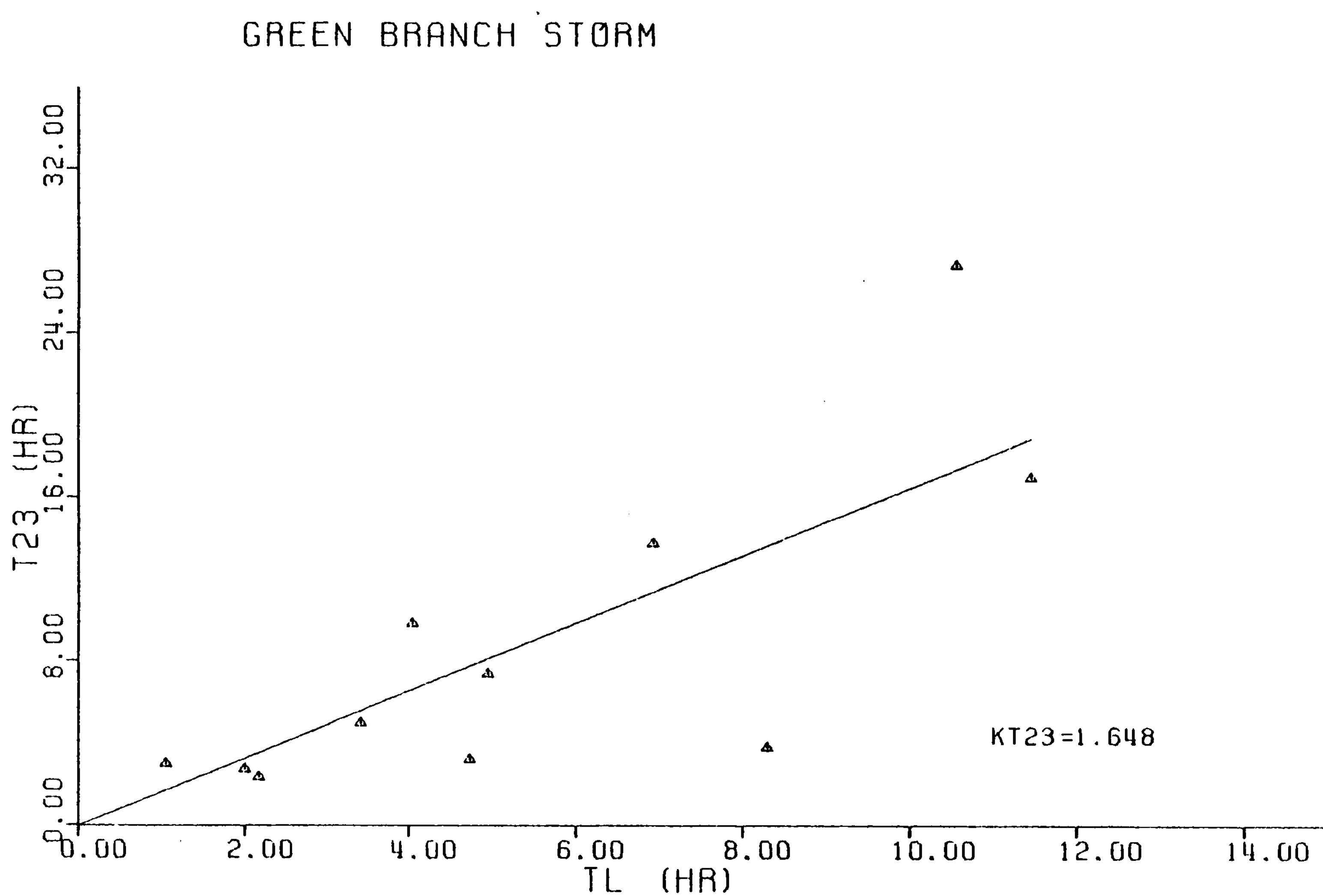

FIGURE B.19

REGRESSION OF T23 VERSUS TL - GREEN BRANCH

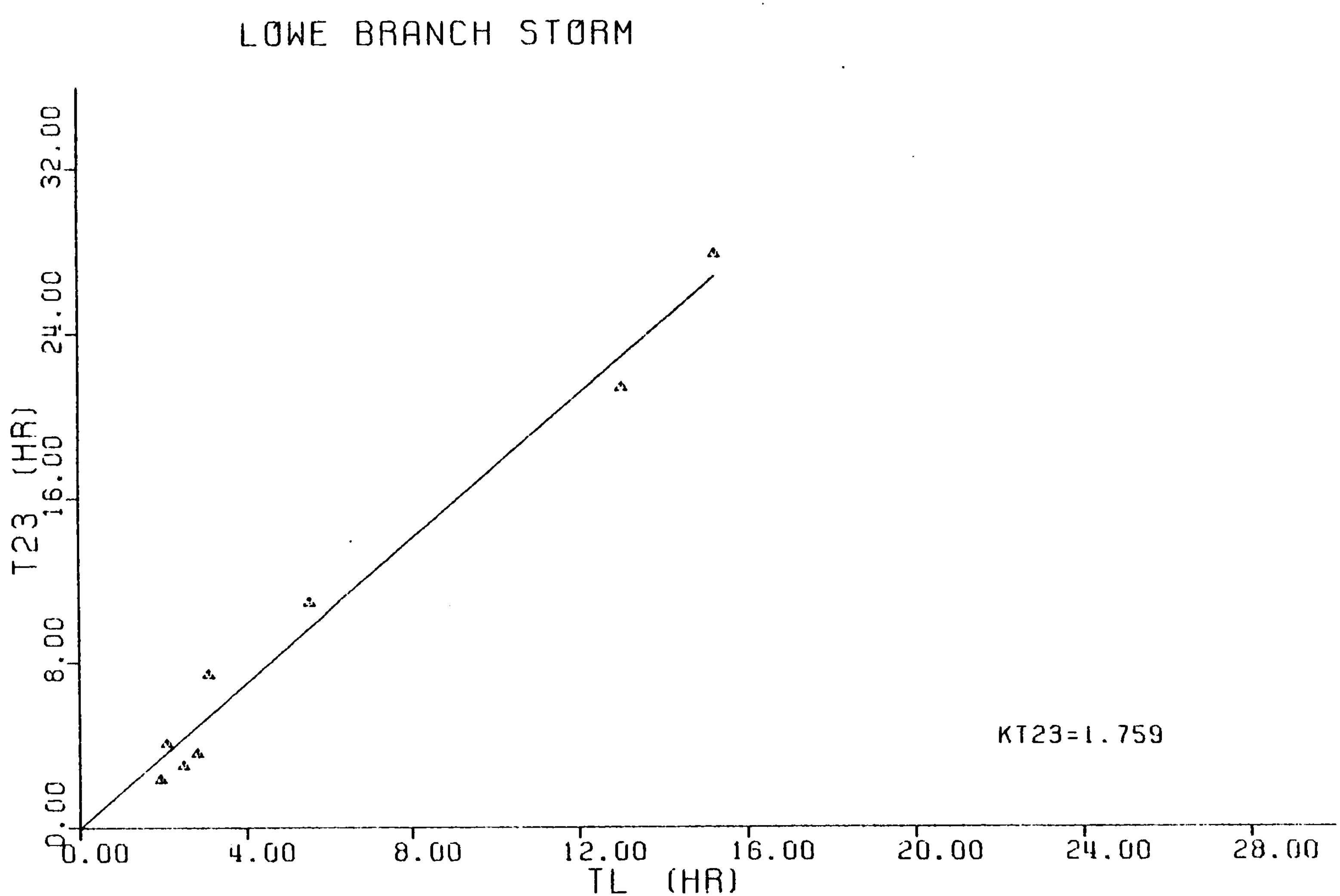

FIGURE B.20

REGRESSION OF T23 VERSUS TL - LOWE BRANCH

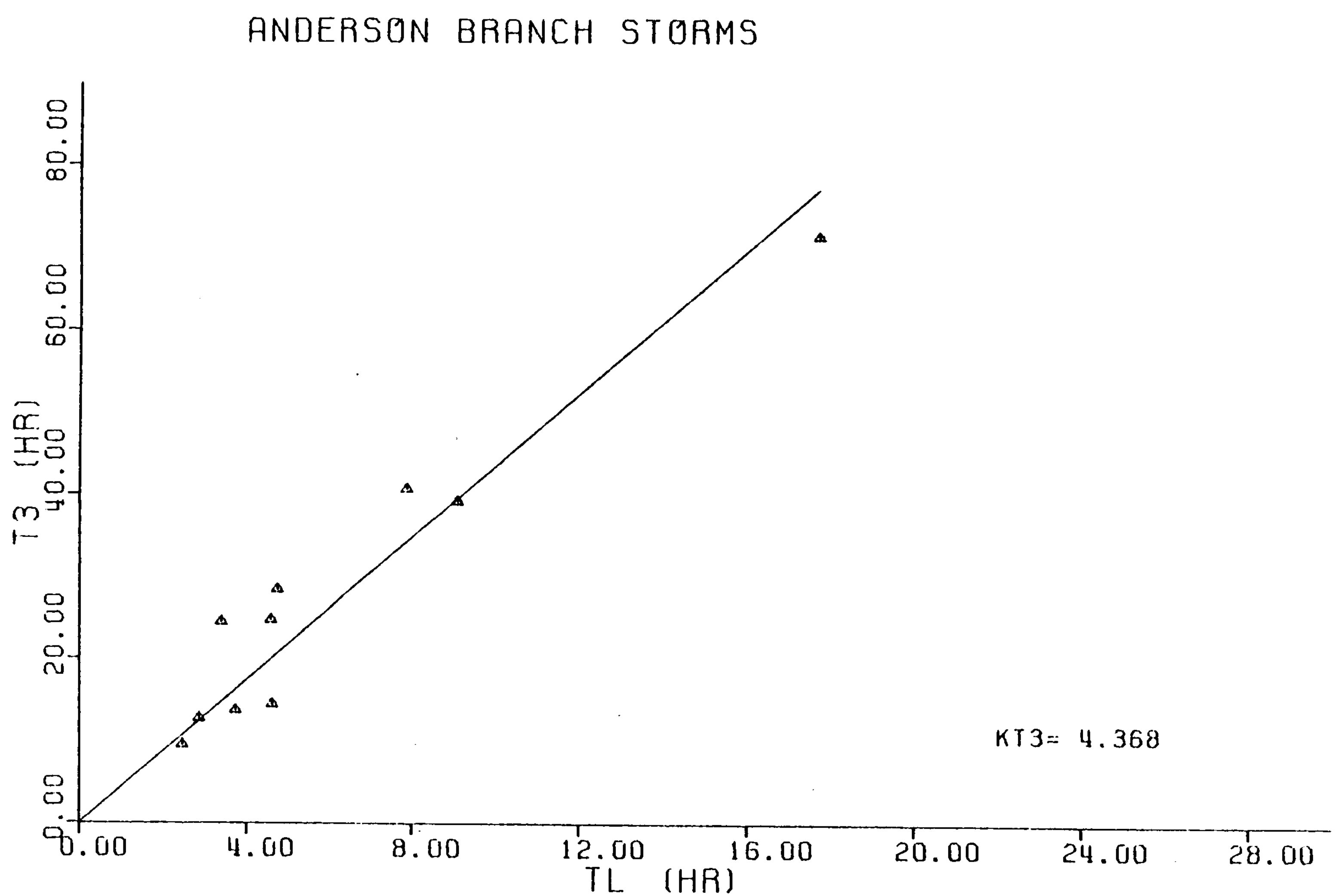

FIGURE B.21

REGRESSION OF T3 VERSUS TL - ANDERSON BRANCH

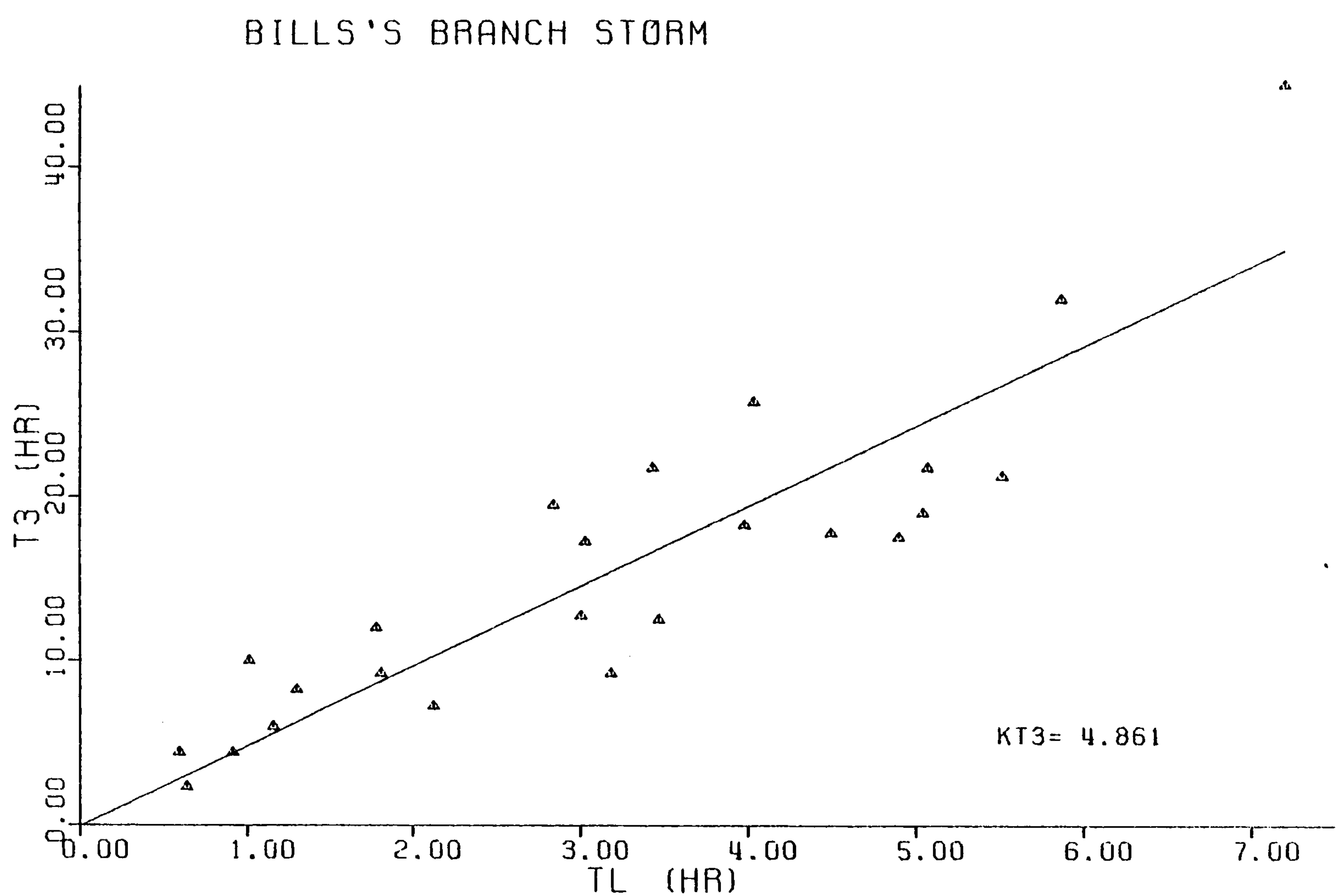

FIGURE B.22

REGRESSION OF T3 VERSUS TL - BILL'S BRANCH

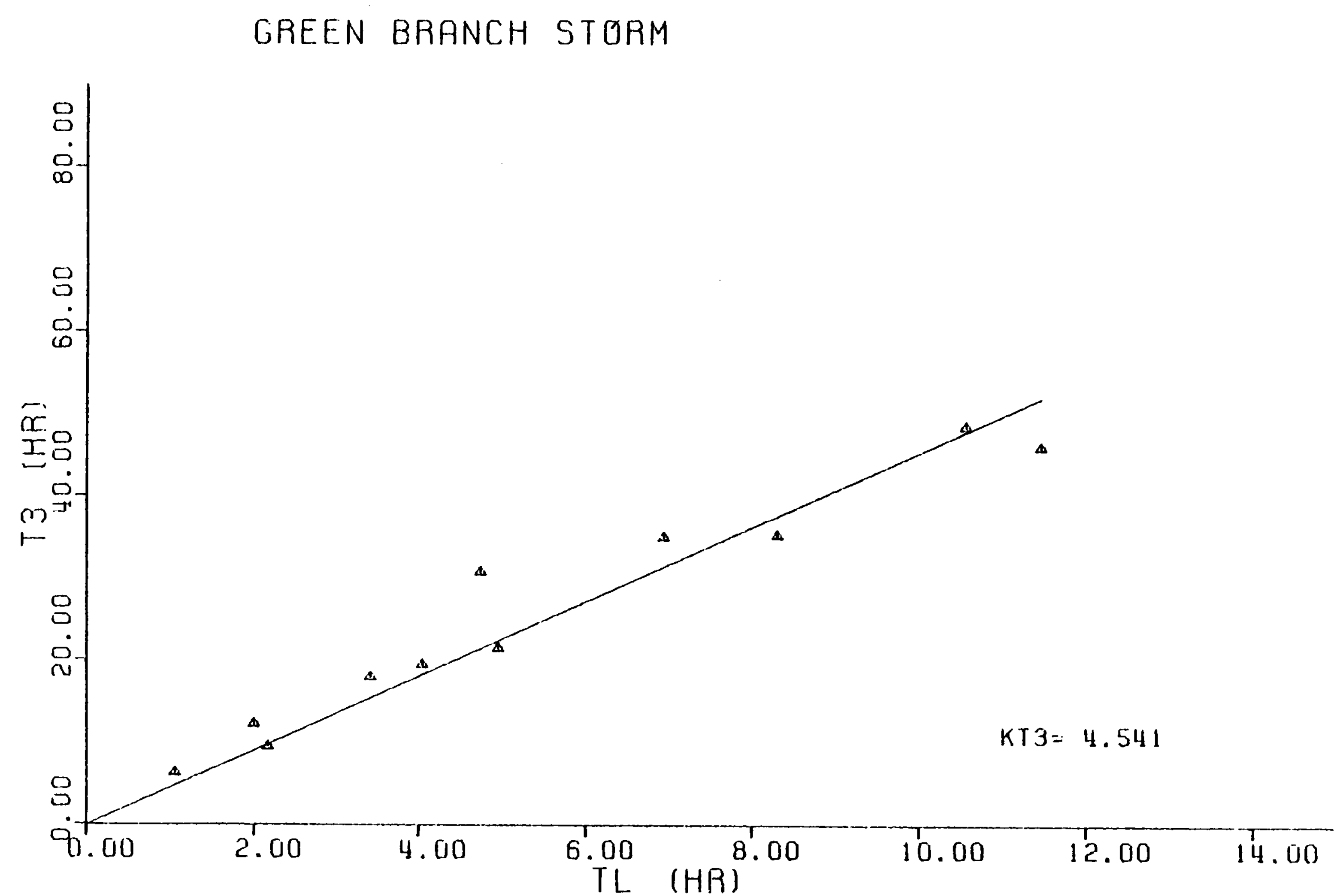

FIGURE B.23

REGRESSION OF T3 VERSUS TL - GREEN BRANCH

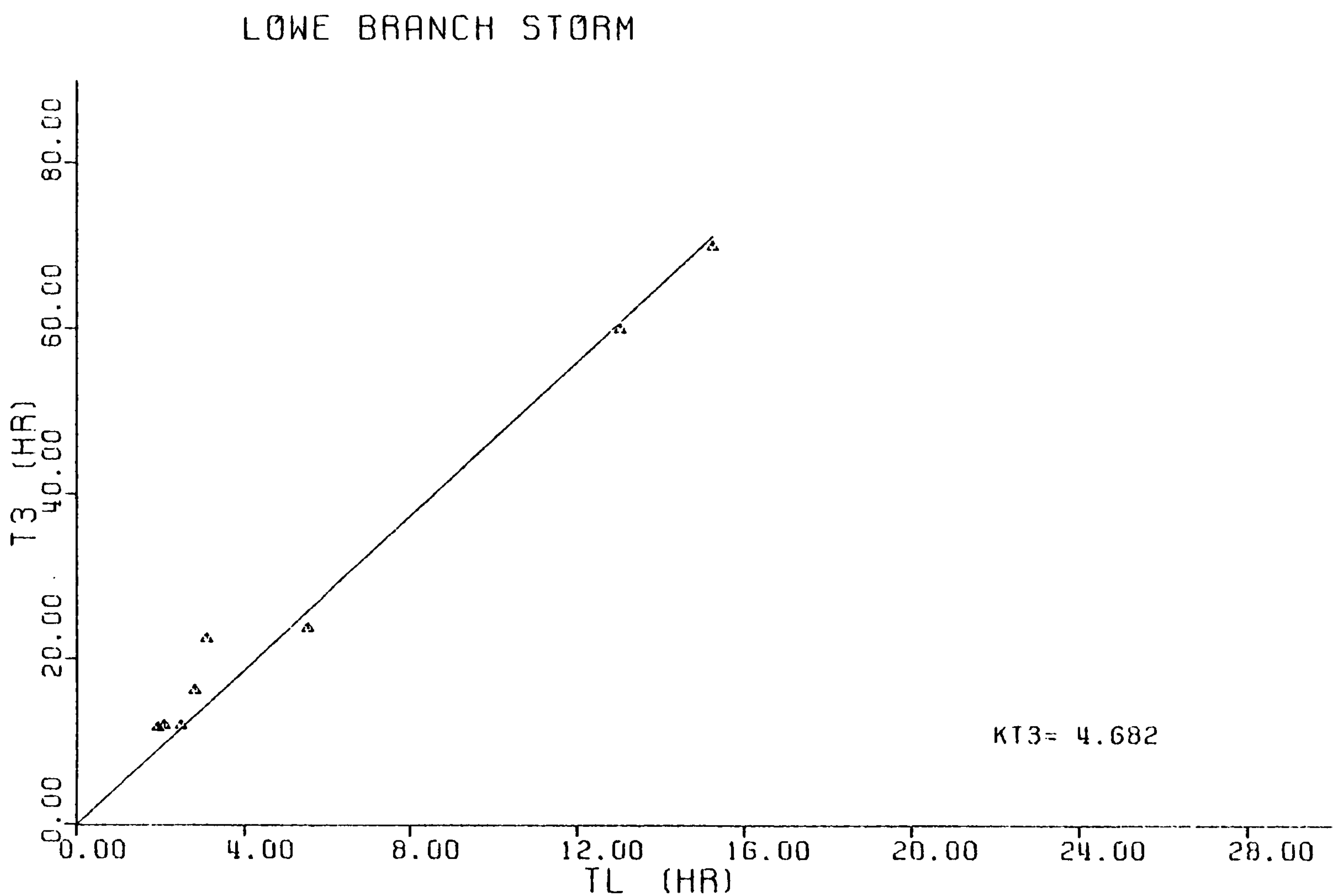

FIGURE B.24

REGRESSION OF T3 VERSUS TL - LOWE BRANCH

VITA

Ernest Clayton Crosby was born in Chicago, Illinois, on December 17, 1944. He graduated from Lemoore High School, Lemoore, California, in June 1963. He received a Bachelor of Science degree in Civil Engineering in August 1969 and a Master of Science degree in Civil Engineering in August 1974 from Memphis State University, Memphis, Tennessee.

He was commissioned an officer in the United States Army Corps of Engineers in July 1970. He served with the United States Army Corps of Engineers from 1970 to 1975 in the Memphis District Office and the Federal Republic of Germany.

He entered the Graduate School at The University of Tennessee in September 1975 and received his Doctor of Philosophy degree with a major in Civil Engineering in August 1979.

He is married to the former Michele M. Przybyszewski, of Memphis, Tennessee.